Volume 65A
Number 6
Nov.–Dec. 1961

Physics and Chemistry

U.S. DEPARTMENT OF COMMERCE

SECTION A

JOURNAL OF RESEARCH

NATIONAL BUREAU OF STANDARDS

Journal of Research

of the

National Bureau of Standards

A. Physics and Chemistry

NOV.-DEC. • 1961

VOLUME • 65A

NUMBER • 6

Editor: U. Fano

Associate Editors: L. M. Kushner
J. M. Richardson

Publication dates:
Feb. 1, Apr. 1, June 1, Aug. 1, Oct. 1, Dec. 1, 1961.

JOURNAL OF RESEARCH

The National Bureau of Standards Journal of Research reports research and development in the fields of activity shown at right. Also included from time to time are survey articles on topics closely related to the Bureau's scientific and technical program.

The Journal is published in four separate sections as follows:

A. Physics and Chemistry

Contains papers of interest primarily to scientists working in these fields. Issued six times a year. Annual subscription: domestic, $4.00; foreign, $4.75.

B. Mathematics and Mathematical Physics

Presents studies and compilations designed mainly for the mathematician and the theoretical physicist. Issued quarterly. Annual subscription: domestic, $2.25; foreign, $2.75.

C. Engineering and Instrumentation

Reports research and development results of interest chiefly to the engineer and the applied scientist. Issued quarterly. Annual subscription: domestic, $2.25; foreign, $2.75.

D. Radio Propagation

Reports work in radio propagation, upper atmospheric physics, and communications. Issued six times a year. Annual subscription: domestic, $4.00; foreign, $4.75.

Functions and Activities

The functions of the National Bureau of Standards are set forth in the Act of Congress, March 3, 1901, as amended. These include the development and maintenance of the national standards of measurement and the provision of means and methods for making measurements consistent with these standards; the determination of physical constants and properties of materials; the development of methods and instruments for testing materials, devices, and structures; advisory services to government agencies on scientific and technical problems; invention and development of devices to serve special needs of the Government; and the development of standard practices, codes, and specifications. The work includes basic and applied research, development, engineering, instrumentation, testing, evaluation, calibration services, and various consultation and information services. The Bureau also serves as the Federal technical research center in a number of specialized fields. The scope of activities of the National Bureau of Standards is suggested in the following listing of the divisions and sections engaged in technical work.

Washington, D.C.

Electricity. Resistance and Reactance. Electrochemistry. Electrical Instruments. Magnetic Measurements. Dielectrics.

Metrology. Photometry and Colorimetry. Refractometry. Photographic Research. Length. Engineering Metrology. Mass and Scale. Volumetry and Densimetry.

Heat. Temperature Physics. Heat Measurement. Cryogenic Physics. Equation of State. Statistical Physics.

Radiation Physics. X-ray. Radioactivity. Radiation Theory. High Energy Radiation. Radiological Equipment. Nucleonic Instrumentation. Neutron Physics.

Analytical and Inorganic Chemistry. Pure Substances. Spectrochemistry. Solution Chemistry. Standard Reference Materials. Applied Analytical Research.

Mechanics. Sound. Pressure and Vacuum. Fluid Mechanics. Engineering Mechanics. Rheology. Combustion Controls.

Organic and Fibrous Materials. Rubber. Textiles. Paper. Leather. Testing and Specifications. Polymer Structure. Plastics. Dental Research.

Metallurgy. Thermal Metallurgy. Chemical Metallurgy. Mechanical Metallurgy. Corrosion. Metal Physics. Electrolysis and Metal Deposition.

Mineral Products. Engineering Ceramics. Glass. Refractories. Enameled Metals. Crystal Growth. Physical Properties. Constitution and Microstructure.

Building Research. Structural Engineering. Fire Research. Mechanical Systems. Organic Building Materials. Codes and Safety Standards. Heat Transfer. Inorganic Building Materials.

Applied Mathematics. Numerical Analysis Computation. Statistical Engineering. Mathematical Physics. Operations Research.

Data Processing Systems. SEAC Engineering Group. Components and Techniques. Digital Circuitry. Digital Systems. Analog Systems. Applications Engineering.

Atomic Physics. Spectroscopy. Infrared Spectroscopy. Solid State Physics. Electron Physics. Atomic Physics.

Instrumentation. Engineering Electronics. Electron Devices. Electronic Instrumentation. Mechanical Instruments. Basic Instrumentation.

Physical Chemistry. Thermochemistry. Surface Chemistry. Organic Chemistry. Molecular Spectroscopy. Molecular Kinetics. Mass Spectrometry.

Office of Weights and Measures.

Boulder, Colorado

Cryogenic Engineering. Cryogenic Equipment. Cryogenic Processes. Properties of Materials. Gas Liquefaction.

Ionosphere Research and Propagation. Low Frequency and Very Low Frequency Research. Ionosphere Research. Prediction Services. Sun-Earth Relationships. Field Engineering. Radio Warning Services.

Radio Propagation Engineering. Data Reduction Instrumentation. Radio Noise. Tropospheric Measurements. Tropospheric Analysis. Propagation-Terrain Effects. Radio-Meteorology. Lower Atmosphere Physics.

Radio Standards. High Frequency Electrical Standards. Radio Broadcast Service. Radio and Microwave Materials. Atomic Frequency and Time Interval Standards. Electronic Calibration Center. Millimeter-Wave Research. Microwave Circuit Standards.

Radio Systems. High Frequency and Very High Frequency Research. Modulation Research. Antenna Research. Navigation Systems. Space Telecommunications.

Upper Atmosphere and Space Physics. Upper Atmosphere and Plasma Physics. Ionosphere and Exosphere Scatter. Airglow and Aurora. Ionospheric Radio Astronomy.

U.S. DEPARTMENT OF COMMERCE
Luther H. Hodges, Secretary

NATIONAL BUREAU OF STANDARDS
A. V. Astin, Director

Order all publications from the Superintendent of Documents
U.S. Government Printing Office, Washington 25, D.C.

Use of funds for printing this publication approved by the Director of the Bureau of the Budget (June 19, 1961).

JOURNAL OF RESEARCH of the National Bureau of Standards—A. Physics and Chemistry
Vol. 65A, No. 6, November–December 1961

Comparison of Lens Response for Sinusoidal and Square-Wave Targets at Several Focal Positions

Sayeda H. Emara*

(June 20, 1961)

A study has been made of the sine-wave and square-wave responses of a lens at two apertures and several focal positions, both on- and off-axis. Two focal positions, one of which gives the best definition and the other the highest contrast for coarse patterns, were located precisely. At these focal positions and at several other arbitrarily chosen positions the sine-wave and square-wave responses were measured. Because of the scattering character of the photographically-made target objects, a special technique has been employed for calibrating the targets to obtain their contrast as seen by the lens under test.

The results show that for large apertures of the lens there is some frequency at which the response (either sine or square) is the same for the two focal positions (curves cross). This phenomenon has been further studied by computing the square-wave response of the lens from its sine-wave response; and it was found that there is close agreement between the computed and experimentally determined responses.

1. Introduction

During the past few years the National Bureau of Standards and a number of other laboratories have been engaged in a research program with the aim of developing a more objective method of assessing the image qualities of a lens than those methods currently in use.

Among numerous procedures, the one based upon Fourier analysis of the object and the image into sinusoidal components is of great theoretical interest. The striking feature of the Fourier approach is the simplicity with which sinusoidally varying luminance patterns are imaged. Diffraction and aberrations have no effect whatsoever on the sinusoidal shape of the image of such a wave, nor on its orientation. In other words, the image of a sinusoidal pattern is also sinusoidal; only the amplitude (or modulation factor) is changed by the imaging process. Thus the performance of an image-forming system may be described by a graph or table that gives the degradation of contrast as a function of spatial frequency for sinusoidal objects. Two such graphs or tables for sinusoidal objects at right angles to each other completely describe the image-forming characteristics at one point in the field.

The easiest method for determining these characteristics makes use of the multiple line object and has been used by several workers [1, 2, 3]. For this method the image of the lines is scanned by a narrow slit to measure the distribution of flux in that image. Recently an improved technique was developed at the National Bureau of Standards which scanned the aerial image directly with a slit and photo-multiplier tube [4]. The resultant variations in illuminance in the image were recorded on the moving chart recorder.

One might suppose that the proper focal plane at which the measurements should be performed would be easily determined as the one at which the response (or transfer function) was maximum. Unfortunately patterns of different frequency give different focuses for their respective maximum responses [5]. Consequently, the selection of the proper focus must be judged by additional criteria. Many investigators have reported the existence of different best focuses, depending upon the criteria. There is a focus that gives the best resolution of fine detail and, presumably, as a consequence, the sharpest reproduction of edges. There is another focus that gives best contrast of coarse detail. If only coarse detail is important, as in 530-line television pictures, this focus may be more nearly optimum than the other. In a previous work a comparison was made between the focal position for highest contrast and the position for best definition, using a coarse parellel line target [6]. Examination of photographs of the pattern indicated a maximum sharpness of edges at one focal position while the maximum amplitude of the traces gave a different position of highest contrast, with a separation of several tenths of a millimeter between the two positions for the particular lens tested. Although the results showed this discrepancy between the focal positions of highest contrast and best definition in a spatial frequency area somewhat removed from the limit of resolution, near this limit the two criteria were satisfied at the same position.

The conclusion arrived at for the location of the position of best definition were based entirely upon visual judgment. Also, all observations were carried

*Guest worker, at the National Bureau of Standards, from Ein-Shams University, Cairo, Egypt.

out using only one coarse pattern and one position, off-axis. Therefore, it was felt that further study of the problem, using more precise measurements, should be made. Thus it is the aim of this paper to present accurate procedures to locate the focuses of best definition and highest contrast and then to measure the sine-wave response and the square-wave response over a wide range of frequencies and apertures for a given lens in the hope of finding a satisfactory explanation of this phenomenon.

Although the work was done with only one lens, a Zeiss Biotar, *f*/2, with a focal length of 58 mm, the results are representative of the performance of practically all high grade photographic lenses.

2. Arrangement of Apparatus

The apparatus was as shown in figure 1. The source was a ribbon filament tungsten lamp focused by a condensing lens on the target located at the focus of the collimator. Thus illumination in this case fulfills the conditions for noncoherence [7]. The lens under test was located on a nodal slide in the collimated beam. The nodal slide and pickup unit were mounted on separate saddles riding on a length of ways alined with the optical axis established by the collimator.

Immediately behind the test lens was the pickup unit consisting of a microscope, slit, and photo tube. In operation the object was moved in the focal plane of the collimator so that the image moved across the slit.

3. Description of Targets

The two targets used in this investigation were transparencies on glass plates, with a transmittance variation forming a square wave for one and a sine wave for the second. There was no variation in transmittance in the orthogonal direction. The square-wave target consisted of 25 patterns, each of which had three dark lines, with lines and spaces of equal width. The spatial frequencies in the image of the patterns ranged from the coarsest, of 6.12 lines per millimeter, to the finest, of 97.6 lines per millimeter. The sine-wave target had 23 patterns producing spatial frequencies in the image of 3 lines per millimeter for the coarsest pattern and approximately 500 lines per millimeter for the finest pattern.

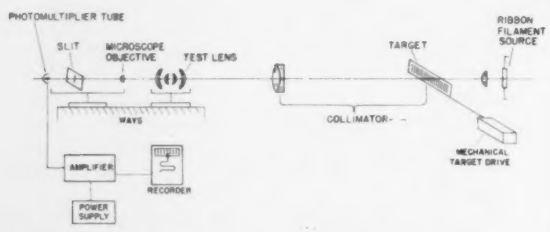

FIGURE 1. *Schematic diagram of the apparatus used.*

The target under investigation was mounted on a carriage and moved through the light beam in a plane parallel to the image plane along a line at right angles to the lines on the target. The scanning speed was constant for a given pattern but for coarse patterns it was faster than for fine patterns. An effort was made to maintain a constant scanning rate in terms of lines per minute for the entire target by changing target speed with gears.

4. Calibration of Targets

Both targets were calibrated using a Leeds and Northrup microdensitometer. The numerical apertures of the microscope and condenser lenses of the microdensitometer were approximately 0.35, whereas those of the collimator and lens being tested were very small, always less than 0.008. This difference of geometry between the system in which the targets were calibrated and that in which they were used resulted in an error. This error was discovered when the measured sine wave responses of the lens were apparently greater than one for some of the coarse patterns. This cannot, of course, be correct. The discrepancy was attributed to the fact that the contrast of photographic materials appears greater with small apertures than with large because of their scattering nature.

It is not possible to eliminate this error by performing the calibration with the aperture of the microdensitometer reduced so as to match the conditions of use. Such a procedure would so reduce the resolving power of the microdensitometer as to render the calibration useless at the higher frequencies. Consequently an indirect calibration process was adopted.

For this calibration a photographic plate was exposed to give a series of fairly broad strips, about 1 cm in width, varying in transmittance by small increments over the entire density scale of the plate. The type of plate was chosen in order to have similar scattering characteristics to that on which the target objects were made. The transmittances of the strips on this plate were measured on the microdensitometer; they were also measured on the test instrument at a numerical aperture of approximately 0.008. The widths of the strips were sufficient that the accuracy of these measurements was not reduced by the low resolving power of the system. The values obtained are exactly the same as if the lens system were free from aberrations and diffraction. A calibration curve was made by plotting transmittance values by test instrument as a function of transmittance by microdensitometer using the data obtained with the step density plate. This is shown in figure 2.

Obviously the end points, zero and unity, are the same on both instruments, but in between there is considerable difference. Correction of target modulations by means of this calibration eliminated responses greater than one and led to satisfactory agreement between measured and computed square-wave responses.

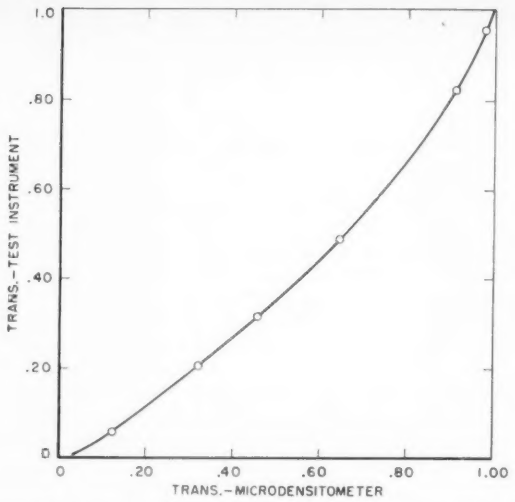

FIGURE 2. *Calibration curve for transmittance measured by the test instrument.*

5. Procedure

The initial requirement of each run was to determine the focal positions of best definition and highest contrast for the selected *f*-stops. Runs were made at lens stop openings of *f*/2 and *f*/8. The position of best definition was determined by using a pattern near the limit of resolution but still giving enough modulation, compared to the noise level, to be measured with moderate accuracy. Several scans were made of the same target pattern with small change in focal position between scans to determine the position yielding the largest signal or modulation. Modulation of the image was calculated using the formula

$$M_i=\frac{T_{\max}-T_{\min}}{T_{\max}+T_{\min}},$$

where M_i is the image modulation produced by the lens under test, $T_{\max}$ the illuminance of a space, and $T_{\min}$ the illuminance of the adjoining line. A plot of image modulation against focal position was drawn. The maximum modulation of this curve determined the position for best definition. The procedure was repeated using a coarse pattern on the square-wave target and a similar curve was drawn to indicate the position of highest contrast. There was little difficulty in finding these focal positions of the lens on axis but at off-axis positions the increased depth of focus of the lens gave flat-top curves, especially for the highest contrast positions, as can be seen in figure 3.

Several runs were made at other apertures, *f*/2.8, *f*/4 and *f*/5–6, where it was found that there was practically no difference between the positions of best definition and best contrast. This is an interesting phenomenon itself, which is worthy of further investigation; but, as we were interested in cases where these two focuses were distinct, no further results are reported for these apertures.

After the correct focal positions had been obtained, the response was determined for several patterns on each target and a plot was made of response as a function of frequency for each focal position. This was accomplished by moving the target through the light beam parallel to the image plane and tracing the resultant image illuminances on the recorder chart. A pattern consisted of a set of lines and spaces of constant spatial frequency. Thus, the target pattern produced a spatial variation in luminance consisting of a sinusoidal component superimposed on a constant component. The ratio of the amplitude of the sinusoidal component to the magnitude of the constant component is the target modulation. An imperfect image of this pattern was formed by the lens under test. This image was further projected onto the plane of the receiver slit with a good low-power microscope objective. Thus the distribution of illuminance in the image was measured.

When the target is imaged by the lens under test, the modulation is reduced, the degree of reduction depending on the quality of the lens. The ratio of the modulation in the image to that in the object is called the response. This factor generally diminishes as the spatial frequency of the pattern increases, the lens acting as a low-pass filter on spatial frequencies. Thus if M_t denotes the modulation of the target and M_i that of the image produced by the lens under test, then the ratio of the two is called response,

$$\Phi=\frac{M_i}{M_t}.$$

The use of the modulation automatically compensates for any factor which changes the signal output of the testing device proportionally such as the transmission factor of the lens, change in brightness of the source, change in gain of the detector amplifier, etc. It must be remembered that the complete response function is actually complex, involving both an amplitude and a phase factor, of which Φ is the amplitude factor. However, for measurements made on axis there is no phase shift involved. In most cases, for evaluation purposes, the phase shift factors can be neglected.

The square-wave response of the lens was computed from its sine-wave response, employing Fourier analysis. A general object was considered to be the summation of a set of sinusoidal waves spatially distributed in the object plane, these component waves differing from each other in amplitude, frequency, phase, and direction. The image consisted of the summation of the images of these component waves.

The square-wave test object can be analyzed into its component harmonics, each of which is attenuated by the Φ corresponding to its frequency, and the square-wave response is obtained by adding these attenuated harmonics [8]. For the response

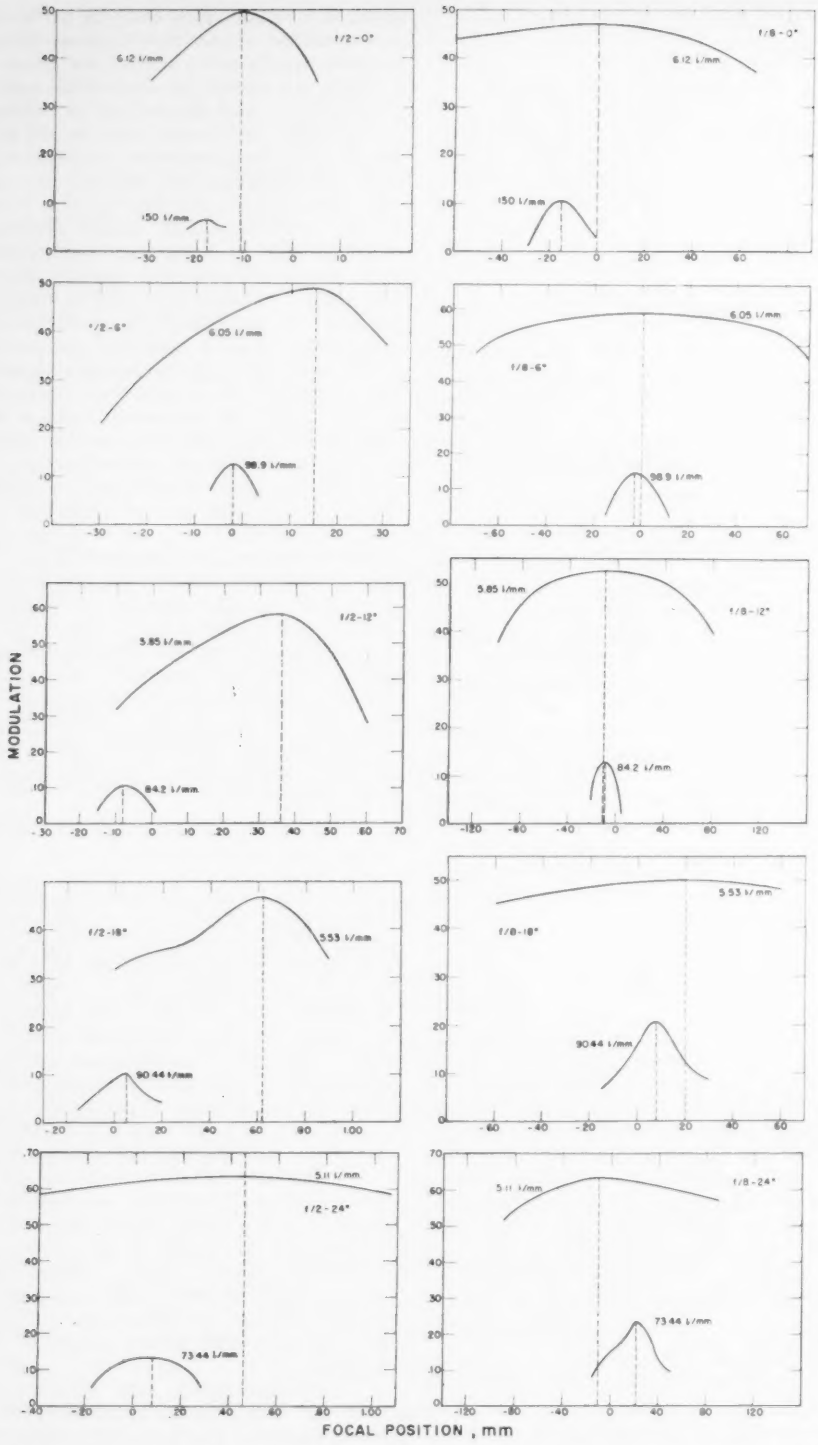

FIGURE 3. *Curves used for obtaining the focal positions for best definition and highest contrast.*

curve we are only interested in the peak-to-peak values which are obtained from the values at the centers of the lines and spaces. The square-wave response curve on axis is then given by:

$$\Psi(\omega)=\frac{4}{\pi}\left[\Phi(\omega)-\frac{1}{3}\Phi(3\omega)+\frac{1}{5}\Phi(5\omega)-\ldots\right]. \quad (1)$$

It should be noticed that there will be only a finite number of terms in the sum because there is a limiting value of ω beyond which Φ is zero for all larger values of ω. This limit exists because of the finite dimensions of the aperture of the system the larger the aperture, the higher the limiting frequency.

Figure 4 shows square-wave target curves or axis using a lens stop of $f/2$. The two solid curves are the experimental curves plotted from data taken in the focal positions of best definition and highest contrast, while the two dotted curves are obtained from values calculated from eq (1). The agreement between the experimental and the calculated curves is very good.

It is to be emphasized that comparison of measured square-wave responses with computed values was entirely unsatisfactory until averages of several runs were used for both the square-wave and sine-wave responses used in the computation. Accordingly, care has been taken to have an average of several runs for each curve shown in this investigation. To convey an idea of the magnitudes of the uncertainties of these results, tables 1 and 2 show the average responses and associated probable errors for two different focuses, best definition and highest contrast, respectively, for the square wave target. These tables represent the results of five runs each.

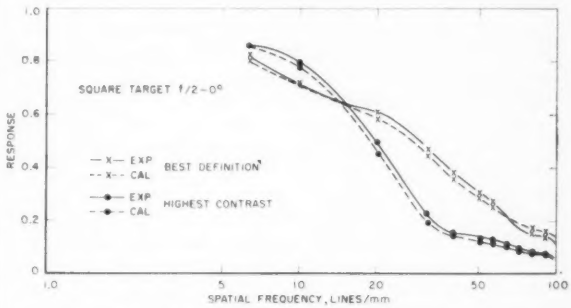

FIGURE 4. *Best definition and highest contrast curves for the square-wave target at f/2 on axis. The two solid curves are those obtained by experiment while the two dotted curves are for values calculated from the sine-wave response using Fourier analysis.*

TABLE 1. *Responses to square waves at the focus of best definition with associated probable errors; measured on axis at f/2.*

Lines/mm	6.12	9.7	19.4	30.7	38.7	49.2	55.2	62.4	69.8	78.5	88.4	97.5
Average response	0.820	0.720	0.626	0.492	0.384	0.310	0.272	0.220	0.177	0.151	0.142	0.111
Probably error	±0.025	±0.027	±0.021	±0.018	±0.018	±0.012	±0.012	±0.008	±0.008	±0.007	±0.008	±0.006

TABLE 2. *Responses to square waves at the focus of highest contrast with associated probable errors; measured on axis at f/2.*

Lines/mm	6.12	9.7	19.4	30.7	38.7	49.2	55.2	62.4	69.8	78.5	88.4	97.5
Average response	0.860	0.800	0.514	0.228	0.158	0.138	0.124	0.114	0.097	0.084	0.079	0.060
Probable error	±0.027	±0.026	±0.035	±0.015	±0.008	±0.014	±0.007	±0.006	±0.007	±0.007	±0.005	±0.002

6. Results

Figure 5 illustrates the square- and sine-wave response curves at an $f/2$ stop opening on axis and at off-axis positions of 6°, 12°, 18°, and 24°. The curves for the square-wave show an interesting phenomenon. On axis the best-definition and highest-contrast curves intersect at a spatial frequency of 14.5 lines per millimeter with a response of 0.66. At 6° off-axis best-definition and highest-contrast curves intersect at the spatial frequency of 11 lines per millimeter, where the response is 0.65. At 12° these curves intersect at a point where the frequency is 11.5 lines per millimeter at a lower response of 0.39. At 18° the frequency at which they intersect reaches a value of approximately 9.6 lines per millimeter at a response as low as 0.34. At 24° the two curves intersect at a spatial frequency of 17 lines per millimeter at a response of 0.65. The curves for the lens at the position of highest contrast show that the finest pattern resolved decreases in frequency at off-axis positions and reaches a minimum of 23 lines per millimeter at 18° but increases again at 24° reaching a value of 46 lines per millimeter, while the best-definition curves show little change.

The sine wave shows characteristics similar to those for the square wave. On-axis the behavior is as expected; but at 6° off-axis the highest contrast and best definition curves intersect at a frequency of 7.8 lines per millimeter, where the response is 0.71. At 12° the two curves intersect at a spatial frequency of 10.8 lines per millimeter with a decreased response of 0.31. At 18° off-axis the spread between the best definition and highest contrast decreases with coincidence at a spatial frequency of 8.2 lines per millimeter and a response of 0.36. As the lens is rotated further about its vertical axis until 24° off-axis is

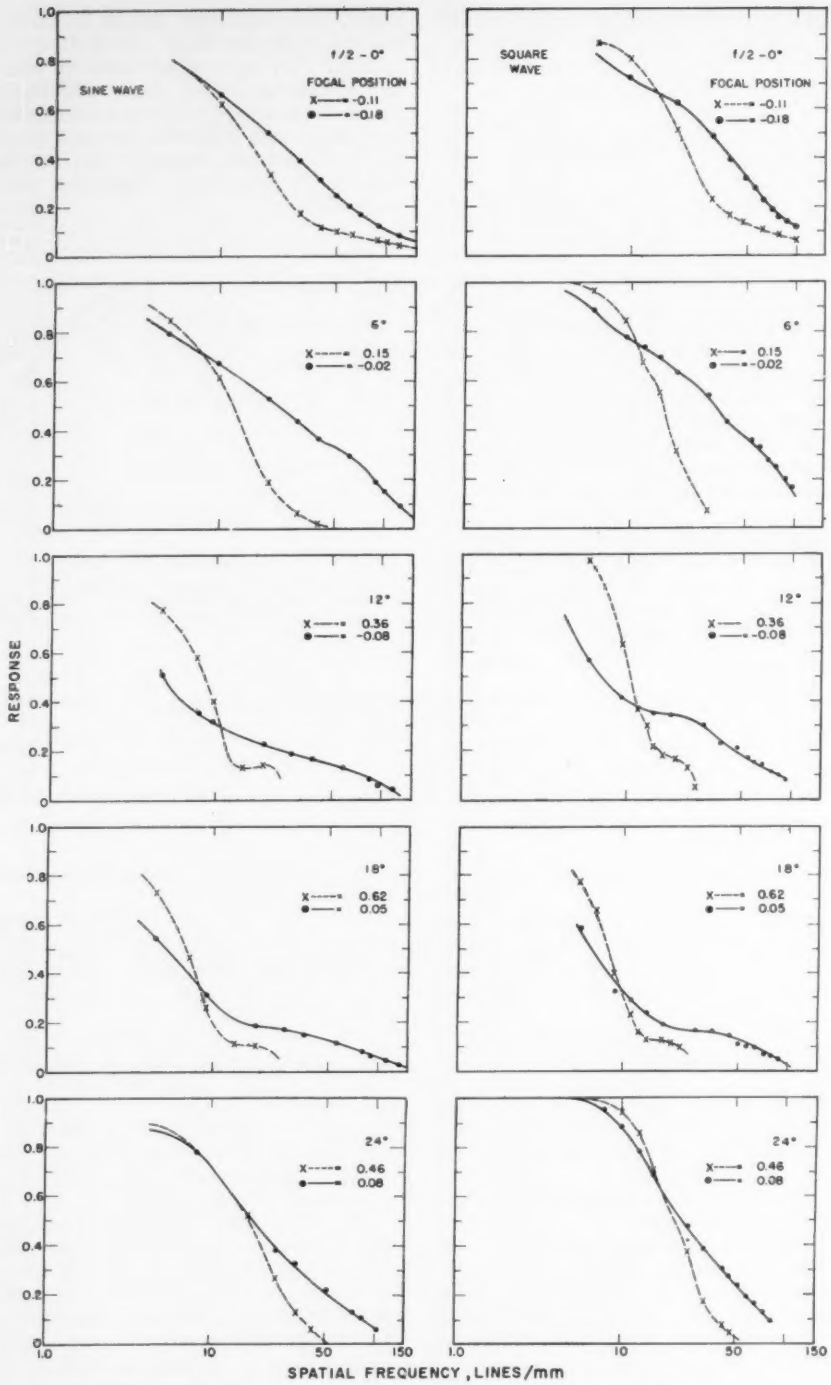

FIGURE 5. *Responses for square-wave and sine-wave targets at f/2 on axis and for four off-axis positions, 6°, 12°, 18° and 24°.*

reached the best definition and highest contrast curves intersect at a spatial frequency of 8.8 lines per millimeter with a response of 0.77. It is of interest to note that at this frequency the response has again reached a higher value, closer to that obtained on axis. The finest pattern resolved for the highest contrast curves decreases in frequency for increasing off-axis angles, reaching a minimum of 18 lines per millimeter at 18° and then increasing to a value of 42 lines per millimeter at 24°.

This suggests that for both targets there is a serious effect from aberrations reaching a maximum near 12° off-axis and then decreasing as off-axis positions approach 24°. This obviously is a consequence of the zonal nature of the corrections in photographic lenses. In this case the observations appear to be most nearly corrected on axis and at about 24° off-axis with some deterioration of image quality in between.

Figure 6 shows a set of curves for both targets using *f*/8 stop of the lens on axis and at 18° and 24° off-axis positions. It is clearly seen that the results obtained with the two targets are similar. The best definition and highest contrast curves differ considerably on axis and at 24° off-axis while the difference at 18° is smaller.

Curves at 6° and 12° with an *f*/8 stop opening are omitted because at these off-axis positions the focal positions for best definition and highest contrast were very close and no appreciable difference in response could be observed on these curves.

Further runs were made, both on- and off-axis, using the *f*/2 lens stop and four different focal positions, two of which were the positions of highest contrast and best definition. Two examples are given illustrating the effect of changing the focal positions. Figure 7 shows curves for the sine-wave target at four different focal positions on axis of the lens. The best focal position is that of best definition. Figure 8 illustrates another set of curves at 18° off-axis. Here again it is clearly seen that in the spatial frequency range of 5 to 6.8 lines per millimeter the highest contrast position (0.62) gives the highest response while in the range of 6.8 to 12 lines per millimeter the position next to highest contrast (0.40) is best. In the area 12 to 29 lines per

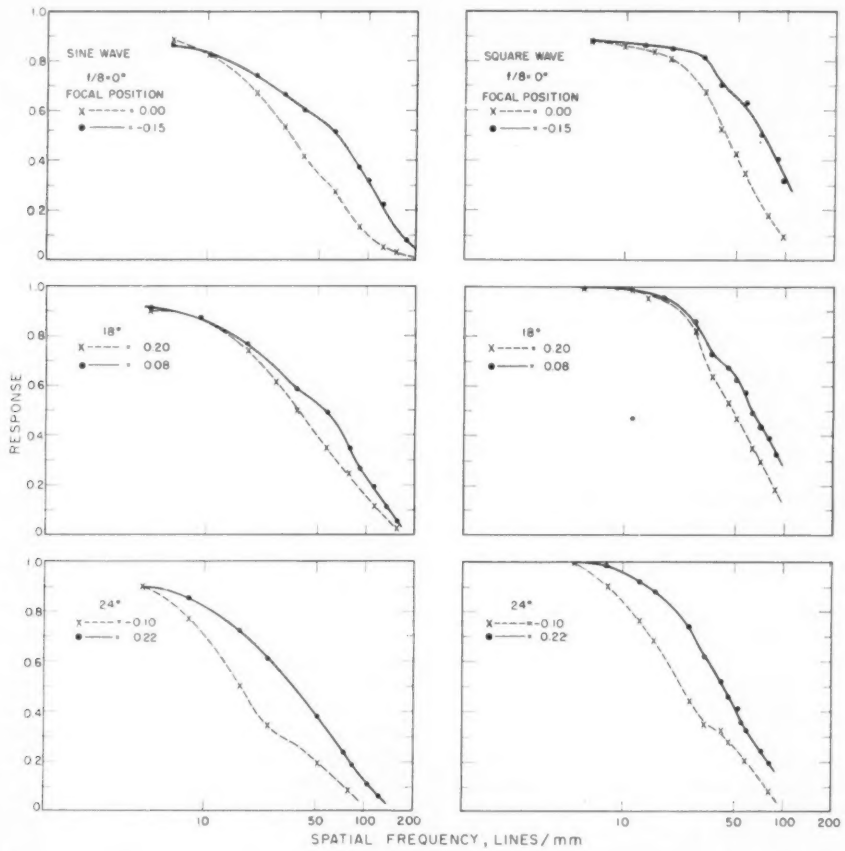

FIGURE 6. *Responses for square-wave and sine-wave targets at* f/8 *on axis and for two off-axis positions, 18° and 24°.*

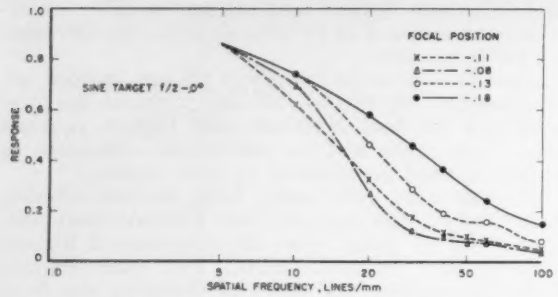

FIGURE 7. *Sine-wave response curves for four different focal positions on-axis.*

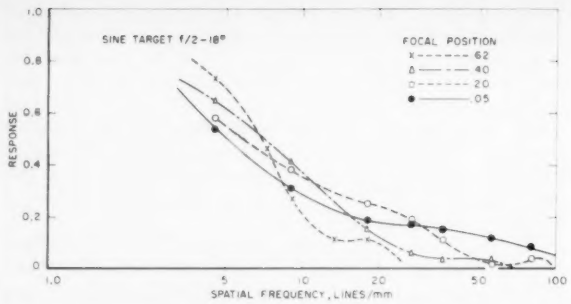

FIGURE 8. *Sine-wave response curves for four different focal positions at 18° off-axis.*

millimeter the next focal position (0.20) is best and, finally, from 29 lines per millimeter up the position of greatest definition (0.05) is best.

7. Conclusions

There are a number of conclusions which can be drawn:

1. The square-wave response can be predicted reasonably well if the sine-wave response is known. It is concluded that for a large aperture of the lens there is a certain spatial frequency at which the best definition and highest contrast curves coincide. Its value differs slightly for off-axis positions.

2. The response for both targets decreases as spatial frequency increases.

3. There is a serious effect caused by lens aberrations at off-axis positions; reaching a maximum for this lens close to 12° and decreasing again at 24°.

4. Displacement of focal positions at large apertures shows that the position of best definition may be inferior for some purposes.

5. Curves drawn for locating the focuses of best definition, and especially those for locating focuses of highest contrast become very flat topped for small apertures. Consequently these two focuses become indistinguishable. This is, of course, a manifestation of the increasing of depth of focus.

The author wishes to express her grateful thanks to the National Bureau of Standards and to A. G. McNish, chief of the Metrology Division, for providing excellent laboratory facilities and greatly appreciates the assistance of staff members. My sincere thanks are due in particular to F. W. Rosberry for his kind interest and encouragement during the course of this work and to R. E. Stephens for invaluable discussions.

8. References

[1] W. Henist, A photo-electric lens bench, J. Opt. Soc. Am. **37**, 472 (1947).
[2] E. Inglestam and P. J. Lindberg, A combined test procedure for camera lenses, and photoelectric examination of intensity distribution in line images, NBS Circular 526 (1951).
[3] O. Schade, A new system of measuring and specifying image definition, NBS Circular 526, 183 (1951).
[4] F. W. Rosberry, Equipment and method for photoelectric determination of image contrast suitable for using square-wave targets, J. Research NBS **64C**, 57 (1960).
[5] F. W. Rosberry, The effect of object frequency on focal position of four photographic objectives (informal communication).
[6] F. W. Rosberry, Measurement of contrast in the aerial image, Photogrammetric Eng. **27**, 155 (1961).
[7] R. V. Shack, Investigations into the correlation between photographic and photo-electric image evaluation (informal communication).
[8] R. V. Shack, Characteristics of an image-forming system, J. Research NBS **56**, 245 (1956) RP2672.

(Paper 65A6–127)

JOURNAL OF RESEARCH of the National Bureau of Standards—A. Physics and Chemistry
Vol. 65A, No. 6, November–December 1961

Wavelength Shifts in Hg^{198} As a Function of Temperature

Sayeda H. Emara*

(July 11, 1961)

The wavelength shifts for the green (5460A) and blue (4358A) lines emitted from an electrodeless discharge lamp of Hg^{198} have been studied as a function of the temperature of the water jacket of the source. The values of the wavelength shifts observed for the green and the blue lines are $(8.5\pm3)\ 10^{-6}$ A/°C and $(2\pm1)\ 10^{-6}$ A/°C, respectively.

1. Introduction

When satisfactory electrodeless discharge lamps containing a single isotope of mercury became available, several reports [1, 2, 3] [1] were given recommending the use of this source as a secondary standard of wavelength.

The ease of construction and operation of electrodeless discharge lamps of Hg^{198} and the high intensity and relative sharpness of the widely spaced lines of this source have contributed to its wide general use for many interferometric and metrological purposes. There are no isotope shifts or hyperfine structure in the lines of Hg^{198} and because the atoms can be excited at relatively low temperature and vapor pressure, the wavelengths can be determined with great accuracy.

Two of the most commonly used spectral lines from this source are the green line (5460A) and the blue line (4358A). For visual adjustment of interferometers the green line of Hg^{198} is highly satisfactory and has been used extensively by several workers because it lies in the spectral region to which the normal eye is most sensitive.

Although an electrodeless Hg^{198} discharge lamp is convenient to use, the radiations emitted from this source suffer small wavelength shifts due to the pressure of the carrier gas and a change of vapor pressure of the mercury. Baird and Smith [4] have measured the shift due to the carrier gas pressure for a number of lines. They also pointed out the necessity for operating the source at a low temperature, preferably below 10 °C, [5] to reduce the asymmetric broadening and self absorption observed at higher temperatures. No quantitative measurement of this shift has as yet been reported.

Precision measurements of the wavelength of the green line have been reported by a number of laboratories. [6–11] These values are in disagreement. The discrepancies among the reported values might be due in part to the differences in the operating temperatures of the lamps. Consequently, a quantitative study of the effect of temperature was made. This paper reports the observed wavelength shifts of the green and blue lines as a function of the temperature of the water jacket of the source.

2. Experimental Details

The source was a Hg^{198} electrodeless discharge lamp of the type described by Meggers and Westfall [12]. It contained 1 mg of mercury. The carrier gas was argon at a pressure of 3 mm of mercury. The lamp was excited with a Raytheon microwave generator at a frequency of 2,450 Mc/s, and was operated in a jacket in which water was circulated. The radiation from this source illuminated a vacuum-enclosed Fabry-Perot interferometer with plate separation of 104.55 mm. The interference patterns were imaged on the slit of a quartz prism spectrograph by an achromatic lens of 75 cm focal length. The temperature of the water was measured to an accuracy of ±0.1 °C with a thermometer placed close to the outlet. When a constant water temperature was indicated, interferograms were taken with Kodak spectroscopic plates 103a–F. The exposure times were ten seconds and one minute at temperatures of 40 and 5 °C, respectively. Twenty-four exposures were made at alternate temperatures of the water jacket of 5 and 40 °C. This procedure was repeated for temperatures of 5 and 22.5 °C. The diameters of nine rings in the interference patterns for the green and blue lines were measured. From these measurements the fractional order at the center of each pattern was determined by using a procedure described by Meissner [13].

3. Results

The formula used for the calculation of the change in wavelength due to a change of temperature of the source is

$$\Delta\lambda=\frac{\lambda^2}{2t}\cdot\frac{\epsilon_1-\epsilon_2}{T_2-T_1}$$

where $\Delta\lambda$ is the change in wavelength per degree centigrade; T_1, T_2 are the lower and higher temperatures of the water jacket of the source.

λ is the wavelength of the line being measured.

t is the plate separation of the interferometer.

ϵ_1, ϵ_2 are the average fractional orders measured at the specified temperatures.

*Guest worker, at the National Bureau of Standards from Ein-Shams University, Cairo, Egypt.

[1] Figures in brackets indicate the literature references at the end of this paper.

The results obtained are summarized in the following table:

Nominal wavelength	T_1	T_2	No. of determinations	Wavelength shift $\times 10^6$
A	°*C*	°*C*		*A*/°*C*
5460	5	40	10	$+9.5 \pm 3.0$
5460	5	22.5	10	$+7.5 \pm 2.5$
			Average	$+8.5 \pm 3$
4358	5	40	10	$+2.0 \pm 0.8$
4358	5	22.5	10	$+2.1 \pm 1.3$
			Average	$+2.0 \pm 1$

The precisions indicated in the last column are average deviations.

The results indicate that the wavelength shift is nearly a linear function of temperature. Note, however, that the shift observed for the green line is about four times greater than that for the blue line and in the same direction. In both cases the wavelength increases with temperature. The green line also suffers to a greater extent from self absorption. These differences might be attributable to the fact that the lower state of the transition from which the green line arises is metastable. Therefore, for precision work using this source, the blue line at 4358A would appear to have advantages over the green line at 5460A.

The author expresses her thanks to the National Bureau of Standards and to A. G. McNish, Chief of the Metrology Division, for providing laboratory facilities. It is a pleasure to express my sincere thanks to K. G. Kessler, Chief of the Spectroscopy Section, for suggesting the problem and to V. Kaufman for his continuous encouragement and helpful suggestions.

4. References

[1] Compt. rend. 9th Conference Générale des Poids et Measures **24,** M43 (1954).
[2] Compt. rend. 9th Conference Générale des Poids et Measures **44,** (Paris-Gauthier-Villars, 1949).
[3] Meggers, W. F., Sci. Monthly **LXVIII,** No. 1 (Jan. 1949).
[4] Baird, K. M., and D. S. Smith, Can. J. Phys. **35,** No. 4, 455–461 (1957).
[5] Baird, K. M., and D. S. Smith, Proces-verbaux Comité Int. Poids et Mesures **26-B,** M121 (1959).
[6] Meggers, W. F., and K. G. Kessler, J. Opt. Soc. Am. **40,** No. 11, 737–741 (1950).
[7] Terrien, J., Proces-verbaux Comité Int. Poids et Mesures **26-B,** M134 (1958).
[8] Englehard, E., Proces-verbaux Comité Int. Poids et Mesures **26-B,** M63 (1958).
[9] Barrell, H., Proces-verbaux Comité Int. Poids et Mesures **26-B,** M85 (1958).
[10] C.I.I.W.M. (Japan), Proces-verbaux Comité Int. Poids et Mesures **26-B,** M103 (1958).
[11] Baird, K. M., and D. S. Smith, Proces-verbaux Comité Int. Poids et Mesures **26-B,** M119 (1958).
[12] Meggers, W. F., and F. O. Westfall, J. Research NBS **44,** 447–455 (1950) RP2091.
[13] Meissner, K. W., J. Opt. Soc. Am. **31,** No. 6, 405–427 (1941).

(Paper 65A6–128)

JOURNAL OF RESEARCH of the National Bureau of Standards—A. Physics and Chemistry
Vol. 65A, No. 6, November–December 1961

Variability of Spectral Tristimulus Values

Isadore Nimeroff, Joan R. Rosenblatt, and Mary C. Dannemiller

(July 11, 1961)

As the spectral tristimulus values of the CIE Standard Observer System for Colorimetry are measurable quantities, their variabilities should be known. This paper describes a procedure for deriving "within" and "between" variances and covariances in the spectral tristimulus values, based on color-matching data for individual observers. The "within" variances are based on the replications of color-mixture data by an observer. The "between" variances are based on differences among the color-mixture data of individual observers. A statistical model is given for the system in which the experimental data are obtained. Formulas for expected values (means), variances, and covariances are developed. Variances and covariances belonging to different sources of uncertainties in the experimental data are considered. A procedure is developed for determining the uncertainties in the constants of a linear transformation to a system analogous to the present CIE system. The formulas for variances and covariances after linear transformation are given, for a rigorous empirically-based choice, and also for an arbitrary choice of transformation constants. The complete standard observer system for every 10 mμ consisting of means, variances, and covariances derived from an arbitrary transformation, is listed. The between-observer variabilities are found to be about 10 percent of the averages of the color-mixture data and the average ratio of the between-observer variabilities to the within-observer variabilities is found to be about 5.7.

1. Introduction

Since 1931 the International Commission on Illumination has recommended the use of a Standard Observer System for Colorimetry [1].[1] This system defines the manner in which spectral data for materials are to be reduced to three numbers, called tristimulus values, that describe colors of emitted, reflected, or transmitted lights. The defining equations for these tristimulus values are:

$$X \equiv \int_0^\infty \bar{x}_\lambda N_\lambda T_\lambda d\lambda \doteq \sum_0^\infty \bar{x}_\lambda N_\lambda T_\lambda \Delta_\lambda$$

$$Y \equiv \int_0^\infty \bar{y}_\lambda N_\lambda T_\lambda d\lambda \doteq \sum_0^\infty \bar{y}_\lambda N_\lambda T_\lambda \Delta_\lambda$$

$$Z \equiv \int_0^\infty \bar{z}_\lambda N_\lambda T_\lambda d\lambda \doteq \sum_0^\infty \bar{z}_\lambda N_\lambda T_\lambda \Delta_\lambda$$

The quantities $\bar{x}_\lambda$, $\bar{y}_\lambda$, and $\bar{z}_\lambda$ are called spectral tristimulus values and are intended to be descriptive of the spectral-light response of the average human observer with normal color vision. The quantity N_λ describes the spectral emittance of light sources and the quantity T_λ describes the spectral character of the reflecting or transmitting materials.

Tristimulus values are usually reduced to chromaticity coordinates by the equations:

$$x = X/S,\ y = Y/S, \text{ and } z = Z/S,$$

where S is the sum of the tristimulus values X, Y, and Z. As $\bar{x}_\lambda$, $\bar{y}_\lambda$, $\bar{z}_\lambda$, N_λ, and T_λ are measured quantities, they are subject to measurement uncertainty. Nimeroff [2,3] has treated, by means of propagation of error theory, the manner in which variabilities in T_λ and in N_λ affect the chromaticity coordinates, x, y, and z.

The general problem and several special cases of propagation of errors in tristimulus colorimetry have been treated by Nimeroff [3]. In that treatment the mean spectral tristimulus values, $\bar{x}$, $\bar{y}$, and $\bar{z}$, were estimated by averaging the mean CIE (17 observers) and mean Stiles' 2°- and 10°-field pilot data (10 observers each). The variances in these values were estimated in the usual manner by using deviations of these three mean data from the estimated overall mean values; the covariances were ignored. The variances as well as the covariances should, however, be more fundamentally estimated; that is, they should be estimated from differences among color-mixture functions of individual observers. Such data became available in 1959. This paper describes how this fundamental estimation of the between-observer variances and covariances may be made for the 10°-field color-mixture data of the 53 observers of Stiles-Burch [4] and the 27 observers of Speranskaya [5], and gives estimates of the average within-observer variances and covariances of two observers, one with 4 and the other with 5 replications. The estimates of covariances are developed on the basis of the data of the 53 observers of Stiles-Burch.

2. Statistical Model

Fundamental color-matching data are obtained on a device where an observer is presented two fields which he is asked to color-match, by adjusting the

[1] Figures in brackets indicate the literature references at the end of this paper.

amounts of three primary colors. In one field, there is a fixed amount, E_λ, of a given spectral color of wavelength λ. The three adjustable primaries having wavelengths 645.2, 526.3, and 444.4 mμ may be denoted R, G, B, respectively. One is added to the field containing the given color, and the other two are mixed in the second field. If R_λ is the amount of the Red (R) primary (in energy units) used in matching E_λ, and G_λ and B_λ are similarly defined, then the condition of color-matching may be expressed:

$$E_\lambda \overset{m}{\equiv} R_\lambda + G_\lambda + B_\lambda, \tag{1}$$

where the primary which was mixed with the given color is represented by a negative quantity on the right-hand side of this symbolic equation.

The complete set of color-mixture data for a single observer consists of the amounts of the three primaries used in matching a series of spectrum colors sampling the entire visible portion. These data are adjusted so that, in suitable units, (R_λ, G_λ, B_λ) represent the amounts used in matching a unit amount (energy) of the spectrum color at wavelength λ.

The empirical results for the ith observer may be denoted ($R_{\lambda i}$, $G_{\lambda i}$, $B_{\lambda i}$). Omitting the subscript λ we consider the following model:

$$\begin{aligned} R_i &= R + b_{Ri} + \epsilon_{Ri} \\ G_i &= G + b_{Gi} + \epsilon_{Gi} \\ B_i &= B + b_{Bi} + \epsilon_{Bi}, \end{aligned} \tag{2}$$

where each of R_i, G_i, B_i is represented as the sum of three terms: R, the average amount which would be used in color-matching in a population of observers with normal color vision; the "bias" b_{Ri} of the ith observer; and an "error" ϵ_{Ri}. The bias b_{Ri} is the amount by which the ith observer's "true" average differs from the population average R. The error ϵ_{Ri} is the difference between a given observation R_i and the ith observer's true average which is $(R+b_{Ri})$. The terms of the second and third eqs of (2) are similarly defined. The expected value (true average) of error ϵ_i is assumed to be zero; thus, for the ith observer,

$$\begin{aligned} E_i[R_i] &= R + b_{Ri} \\ E_i[G_i] &= G + b_{Gi} \\ E_i[B_i] &= B + b_{Bi} \end{aligned}$$

where E_i denotes the operation of averaging (taking the expected value) over the hypothetical set of repeated observations by the ith observer.

The "within" variance for the ith observer (for the red primary, say) is the average squared deviation of R_i from $E_i[R_i]$,

$$V_i(R_i) = E_i[R_i - E_i[R_i]]^2 = E_i[\epsilon^2_{Ri}].$$

If all observers have the same "within" variance, then this common variance is denoted by ${}_w\sigma^2_R$; when it is desired to specify the dependence of this variance on the wavelength of the spectrum color being matched, the subscript λ is restored and the within variance is denoted by ${}_w\sigma^2_{R\lambda}$.

Now, referring again to eq(2), the average or expected value of R_i over the whole population of observers is R; $E[R_i]=R$, where E (without subscript i) denotes the operation of averaging over the population of observers. Therefore, it follows that $E[b_{Ri}]=0$.

The "between" variance, in the population of observers, is the average squared deviation of the ith observer's average $(R+b_{Ri})$ from the population average R,

$${}_b\sigma^2_R = E[b^2_{Ri}].$$

It is assumed that the error ϵ_{Ri} is statistically independent of the observer bias b_{Ri}. Thus, the total variance σ^2_R of the observed value R_i for one observation by one observer is the sum of the within and between variances, and similarly for the green and blue primaries:

$$\begin{aligned} \sigma^2_R &= {}_b\sigma^2_R + {}_w\sigma^2_R \\ \sigma^2_G &= {}_b\sigma^2_G + {}_w\sigma^2_G \\ \sigma^2_B &= {}_b\sigma^2_B + {}_w\sigma^2_B. \end{aligned} \tag{3}$$

Although it is perhaps reasonable to assume that an observer's "errors" are not correlated with his "biases", the analyses of empirical data below will show that it cannot be assumed that the three observations R_i, G_i, B_i for the ith observer are independent. Accordingly, it is necessary to know the covariances. The "between" covariances are:

$$E[b_{Ri}b_{Gi}],\ E[b_{Ri}b_{Bi}],\ E[b_{Gi}b_{Bi}].$$

The "within" covariances are:

$$C_i(R_i,G_i) = E_i[(R_i - E_i[R_i])(G_i - E_i[G_i])] = E_i[\epsilon_{Ri}\epsilon_{Gi}].$$

When we assume that the within covariances are equal for all observers, we may then write the total covariances as:

$$\begin{aligned} C(R,G) &= {}_b\sigma_{RG} + {}_w\sigma_{RG}, \\ C(R,B) &= {}_b\sigma_{RB} + {}_w\sigma_{RB}, \\ C(G,B) &= {}_b\sigma_{GB} + {}_w\sigma_{GB}, \end{aligned} \tag{4}$$

where, for example,

$${}_b\sigma_{RG} = E[b_{Ri}b_{Gi}]$$

and

$${}_w\sigma_{RG} = E_i[\epsilon_{Ri}\epsilon_{Gi}].$$

No attempt will be made in this paper to estimate the within and between covariances separately; estimates are given for the total correlations such as ρ_{RG}, defined by eqs (3), (4), and

$$C(R,G) = \rho_{RG}\sigma_R\sigma_G \tag{5}$$

The total variances and covariances are estimated in the usual way. For example, the estimate for σ_R^2 is

$$\hat{\sigma}_R^2 = \sum_{i=1}^{n} (R_i - \bar{R})^2/(n-1)$$

where n is the number of observers and $\bar{R}$ is the average of the R_i for the n observers.

3. Rigorous Transformation to a System Analogous to CIE

Spectral tristimulus values, $\bar{r}$, $\bar{g}$, $\bar{b}$, have been derived from measured color-matching data of the primaries, wavelengths 645.2, 526.3, and 444.4 mμ. An empirically-based system of spectral tristimulus values, $\bar{x}$, $\bar{y}$, $\bar{z}$, analogous to the present CIE system, may be derived from these tristimulus values, $\bar{r}$, $\bar{g}$, $\bar{b}$, by means of the eqs (6) below. If we wish to locate the chromaticity coordinates of the equal-energy point (x_n, y_n, z_n) at the point (1/3, 1/3, 1/3) we must set a restriction that $\Sigma\bar{x}_\lambda = \Sigma\bar{y}_\lambda = \Sigma\bar{z}_\lambda$. This is the purpose of the adjustment factors, f_x, f_y, and f_z, respectively.

$$\begin{aligned}
\bar{x}_\lambda &= f_x(k_1\bar{r}_\lambda + k_2\bar{g}_\lambda + k_3 b_\lambda) = f_x\bar{x}'_\lambda \\
\bar{y}_\lambda &= f_y(k_4\bar{r}_\lambda + k_5\bar{g}_\lambda + k_6\bar{b}_\lambda) = f_y\bar{y}'_\lambda \\
\bar{z}_\lambda &= f_z(k_7\bar{r}_\lambda + k_8\bar{g}_\lambda + k_9\bar{b}_\lambda) = f_z\bar{z}'_\lambda.
\end{aligned} \tag{6}$$

We may impose two additional restrictions on the system:

1. That the tristimulus values be not less than zero.

2. That no one of the functions, $\bar{x}$, $\bar{y}$, $\bar{z}$, be equivalent to a linear combination of the other two. This restriction is established if the determinant of coefficients k_i does not vanish, that is,

$$\begin{vmatrix} k_1 & k_2 & k_3 \\ k_4 & k_5 & k_6 \\ k_7 & k_8 & k_9 \end{vmatrix} \neq 0. \tag{6a}$$

If all the luminosity, V_λ, is placed in the $\bar{y}_\lambda$ primary, and if f_y is set equal to 1, then k_4, k_5, and k_6 are determined by

$$V_\lambda = \bar{y}'_\lambda = L_r\bar{r}_\lambda + L_g\bar{g}_\lambda + L_b\bar{b}_\lambda = k_4\bar{r}_\lambda + k_5\bar{g}_\lambda + k_6\bar{b}_\lambda \tag{7}$$

thereby making $k_4 = L_r$, $k_5 = L_g$, and $k_6 = L_b$. The symbols L_r, L_g, and L_b are the luminous units of the $\bar{r}\ \bar{g}\ \bar{b}$ system.

The solutions for the k_i's in the $\bar{x}$ and $\bar{z}$ spectral tristimulus functions are not obtained as directly as those for the k_i's in the $\bar{y}$ function. Equations (8) to (8e) below show how a solution of the k_i's in the $\bar{x}$ function may be obtained.

The $\bar{x}'$ equation (eq 8) contains three k_i's to be determined. A unique solution for k_1, k_2, and k_3 requires three simultaneous equations. By assigning, tentatively, a value of unity to k_1 (eq 8a), no loss of generality is encountered that cannot be accounted for by the adjustment factor, f_x, in eq (6).

$$\bar{x}'_\lambda = k_1\bar{r}_\lambda + k_2\bar{g}_\lambda + k_3\bar{b}_\lambda \tag{8}$$

$$\bar{x}'_\lambda = \bar{r}_\lambda + k_2\bar{g}_\lambda + k_3\bar{b}_\lambda. \tag{8a}$$

When this is done, only two simultaneous equations are required to solve for the remaining two constants. The equations are set up by selecting, at two wavelengths (λ_1 and λ_2), numerical values for say, $\bar{x}_1$ and $\bar{x}_2$, that will satisfy the requirement that all the tristimulus values be positive. Equation (8a) then becomes

$$\bar{x}'_1 = r_1 + k_2\bar{g}_1 + k_3\bar{b}_1 \tag{8b}$$

$$\bar{x}'_2 = \bar{r}_2 + k_2\bar{g}_2 + k_3\bar{b}_2 \tag{8c}$$

and the solutions for k_2 and k_3 are given by:

$$k_2 = [(\bar{x}'_1 - \bar{r}_1)\bar{b}_2 - (\bar{x}'_2 - \bar{r}_2)\bar{b}_1]/(\bar{g}_1\bar{b}_2 - \bar{g}_2\bar{b}_1) \tag{8d}$$

$$k_3 = [(\bar{x}'_2 - \bar{r}_2)\bar{g}_1 - (\bar{x}'_1 - \bar{r}_1)\bar{g}_2]/(\bar{g}_1\bar{b}_2 - \bar{g}_2\bar{b}_1). \tag{8e}$$

The constants k_i of the $\bar{z}$ function are solved in a similar manner as shown by eqs (9) to (9e):

$$\bar{z}'_\lambda = k_7\bar{r}_\lambda + k_8\bar{g}_\lambda + k_9\bar{b}_\lambda \tag{9}$$

$$\bar{z}'_\lambda = k_7\bar{r}_\lambda + k_8\bar{g}_\lambda + \bar{b}_\lambda \tag{9a}$$

$$\bar{z}'_3 = k_7\bar{r}_3 + k_8\bar{g}_3 + \bar{b}_3 \tag{9b}$$

$$\bar{z}'_4 = k_7\bar{r}_4 + k_8\bar{g}_4 + \bar{b}_4 \tag{9c}$$

$$k_7 = [(\bar{z}'_3 - \bar{b}_3)\bar{g}_4 - (\bar{z}'_4 - \bar{b}_4)\bar{g}_3]/(\bar{r}_3\bar{g}_4 - \bar{r}_4\bar{g}_3) \tag{9d}$$

$$k_8 = [(\bar{z}'_4 - \bar{b}_4)\bar{r}_3 - (\bar{z}'_3 - \bar{b}_3)\bar{r}_4]/(\bar{r}_3\bar{g}_4 - \bar{r}_4\bar{g}_3). \tag{9e}$$

4. Variances and Covariances in a Rigorous Transformation

In general, variances and covariances based on propagation of error theory are:

$$\sigma_U^2 = \sum_{n=1}^{k}\left(\frac{\partial U}{\partial v_n}\right)^2 \sigma_{v_n}^2 + \sum_{m\neq n}\left(\frac{\partial U}{\partial v_n}\right)\left(\frac{\partial U}{\partial v_m}\right)\sigma_{v_m v_n} \tag{10}$$

$$\sigma_{UV} = \sum_{n=1}^{k}\left(\frac{\partial U}{\partial v_n}\right)\left(\frac{\partial V}{\partial v_n}\right)\sigma_{v_n}^2 + \sum_{m\neq n}\left(\frac{\partial U}{\partial v_m}\right)\left(\frac{\partial V}{\partial v_n}\right)\sigma_{v_m v_n} \tag{11}$$

where U and V are functions of $(v_1, \ldots, v_k)$, and the partial derivatives are understood to be evaluated at the average values of these variables. The variances of $v_1, \ldots, v_k$ are $\sigma_{v_1}^2, \ldots, \sigma_{v_k}^2$ and $\sigma_{v_m v_n}$ denotes the covariance of v_n, v_m.

As $\bar{x}$ is a function of 9 variables ($\bar{r}$, $\bar{g}$, $\bar{b}$, $\bar{r}_1$, $\bar{g}_1$, $\bar{b}_1$, $\bar{r}_2$, $\bar{g}_2$, $\bar{b}_2$), $\bar{y}$ is a function of 6 variables ($\bar{r}$, $\bar{g}$, $\bar{b}$, L_r, L_g, L_b), and $\bar{z}$ is a function of 9 variables ($\bar{r}$, $\bar{g}$, $\bar{b}$, $\bar{r}_3$, $\bar{g}_3$,

$\bar{b}_3$, $\bar{r}_4$, $\bar{g}_4$, $\bar{b}_4$), the numbers of terms required by our problem can be counted readily. The numbers of terms in the variance equations are shown in table 1, and the numbers of terms in the covariance equations are shown in table 2.

TABLE 1. *Number of terms in the variance equations*

Variables	Variance terms	Covariance terms	Total
6	6	15	21
9	9	36	45

TABLE 2. *Number of terms in the covariance equations*

Variables		Terms
n	m	
9	6	54
9	9	81

Thus, for every wavelength there are required in a rigorous transformation from $\bar{r}\bar{g}\bar{b}$ to $\bar{x}\bar{y}\bar{z}$, 45+21+45=11 terms for the variances and 54+81+54=189 terms for the covariances, or a total of 300 terms for each wavelength. If the computation of the variances and covariances is performed at every 1 mμ step, as the $\bar{x}$, $\bar{y}$, $\bar{z}$ functions have been derived by Judd [6], from 360 to 830 mμ or at 471 wavelengths, some 141,300 terms would need to be computed.

Observe further that eqs (10) and (11) would include covariances between observations belonging to different spectral colors. That is, the possible correlation between (for example) $\bar{g}_3$ and $\bar{g}_4$ would be included in eq (10) and between $\bar{b}_1$ and $\bar{b}_3$ in eq (11).

5. Variances and Covariances in an Arbitrary Transformation

The foregoing procedure is completely general and rigorous for the conditions where empirical data are asked to indicate the choice of transformation constants, k_i, for a transformation to a system analogous to the present CIE system. Where one wishes to make an arbitrary choice of transformation constants he indicates that the constants are without error or correlation with other variables.

In an arbitrary transformation the variances and covariances involving k_i are chosen equal to zero thus:

$$V(k_i)=C(k_i,\,k_j)=C(k_i,\,v_i)=0 \tag{12}$$

where v_i denotes any of the variables, $\bar{r}$, $\bar{g}$, $\bar{b}$, L, with various subscripts. Thus in the transformation,

$$\left.\begin{aligned}\bar{x}_\lambda&=k_1\bar{r}_\lambda+k_2\bar{g}_\lambda+k_3\bar{b}_\lambda\\ \bar{y}_\lambda&=k_4\bar{r}_\lambda+k_5\bar{g}_\lambda+k_6\bar{b}_\lambda\\ \bar{z}_\lambda&=k_7\bar{r}_\lambda+k_8\bar{g}_\lambda+k_9\bar{b}_\lambda\end{aligned}\right\} \tag{13}$$

the variance equations are:

$$\left.\begin{aligned}V(\bar{x})&=k_1^2V(\bar{r})+k_2^2V(\bar{g})+k_3^2V(\bar{b})\\&\quad+2[k_1k_2C(\bar{r},\bar{g})+k_1k_3C(\bar{r},\bar{b})+k_2k_3C(\bar{g},\bar{b})]\\ V(\bar{y})&=k_4^2V(\bar{r})+k_5^2V(\bar{g})+k_6^2V(\bar{b})\\&\quad+2[k_4k_5C(\bar{r},\bar{g})+k_4k_6C(\bar{r},\bar{b})+k_5k_6C(\bar{g},\bar{b})]\\ V(z)&=k_7^2V(\bar{r})+k_8^2V(g)+k_9^2V(\bar{b})\\&\quad+2[k_7k_8C(\bar{r},\bar{g})+k_7k_9C(\bar{r},\bar{b})+k_8k_9C(\bar{g},\bar{b})]\end{aligned}\right\}, \tag{14}$$

$$\left.\begin{aligned}C(\bar{x},\bar{y})&=k_1k_4V(\bar{r})+k_2k_5V(\bar{g})+k_3k_6V(\bar{b})+(k_1k_5+k_2k_4)C(\bar{r},\bar{g})+(k_1k_6+k_3k_4)C(\bar{r},\bar{b})+(k_2k_6+k_3k_5)C(\bar{g},\bar{b})\\ C(\bar{x},\bar{z})&=k_1k_7V(\bar{r})+k_2k_8V(\bar{g})+k_3k_9V(\bar{b})+(k_1k_8+k_2k_7)C(\bar{r},\bar{g})+(k_1k_9+k_3k_7)C(\bar{r},\bar{b})+(k_2k_9+k_3k_8)C(\bar{g},\bar{b})\\ C(\bar{y},\bar{z})&=k_4k_7V(\bar{r})+k_5k_8V(\bar{g})+k_6k_9V(\bar{b})+(k_4k_8+k_5k_7)C(\bar{r},\bar{g})+(k_4k_9+k_6k_7)C(\bar{r},\bar{b})+(k_5k_9+k_6k_8)C(\bar{g},\bar{b})\end{aligned}\right\}. \tag{15}$$

To estimate these variances and covariances from the data obtained in color-matching by n observers, the following formulas are used:

$$\left.\begin{aligned}\hat{V}(\bar{r})&=\sum_{i=1}^{n}(\bar{r}_i-\hat{\mu}_r)^2/(n-1)=\hat{\sigma}_r^2\\ \hat{V}(\bar{g})&=\sum_{i=1}^{n}(\bar{g}_i-\hat{\mu}_g)^2/(n-1)=\hat{\sigma}_g^2\\ \hat{V}(\bar{b})&=\sum_{i=1}^{n}(\bar{b}_i-\hat{\mu}_b)^2/(n-1)=\hat{\sigma}_b^2\end{aligned}\right\} \tag{16}$$

$$\left.\begin{aligned}\hat{C}(\bar{r},\bar{g})&=\sum_{i=1}^{n}(\bar{r}_i-\hat{\mu}_r)(\bar{g}_i-\hat{\mu}_g)/(n-1)=\hat{\sigma}_{rg}\\ \hat{C}(\bar{r},\bar{b})&=\sum_{i=1}^{n}(\bar{r}_i-\hat{\mu}_r)(\bar{b}_i-\hat{\mu}_b)/(n-1)=\hat{\sigma}_{rb}\\ \hat{C}(\bar{g},\bar{b})&=\sum_{i=1}^{n}(\bar{g}_i-\hat{\mu}_g)(\bar{b}_i-\hat{\mu}_b)/(n-1)=\hat{\sigma}_{gb}\end{aligned}\right\} \tag{17}$$

and

$$\hat{\mu}_r=\sum_{i=1}^{n}\bar{r}_i/n,\quad \hat{\mu}_g=\sum_{i=1}^{n}\bar{g}_i/n,\quad \hat{\mu}_b=\sum_{i=1}^{n}\bar{b}_i/n.$$

The transformation equations derived by Kelly and Judd [6] and being considered for recommendation by the CIE for a 10°-field standard observer system for colorimetry are:

$$\left.\begin{aligned}\bar{x}_{10}&=0.341080\,\bar{r}_{10}+0.189145\,\bar{g}_{10}+0.387529\,\bar{b}_{10}\\ \bar{y}_{10}&=0.139058\,\bar{r}_{10}+0.837460\,\bar{g}_{10}+0.073316\,\bar{b}_{10}\\ \bar{z}_{10}&=0.000000\,\bar{r}_{10}+0.039553\,\bar{g}_{10}+2.026200\,\bar{b}_{10}\end{aligned}\right\}. \quad (18)$$

As the constants, k_i, of these equations were derived in a very complex way, the transformation will be treated as an arbitrary one.

6. Variability of Color-Mixture Data

The results of a statistical analysis of the Stiles-Burch color-matching data may be useful in determining the variances and covariances for the transformation to the proposed new CIE standard observer system. The Stiles-Burch data were analyzed because in the development of the new system they are being given greater weight than those of other investigators and because they are available in terms of individual observer data. Such an analysis was reported by Nimeroff, Rosenblatt, and Dannemiller [7] at the October 1959 meeting of the Optical Society of America and the results are given below.

The Stiles-Burch data were obtained under two experimental conditions. For condition I, 24 observers were used, while for condition II, 29 observers were employed. These two conditions differ in that the blue instrumental primary of condition I was located at 445.4 mμ (22,450 cm^{-1}) while that of condition II was located at 470.6 mμ (21,250 cm^{-1}). The data taken under these two conditions were transformed by Stiles-and Burch to an $\bar{r}\bar{g}\bar{b}$ system system in which the blue primary is located at 444.4 mμ. To test whether these two sets of transformed data are significantly different from each other the Hotelling T^2 test [8] was used. The T^2 test provides a comparison between the two sets of averages $\bar{p}_1$, representing $\bar{r}_1$, $\bar{g}_1$, $\bar{b}_1$, of condition I and $\bar{p}_2$, representing $\bar{r}_2$, $\bar{g}_2$, $\bar{b}_2$, of condition II in which the three correlated differences between corresponding averages are evaluated simultaneously against the variability present in the data from which the averages were estimated. In this test a high value of T^2 implies that the differences between the averages compared are large. The T^2 statistic in quadratic form for our problem of three variables in each of two conditions for N_1 and N_2 observers is:

$$T^2=\frac{N_1N_2}{N_1+N_2}\sum_{i,j=1}^{3}S^{ij}(\bar{p}_{1i}-\bar{p}_{2i})(\bar{p}_{1j}-\bar{p}_{2j}), \quad (19)$$

where S^{ij} is the (i,j) element of the inverse of the three by three matrix with elements

$$S_{ij}=\frac{1}{N_1+N_2-2}\left[\sum_{k=1}^{N_1}(\bar{p}_{1ik}-\bar{p}_{1i})(\bar{p}_{1jk}-\bar{p}_{1j})+\sum_{k=1}^{N_2}(\bar{p}_{2ik}-\bar{p}_{2i})(\bar{p}_{2jk}-\bar{p}_{2j})\right] \quad (20)$$

The subscripts 1 and 2 refer to the two conditions, i and j refer to the three primaries compared two at a time, and k identifies the observer for each condition.

The results of this test are plotted on figure 1 and indicate that the data obtained by Stiles under the two experimental conditions are in general statistically different even at the 2.5 percent level of significance, the exceptions lying between 470 and 580mμ. The difference may result from either an improper evaluation of the transformations of the two sets of data to a common primary system or an inherent dependence on the choice of instrumental primary. This latter supposition, if true, would invalidate any attempt to make the data obtained under the two sets of conditions comparable through such transformation. The differences between conditions I and II, while statistically significant, are in practical terms small.

In spite of these differences the CIE is proceeding to average these data as well as those of Speranskaya for 27 observers, to derive the 10°-field tristimulus functions, $\bar{x}\bar{y}\bar{z}$. Figure 2 shows the averaged $\bar{r}$ function with its three lobes, two positive and one negative. Also shown are the estimates of between-observer standard deviations for the $\bar{r}$ function, based on the Stiles-Burch combined data and the Speranskaya data. Note that the standard deviations of these independent investigations are essentially of the same order of magnitude and range approximately from 10 to 20 percent of the mean function.

Strictly, the estimates shown in figure 2 (likewise figs. 3, 4) are estimates of the total standard deviation (see eq (3)). As the within-observer variances are relatively small, the estimated between-observer variances are only slightly over-stated. A satisfactory estimate of between-observer variance alone can be made only when the data include repeated observations by many (if not all) observers.

The lower curve gives the estimated within-observer standard deviations for the $\bar{r}$ function.

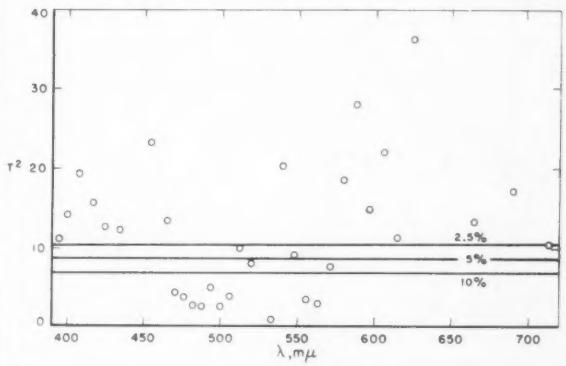

FIGURE 1. *Values of the* T^2 *statistic for evaluating differences between Stiles' data obtained under condition I and under condition II.*

Critical values of T^2 at three probability levels are indicated, showing that even at the 2.5% level the results obtained under the two conditions are for the most part significantly different.

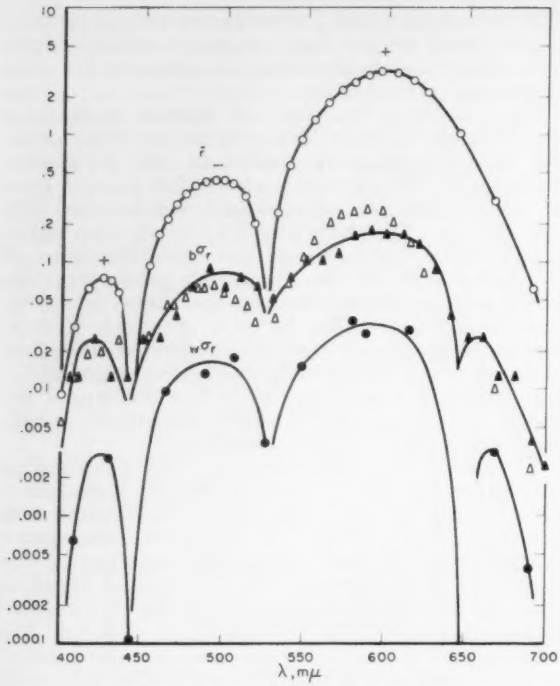

FIGURE 2. *Means and variability of the red-primary data.* Means, ○; standard deviations between observers ($_b\sigma_r$): Stiles Δ, Speranskaya ▲; standard deviations within observer ($_w\sigma_r$).

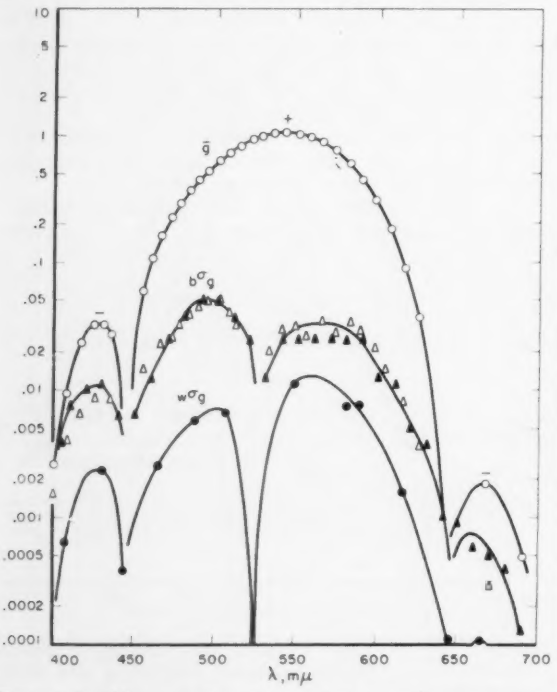

FIGURE 3. *Means and varibility of the green-primary data.* Means ○; standard deviations between observers ($_b\sigma_g$): Stiles Δ, Speranskaya ▲; standard deviations within observer ($_w\sigma_g$).

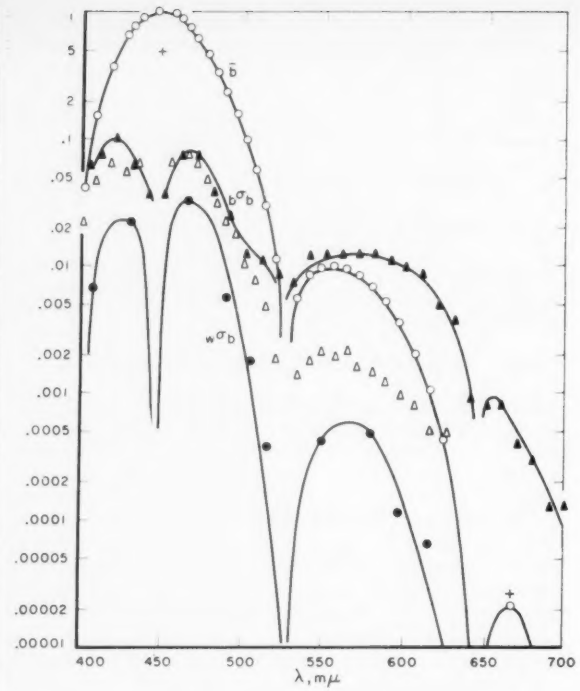

FIGURE 4. *Means and variability of the blue-primary data.* Means ○; standard deviation between observers ($_b\sigma_b$): Stiles Δ, Speranskaya ▲; standard deviation within observer ($_w\sigma_b$).

These data are based on the average of individual variability of two observers, one repeating his measurements four times and the other repeating his measurements five times. As might be expected, the within-observer standard deviations are approximately an order of magnitude lower than the between-observer standard deviations. Note that because settings in matches of the primaries themselves are assumed to be free from error the curves for the standard deviations are extended so as to approach zero at the location of the $\bar{r}\,\bar{g}\,\bar{b}$ primaries, that is at wavelengths 444.4, 526.3, and 645.2 mμ.

Figure 3 shows the same kind of information for the $\bar{g}$ function with its three lobes, two negative and one positive. Here also there is the same agreement between the Stiles-Burch data and the Speranskaya data; the within standard deviations are about an order of magnitude lower than the between standard deviations. The standard deviations approach zero at the location of the primaries.

Figure 4 shows the data for the $\bar{b}$ function. Here there is a disparity between the Stiles-Burch and the Speranskaya data in the longwave region. This disparity may result from the transformation from the instrumental primaries used in the Speranskaya investigation to those of the $\bar{r}\,\bar{g}\,\bar{b}$ system. It is more likely, however, that the procedure used by Stiles, that of employing for longwave matches a yellow

primary at 588.2 rather than a green instrumental primary, is responsible for the lower variability of the $\bar{b}$ function in this region.

On figure 5 are shown averages of the between standard deviations derived from the data of the 53 Stiles-Burch observers and the data of the 27 Speranskaya observers. In the longwave (640 mμ and beyond) region of the $\bar{b}$ function the averages are based on the same weights used by Judd in deriving the mean $\bar{b}$ function itself from the British and Russian data. The weights for the British data are greater than those for the Russian data and increase with wavelength.

It was noted above that the within standard deviations are about an order of magnitude lower than the between standard deviations. We are interested in learning whether the ratio of between to within standard deviations for the three functions can be represented by a single constant independent of wavelength and, if so, in determining the magnitude of such a constant. The computation of within-observer variability in a transformation to an $\bar{x}\bar{y}\bar{z}$ system would be simplified were this permissible. Figure 6 shows these ratios for the three color-mixture functions. The overall average ratio was derived from the geometric mean and is 5.7 in the spectral region 400 to 700 mμ. The geometric mean was used because of the wide disparity between the extreme values, namely 2.0 and 30.9. We consider this value reasonably representative of the ratio of between to within standard deviations, as better than 80 percent of the ratios lie between half and twice 5.7.

In the transformations from color-mixture functions, $\bar{r}\bar{g}\bar{b}$, to tristimulus values, $\bar{x}\bar{y}\bar{z}$, covariances as well as variances need to be known. The correlation coefficient, ρ_{ij}, relates the covariance, σ_{ij}, to the variances, σ_i^2, σ_j^2, thus:

$$\rho_{ij} = \sigma_{ij}/\sigma_i\,\sigma_j.$$

On figure 7 are plotted the correlation coefficients, $\rho_{\bar{r}\bar{g}}$, $\rho_{\bar{r}\bar{b}}$, and $\rho_{\bar{g}\bar{b}}$. In these data, a positive correlation coefficient implies that if an observer uses more or less than average of one instrumental primary in making a match he uses more or less, respectively, than average of the other primary, also. Conversely, a negative correlation coefficient implies that if more or less than average of one primary is used, less or more, respectively, than average of the other primary is used. We note that $\rho_{\bar{r}\bar{b}}$ is always positive or zero, while $\rho_{\bar{r}\bar{g}}$ is almost always negative or zero. On the other hand, $\rho_{\bar{g}\bar{b}}$ is negative in the shortwave spectral region, 380 to 590 mμ, and positive in the longwave region, 600 to 720 mμ.

Approximately two-thirds of the correlation coefficients are significantly different from zero at the 5 percent level of significance. The general consistency of sign and magnitude among values of the correlation coefficients at adjacent wavelengths provides further confirmation for the general pattern of values shown. Although some of the correlation coefficients are small in magnitude they should not be neglected in determining the variances and covariances in the $\bar{x}\bar{y}\bar{z}$ system transformed from the color-mixture data.

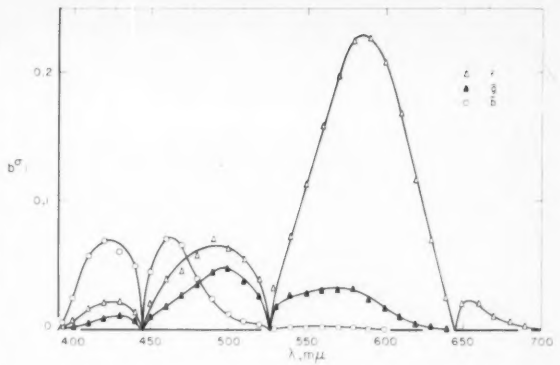

FIGURE 5. *Mean standard deviation between observers for the Stiles-Burch and the Speranskaya data.*

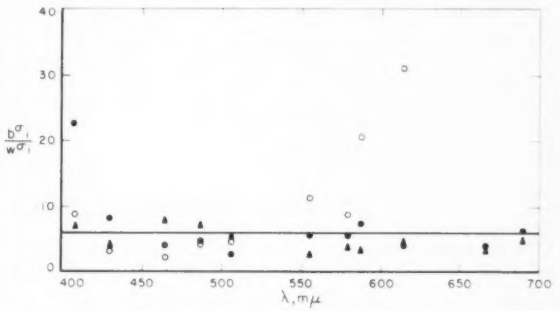

FIGURE 6. *Ratio of the between to within standard deviations, for the three primaries,* $\bar{r}$ (●), $\bar{g}$(▲), *and* $\bar{b}$(○), *showing overall average ratio at 5.7.*

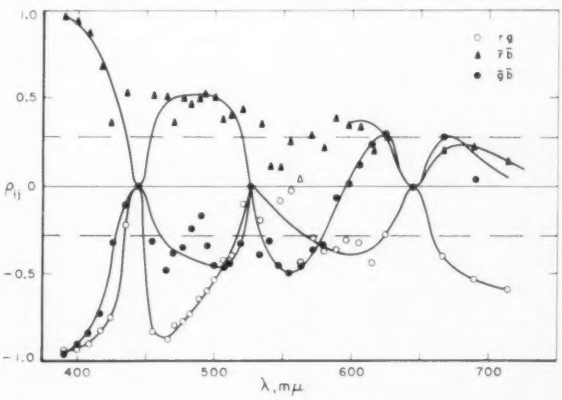

FIGURE 7. *Correlation coefficients,* ρ_{ij}, *for* ij *equal to* $\bar{r}\,\bar{g}$ (○), $\bar{r}\,\bar{b}$ (▲), $\bar{g}\,\bar{b}$ (●).

Dashed lines define the region within which these coefficients are not (statistically) significantly different from zero at the 5% level.

A few qualifications to the interpretation of the statistical analyses should be mentioned. First, statements concerning "statistical significance" are based on the assumption that the observations are normally distributed.

There has been reported, however, by Judd [9] for 7 observers and by Wyszecki [10] for 10 observers, some evidence that the population of observers with normal color vision may be bimodally distributed. A limited analysis of the Stiles-Burch data for the 53 observers was undertaken to see if bimodality is revealed in their individual observer data. This analysis showed (see for example fig. 8 for R_{500} against G_{500}) that although the distribution may be slightly skewed, there is insufficient data to conclude the existence of any bimodality. If more extensive data should lead to a reliable statement that the distribution of the population is bimodal, two standard observer systems might be required, one for each group.

A second qualification is required since possible correlations among observations for different spectral colors have been ignored because of the arbitrary choice of constants in the transformation. For example, the presence of correlation could account in part for the apparently consistent difference between conditions I and II, as shown in figure 1.

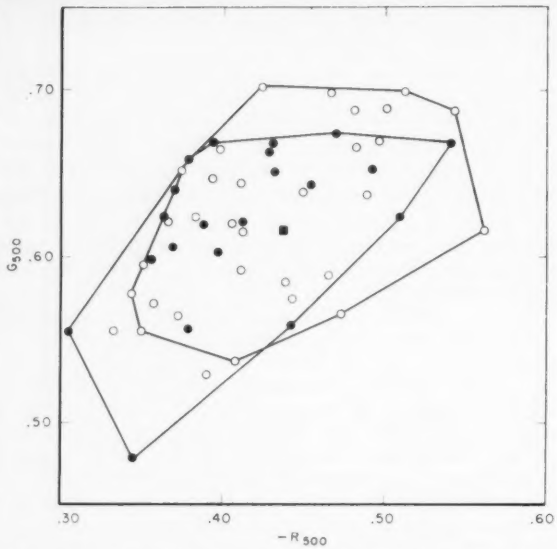

FIGURE 8. *Plot of* R_{500} *against* G_{500} *for Stiles' individual observers indicating no bimodality and very little skewness.*
Condition I (●), condition II (○), and mean (■). Straight lines join outlying values obtained under the two conditions.

7. Complete Standard Observer System

A complete standard observer system should contain not only the mean spectral tristimulus functions, $\bar{x}_\lambda$, $\bar{y}_\lambda$, $\bar{z}_\lambda$, derived from the color mixture data, but should contain, also, the variances and covariances of these functions as derived from the within- and between-observer variability of the color mixture data.

Table 3 lists, for every 10 mμ, the spectral tristimulus values of the proposed standard observer system for colorimetry and the estimated total vari-

TABLE 3. *Proposed CIE tristimulus functions for 10°-field and between variances and covariances in* $\bar{x},\bar{y},\bar{z}$

λ(mμ)	$\bar{x}_{10}$	$\bar{y}_{10}$	$\bar{z}_{10}$	$V(\bar{x})$	$V(\bar{y})$	$V(\bar{z})$	$C(\bar{x},\bar{y})$	$C(\bar{x},\bar{z})$	$C(\bar{y},\bar{z})$
400	0.0191097	0.0020044	0.0860109	0.000126	0.00000118	0.00256	+0.0000104	+0.000568	+0.0000467
10	.084736	.008756	.389366	.000661	.0000110	.0132	+.0000708	+.00294	+.000321
20	.204492	.021391	.972542	.000937	.0000262	.0193	+.0000731	+.00421	+.000350
30	.314679	.038676	1.55348	.000737	.0000671	.0154	+.000106	+.00329	+.000509
40	.383734	.062077	1.96728	.000385	.0000448	.00978	+.0000816	+.00189	+.000355
450	.370702	.089456	1.99480	.000353	.0000561	.00815	+.0000413	+.00161	+.000185
60	.302273	.128201	1.74537	.00109	.0000995	.0206	−.0000151	+.00454	+.000136
70	.195618	.185190	1.31756	.00110	.000272	.0180	−.000101	+.00423	−.000131
80	.080507	.253589	0.772125	.000716	.000602	.00606	−.000108	+.00182	−.00000827
90	.016172	.339133	.415254	.000675	.00105	.00234	−.0000633	+.000973	+.0000759
500	.003816	.460777	.218502	.000414	.00129	.000593	+.000000553	+.000279	−.000245
10	.037465	.606741	.112044	.000325	.000829	.000190	+.0000884	+.000112	−.0000999
20	.117749	.761757	.060709	.000183	.000457	.0000549	+.000109	+.0000325	−.0000185
30	.236491	.875211	.030451	.000143	.000253	.0000271	+.000100	+.00000547	−.00000204
40	.376772	.961988	.013676	.000622	.000590	.0000431	+.000301	+.0000133	−.0000285
550	.529826	.991761	.003988	.00143	.000668	.000105	+.000528	+.0000531	−.0000700
60	.705224	.997340	.000000	.00283	.000847	.000100	+.000960	+.000102	−.0000513
70	.878655	.955552		.00437	.000998	.0000942	+.00142	+.000147	−.0000107
80	1.01416	.868934		.00569	.00113	.0000778	+.00181	+.000184	+.0000381
90	1.11852	.777405		.00588	.000947	.0000652	+.00194	+.000194	+.0000806
600	1.12399	.658341		.00493	.000731	.0000379	+.00170	+.000148	+.0000720
10	1.03048	.527963		.00324	.000475	.0000248	+.00116	+.000102	+.0000518
20	0.856297	.398057		.00159	.000240	.0000123	+.000601	+.0000449	+.0000222
30	.647467	.283493		.000575	.0000918	.00000587	+.000226	+.0000120	+.00000591
40	.431567	.179828		.0000750	.0000127	.000000280	+.0000305	+.000000138	+.000000067
650	.268329	.107633		.0000470	.00000794	.000000050	+.0000191	+.000000052	+.000000032
60	.152568	.060281		.0000458	.00000713	.000000043	+.0000179	+.000000166	+.000000091
70	.0812606	.0318004		.0000129	.00000192	.000000016	+.00000492	+.000000084	+.000000044
80	.0408508	.0159051		.00000427	.000000619	.0000000017	+.00000161	+.000000013	+.0000000077
90	.0199413	.0077488		.000000894	.000000128	.00000000043	+.000000335	+.0000000030	+.0000000016
700	.00957688	.00371774		.000000366	.000000052	.00000000016	+.000000137	+.00000000088	+.00000000049
10	.00455263	.00176847		.000000114	.000000016	.000000000039	+.000000042	+.00000000012	+.000000000086
20	.00217496	.00084619		.000000019	.0000000026	.0000000000043	+.0000000069	+.0000000000027	+.0000000000051

ances, $V(\bar{x})$, $V(\bar{y})$, $V(\bar{z})$, and covariances, $C(\bar{x},\bar{y})$, $C(\bar{x},\bar{z})$, $C(\bar{y},\bar{z})$, for these spectral tristimulus values derived on the basis of an arbitrary transformation. It should be noted that the variances in table 3 are $(5.7)^2$ or 32.5 times those in table 4.

TABLE 4. *Within variances in* $\bar{x}$, $\bar{y}$, $\bar{z}$

λ (mμ)	$v(\bar{x})$	$v(\bar{y})$	$v(\bar{z})$
400	0.00000390	0.0000000364	0.0000788
10	.0002204	.0000003338	.000407
20	.0000288	.0000000806	.000595
30	.0000227	.0000000207	.000475
40	.0000119	.00000138	.000301
450	.0000109	.00000173	.000251
60	.0000337	.00000306	.000635
70	.0000340	.00000837	.000556
80	.0000220	.0000185	.000187
90	.0000208	.0000322	.0000720
500	.0000128	.0000396	.0000183
10	.0000100	.0000255	.00000587
20	.00000562	.0000141	.00000200
30	.00000440	.00000779	.000000834
40	.0000192	.0000182	.00000133
550	.0000441	.0000206	.00000324
60	.0000871	.0000261	.00000309
70	.000135	.0000307	.00000290
80	.000172	.0000347	.00000240
90	.000181	.0000292	.00000201
600	.000152	.0000225	.00000117
10	.0000999	.0000146	.000000764
20	.0000489	.00000740	.000000380
30	.0000177	.00000283	.000000181
40	.00000231	.000000391	.00000000862
650	.00000145	.000000245	.00000000154
60	.00000141	.000000220	.00000000132
70	.000000398	.0000000591	.00000000493
80	.000000131	.0000000191	.000000000524
90	.0000000275	.00000000394	.0000000000132
700	.0000000113	.00000000160	.00000000000493
10	.00000000351	.00000000493	.00000000000120
20	.000000000585	.000000000801	.00000000000132

8. Applications of the Complete System

As the individual observer data, on which the 1931 system is based, have been lost in antiquity, this system can be used only to determine what color matches the standard observer would make. A comprehensive analysis of color-mixture data in terms of means, variances, and covariances permits use of the proposed system to determine, in addition, the region of within and between uncertainties; that is, the extent to which a normal observer tends to make different matches on successive attempts, and the extent to which different normal observers vary one from another.

Some applications of the variances and covariances in the $\bar{x}\,\bar{y}\,\bar{z}$ system have been reported by Nimeroff [3] and by Wyszecki [11]. Further applications are sure to be suggested when a complete standard observer system for colorimetry, consisting of means, variances, and covariances, is established.

The authors are pleased to acknowledge the encouragement, advice, and assistance afforded by the following persons: D. L. MacAdam for his encouragement, N. C. Severo for discussions of the statistical model which describes the experimental arrangement for the color-mixture data, W. S. Stiles for so graciously supplying his individual observer data, E. H. Miller for checking of computations, and R. J. Stanekenas for preparing the figures.

9. References

[1] Commission International de l'Éclairage, Proc. Eighth Session, Cambridge, England, 19–29 (September, 1931).
[2] I. Nimeroff, J. Opt. Soc. Am. **43,** 531 (1953).
[3] I. Nimeroff, J. Opt. Soc. Am. **47,** 697 (1957).
[4] W. S. Stiles and J. M. Burch, Optica Acta **6,** 1 (1959).
[5] N. I. Speranskaya, CIE Committee Report, and in part, NPL Symp. 8, Her Majesty's Stationery Office, London **1,** 317 (1958); Optics and Spectroscopy VII, 429 (1959), (OSA Translation).
[6] D. B. Judd, Detailed Report of Progress (Sept. 1957 to Apr. 1959) CIE Working Committee W-1.3.1, Colorimetry.
[7] I. Nimeroff, J. R. Rosenblatt, and M. C. Dannemiller, J. Opt. Soc. Am. **49,** 1137 (1959).
[8] H. Hotelling, Ann. math. stat. **2,** 360 (1931), and J. E. Jackson, J. Opt. Soc. Am. **49,** 585 (1959).
[9] D. B. Judd, J. Research NBS **43,** 277 (1949).
[10] G. Wyszecki, Natl. Research Council of Canada Report APOI–907, June 1959.
[11] G. Wyszecki, J. Opt. Soc. Am. **49,** 389 (1959).

(Paper 65A6–129)

JOURNAL OF RESEARCH of the National Bureau of Standards—A. Physics and Chemistry
Vol. 65A, No. 6, November–December 1961

Extension of the Flory-Rehner Theory of Swelling to an Anisotropic Polymer System

Stephen D. Bruck

(July 26, 1961)

The Flory-Rehner theory for isotropic swelling of rubber crosslinked in the dry state is extended to an anisotropic system crosslinked in the dry, oriented state. The new parameters introduced into the equation can be readily determined from dimensional changes of the fiber in a suitable solvent using a photomicrographic technique. Unlike other methods, such as the cathetometric and weight methods, this technique enables the attainment of swelling equilibrium usually within 30 minutes. Good agreement is obtained between the equivalents of crosslinks calculated from chemical analyses and from swelling measurements, respectively.

1. Introduction

An important objective in the proper evaluation of network structures is the determination of the swelling [equilibrium volume ratio $q_m=\frac{V}{V_0}$, and the calculation of the average molecular weight between crosslinks ($\overline{M}_c$). There are two classical methods for the determination of the swelling equilibrium volume ratios: (a) the weight method, and (b) the linear method with a cathetometer. Using the weight method one obtains the ratio of the weight of the swollen network at equilibrium to the weight of the unswollen crosslinked polymer, and from a knowledge of the densities of the solvent and polymer, one can calculate $q_m=\frac{V}{V_0}$, (where V= volume of the swollen network at equilibrium and V_0= volume of the unswollen crosslinked network). Using the linear method one measures the length of the fiber at swelling equilibrium (L), and the length of the original fiber in the dry state (L_0). The equilibrium volume swelling ratio, q_m, will then be equal to $\left(\frac{L}{L_0}\right)^3$ if the system is isotropic.

With relatively highly crosslinked networks, especially in case of oriented fibers, neither of the above-mentioned methods is practical. Swelling equilibrium in this case is reached very slowly (up to several weeks) because of surface effects of the fiber. Also, because the system is anisotropic, q_m is no longer equal to $(L/L_0)^3$.

It is the object of this paper to present a modification of the Flory-Rehner theory of swelling and to describe a photomicrographic technique for the rapid determination of swelling equilibrium volume ratios in crosslinked fibers. The Flory-Rehner theory for isotropic swelling of rubber crosslinked in the dry state is extended to an anisotropic system crosslinked in the dry, oriented state. It is shown that good agreement is obtained between the equivalents of crosslinks calculated from chemical analyses and from swelling measurements, respectively.

Modification of the Flory-Rehner Theory of Swelling. Although the Flory-Rehner treatment [1, 2] [1] of the isotropic swelling of rubber crosslinked in the dry state has been found to apply to radiation crosslinked, essentially *isotropic* polyamide films [3], *oriented* (*hence anistropic*) *structures* represent a difficulty. The Flory-Rehner expression for the isotropic swelling of rubber is:

$$-[\ln(1-v_{2m})+v_{2m}+\chi_1 v_{2m}^2]=\frac{V_1}{\bar{v}\overline{M}_c}\left(1-\frac{2\overline{M}_c}{M}\right)\left(v_{2m}^{1/3}-\frac{v_{2m}}{2}\right) \quad (1a)$$

where $v_{2m}=1/q_m$, which is the ratio of the volume of the unswollen network (V_0) to the volume of the swollen network at equilibrium (V); V_1=molar volume of solvent; $\bar{v}$=specific volume of swollen polymer; $\overline{M}_c$=number average molecular weight between crosslinks; M=primary number average molecular weight of polymer (before crosslinking); χ_1=interaction parameter which is a measure of the interaction energy of solvent molecules with polymer.

According to Flory [4] the term $1/v_{2m}=\alpha_s^3$, where α_s is the linear deformation factor; hence the above equation may be rewritten as follows:

$$-[\ln(1-v_{2m})+v_{2m}+\chi_1 v_{2m}^2]=\frac{V_1}{2\bar{v}\overline{M}_c}\left(1-\frac{2\overline{M}_c}{M}\right)\left(\frac{2}{\alpha_s}-\frac{1}{\alpha_s^3}\right) \quad (1b)$$

Since in the case of crosslinked, *anisotropic* fibers swelling does not take place equally in three dimensions, the linear deformation factor, α_s, must be so expressed as to identify the swelling components in the x and y directions. Hence the equilibrium volume swelling ratio for an anisotropic crosslinked fiber (2-dimensional isotropy where $\alpha_x\neq\alpha_y=\alpha_z$) may be expressed as:

$$q_m=\frac{V}{V_0}=\frac{L\times D^2}{L_0\times D_0^2} \quad (2)$$

[1] Figures in brackets indicate the literature references at the end of this paper

where V=volume of swollen structure at equilibrium; V_0=volume of unswollen network; L=length of swollen structure at equilibrium; D=diameter of swollen structure at equilibrium; L_0=length of unswollen structure; D_0=diameter of unswollen structure.

In order to utilize the parameters L, L_0, D, and D_0, additional terms must be introduced into the original Flory-Rehner equation. The modified equation is derived using the equations in the Flory-Rehner treatment, as follows (see also references [1, 2, and 4]):

$$\Delta F=\Delta F_m+\Delta F_{el} \tag{3}$$

where ΔF=total free energy change involved in the mixing of pure solvent with the crosslinked network; ΔF_m=free energy of mixing; ΔF_{el}=elastic free energy.

The free energy change on mixing is:

$$\Delta F_m=\Delta H_m-T\Delta S_m=kT[n_1 \ln v_1+\chi_1 n_1 v_2] \tag{4}$$

where v_1=volume fraction of pure solvent; v_2=volume fraction of polymer; n_1=number of solvent molecules.

Also the elastic free energy is:

$$\Delta F_{el}=\Delta H_{el}-T\Delta S_{el} \tag{5}$$

where ΔS_{el}=change in entropy due to configurational change of the network; ΔH_{el}=change of enthalpy of the network which approximately=0 because (by analogy with the deformation of rubber) the deformation process during swelling is assumed to occur without appreciable change in internal free energy of the network. From the statistical theory of rubber elasticity,

$$\Delta F_{el}=-T\Delta S_{el}=\frac{kT\nu_e}{2}[\alpha_x^2+\alpha_y^2+\alpha_z^2-3-\ln(\alpha_x\alpha_y\alpha_z)] \tag{6}$$

where α_y=linear deformation factor in y direction; α_x=linear deformation factor in x—direction; α_z=linear deformation factor in z direction; and ν_e=effective number of chains in the network.

Since in the case of two-dimensional isotropy, such as in crosslinked fibers, $\alpha_x\neq\alpha_y=\alpha_z$, then, calling $\alpha=\alpha_y=\alpha_z$

$$\Delta F_{el}=-T\Delta S_{el}=\frac{kT\nu_e}{2}[2\alpha^2+\alpha_x^2-3-\ln(\alpha^2\alpha_x)]. \tag{7}$$

The chemical potential of the solvent in the swollen network with two-dimensional isotropy (fibers) is:

$$\mu_1-\mu_1^0=N\left(\frac{\partial\Delta F_m}{\partial n_1}\right)_{T,P}+\frac{N}{2}\left[\left(\frac{\partial(\Delta F_{el})}{\partial(\alpha)}\right)\left(\frac{\partial(\alpha)}{\partial(n_1)}\right)+\left(\frac{\partial(\Delta F_{el})}{\partial(\alpha_x)}\right)\left(\frac{\partial(\alpha_x)}{\partial(n_1)}\right)\right]_{T,P} \tag{8}$$

where N=Avogadro's number. Evaluating the terms in eq (8) and noting that at equilibrium swelling $\mu_1=\mu_1^0$ and $v_2=v_{2m}$ we get:

$$-[\ln(1-v_{2m})+v_{2m}+\chi_1 v_{2m}^2]=\frac{V_1}{2\bar{v}M_c}\left(1-\frac{2M_c}{M}\right)\left(\frac{1}{\alpha_x}-\frac{1}{\alpha^2\alpha_x}+\frac{\alpha_x}{\alpha^2}\right) \tag{9a}$$

or

$$\overline{M}_c=\frac{\frac{V_1}{2\bar{v}}\left(\frac{1}{\alpha_x}-\frac{1}{\alpha^2\alpha_x}+\frac{\alpha_x}{\alpha^2}\right)}{-[\ln(1-v_{2m})+v_{2m}+\chi_1 v_{2m}^2]+\frac{V_1}{\bar{v}\overline{M}}\left(\frac{1}{\alpha_x}-\frac{1}{\alpha^2\alpha_x}+\frac{\alpha_x}{\alpha^2}\right)} \tag{9b}$$

In the above equation, $\alpha_x=\frac{L}{L_0}$ and $\alpha=\frac{D}{D_0}$.

2. Experimental Procedure

Experiments were conducted on a series of 7.8 Tex (60 denier)/32 filament nylon-6 (polycaprolactam) fibers, $\overline{M}_n$ (number average molecular weight)=14,000 (from end-group analyses). Crosslinking was carried out with gaseous formaldehyde on the solid, oriented (drawn) fibers [5]. It can be shown that the total equivalents of amide groups in 10^6 g of nylon-6 polymer is 8,850 (neglecting end-groups), which corresponds to a theoretical maximum of approximately 4,425 equivalents of crosslinkages if all nitrogen atoms (in crystalline and amorphous regions) were substituted. Since nylon-6 fiber is approximately 50 percent crystalline, there would be a maximum of approximately 2,212 equivalents of crosslinkages in the amorphous portions of 10^6 g of polymer.

The values L, L_0, D, and D_0 are obtained from the dimensional changes of small segments (about 0.5 mm) of single filaments in a suitable solvent (such as m-cresol) using a microscope and a micrometer eyepiece or a photomicrographic assembly. A small segment of the yarn is placed on a microscope slide and onto the phase-microscope stage. The specimen is photographed using a Polaroid camera (or measured with a micrometer eyepiece) with a magnification of between 100× to 400× depending on the dimensions of the fiber. From the photographs the values L, L_0, D, and D_0 can then be readily measured.

Swelling measurements were carried out with m-cresol as the swelling agent at 25 ° C. Figure 1 illustrates the relationship between the calculated $\overline{M}_c$ (average molecular weight between crosslinks) and the experimentally determined q_m (equilibrium swelling volume ratio) values. The values for $\overline{M}_c$ were calculated by using eq(9b), above, where χ_1=−0.38 which value was obtained from the literature [3]. Figure 2 shows the equivalent number of crosslinks (−CH_2−) between adjacent amide nitrogen atoms, calculated from chemical analyses and from swelling measurements, respectively, and their relationships to the percent formaldehyde. There is a good agreement between the results obtained from swelling measurements and chemical analyses, at least up to 1,000 equivalents of crosslinks per 10^6 g of polymer (or 3 percent formaldehyde). This is

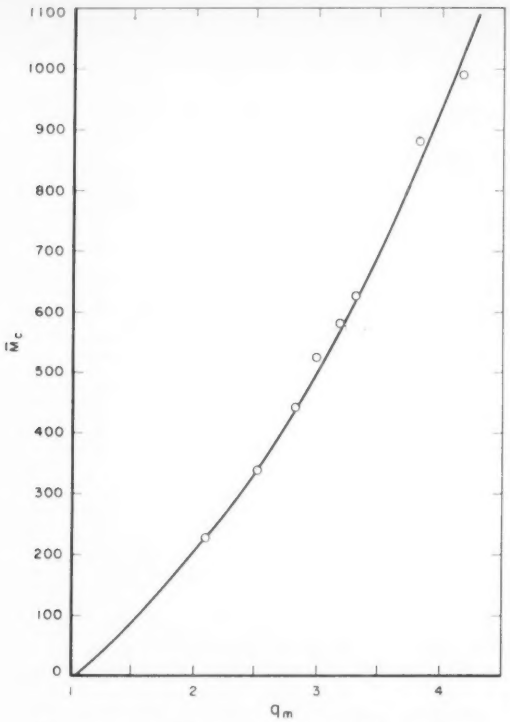

FIGURE 1. *The relationship between* $\overline{M}_c$ *and* q_m.

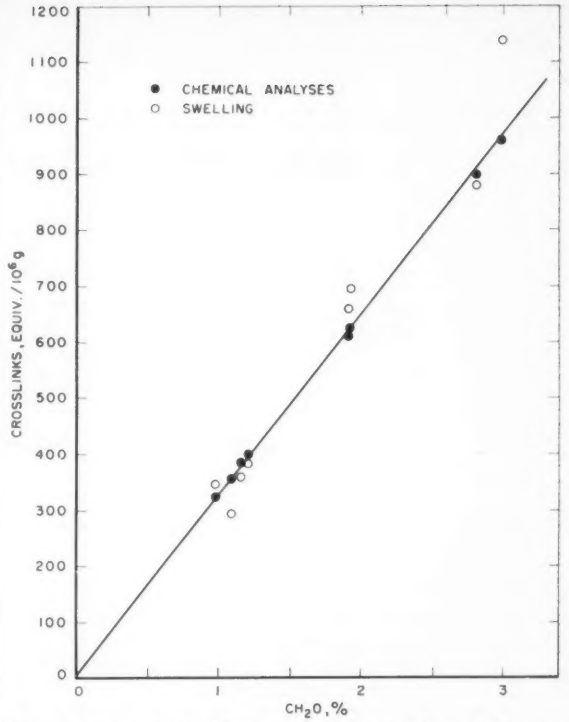

FIGURE 2. *Correlation between percent formaldehyde and equivalent number of crosslinks.*

further illustrated by figure 3 in which the equivalent number of crosslinkages calculated from swelling data is plotted against those calculated from chemical analyses [6]. The approximate margin of error, also indicated in figure 3, arises from the visual limitations of measuring the dimensions of the swollen fibers from photomicrographs. That equilibrium swelling was achieved within 30 min was established from the fact that the q_m values showed no further changes beyond 30 min of swelling.

This good agreement indicates that the Flory-Rehner theory can be extended to this anisotropic system and suggests its possible general application to some anisotropic networks.

It is not yet clear to what extent it is possible to apply a modified Gaussian theory to an anisotropic network. However, the good agreement here with experimental data is encouraging. Current discussions on the theory of network structures [7, 8, 9] indicate that a rigorous analysis of this very complex problem is necessary and the present work suggests the desirability of further experimental data on numerous other polymer systems.

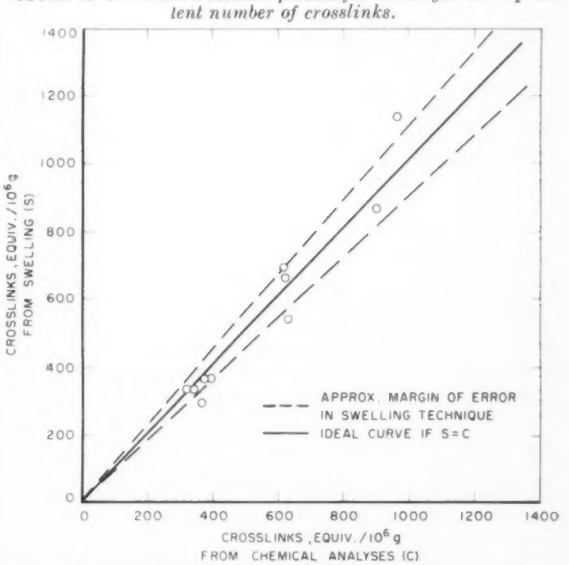
CROSSLINKS, EQUIV./10^6g FROM SWELLING (S)
APPROX. MARGIN OF ERROR IN SWELLING TECHNIQUE
IDEAL CURVE IF S=C
CROSSLINKS, EQUIV./10^6g FROM CHEMICAL ANALYSES (C)

FIGURE 3. *Correlation between equivalent number of crosslinks calculated from chemical analyses and swelling data.*

3. References

[1] P. J. Flory and J. Rehner, Jr., J. Chem. Phys. **11,** 521 (1943).
[2] P. J. Flory, ibid. **18,** 108 (1950).
[3] L. Valentine, J. Polymer Sci. **23,** 297 (1957).
[4] P. J. Flory, Principles of Polymer Chemistry (Cornell University Press, Ithaca, N.Y., 1953).
[5] B. Graham and O. E. Schupp, Jr., U.S. Patent 2,540,726, Example 1.
[6] J. Mitchell, Jr., in Organic Analysis **1,** 288 (Interscience Publ., Inc., New York, 1953).
[7] J. J. Hermans, Abstract of Papers, vol. **1,** No. 2, Division of Polymer Chemistry, ACS, St. Louis Meeting (March 1961).
[8] P. J. Flory, *ibid.*
[9] T. Alfrey, Jr., *ibid.*

(Paper 65A6–130)

JOURNAL OF RESEARCH of the National Bureau of Standards—A. Physics and Chemistry
Vol. 65A, No. 6, November–December 1961

Fiber Structure-Property Relationships: A Disulfide-Crosslinked Self-Crimping Polyamide

Stephen D. Bruck

(June 26, 1961)

A structural modification of nylon-6 fiber (polycaprolactam) was achieved by the introduction of a high density of intermolecular disulfide crosslinkages. The crosslinking process leads to an unexpected three-dimensional crimping in the dry and wet states (similar to wool), and to the formation of helical coils if swelling is carried out in a solvent capable of destroying the crystallites remaining after crosslinking. This phenomenon has not been observed previously in round cross-section synthetic homofibers. A possible explanation is advanced which attributes this crimping and coiling tendency to differential swelling caused by the varying crosslinking density across the fiber axis and to structural asymmetry resulting from the crosslinking process.

1. Introduction

Although the use of crosslinking reactions has markedly changed the properties of rubber, very little work has been published on the chemical intermolecular crosslinking of oriented, semicrystalline structures, such as synthetic fibers. Some work which has appeared in the literature deals with crosslinking reactions on dissolved polymer systems, but such preformed networks cannot be readily spun and drawn into fibers. It seems reasonable to expect, however, that at least some of the numerous known organic reactions could be utilized to bring about structural changes in synthetic homofibers which could markedly affect their properties.

This paper deals with the structural modification of nylon-6 fiber (polycaprolactam) as the result of a four-step disulfide crosslinking reaction. It will be shown that under suitable conditions this process leads to unexpected three-dimensional crimping in the dry and wet states (similar to wool), and to the formation of helical coils if swelling is carried out in a solvent capable of destroying the crystallites remaining after crosslinking. This phenomenon has not been observed previously in round cross-section synthetic homofibers, such as nylon-6.

In general, crimping in synthetic fibers can be induced either by mechanical means or by the preparation of heterofibers in which two polymers of different shrinkage characteristics are spun side-by-side from the same spinneret giving fibers with bilateral structures [1][1]. Among the natural fibers, wool has been found to have a bilateral, heterostructure composed of the orthocortex and the paracortex [2]. Crimped rayon staple is being made by the spinning of asymmetrical cross-section viscose into a specific low-acid coagulating bath and subsequently stretching the filament bundle in a hot bath [3].

[1] Figures in brackets indicate the literature references at the end of this paper.

2. Introduction of Intermolecular Disulfide Crosslinks

The existence of disulfide crosslinkages in wool fibers and other proteins is well known. Many of the unique properties of these systems have been attributed to these crosslinkages. The relative ease with which the sulfhydril groups may be oxidized to the disulfide linkages offers a promising approach to the study of chemical reactions which could lead to similar crosslinking of synthetic fibers. Polycaprolactams appear to possess the necessary requirements by virtue of their amide groups. Instead of using dissolved polycaprolactams, the use of already spun and drawn fibers offers a greater challenge inasmuch as such systems have a "build-in" crystallinity and orientation which should influence the final properties. Thus, for the present study nylon-6 fiber was chosen.

Early work by Cairns and coworkers [4, 5] described the preparation and some properties of *N*-methylol, *N*-alkoxymethyl, and *N*-alkylthiomethyl polyamides. Although these reactions were carried out while the polymers were in the dissolved state, they are of interest as potential precursors for crosslinking. It seemed desirable to investigate techniques aimed at the further development and application of some of these reactions on solid structures with the objective of introducing a large number of disulfide crosslinks into nylon-6 fiber.

The following chemical reactions are involved (for details of procedure, refer to Experimental section):

A.

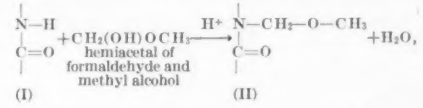

(I) (II)

B.

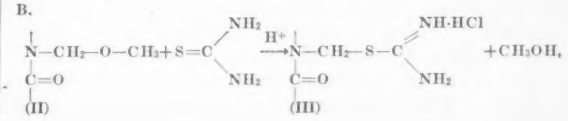

(II) (III)

C.

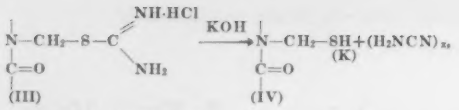

D.

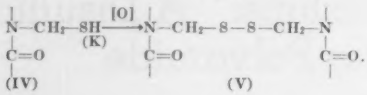

Step A involves the reaction of the amide hydrogen with the hemiacetal of formaldehyde and methyl-alcohol in the presence of strong acids, producing an *N*-methoxy-methylated polycaprolactam (II). The structure of this product has already been established [4] from the facts (a) *N*-methoxy-methylated polyamides produce formaldehyde in good agreement with the expected quantities predicted from methoxyl analyses, (b) polyamides prepared from *N,N'*-alkylated diamines do not react with the hemiacetal of formaldehyde and methyl alcohol, and (c) infrared absorption spectroscopy indicates a substantial decrease in the intensity of certain –NH absorption bands in the *N*-methoxymethylated polyamides.

In the present work, the *N*-methoxymethylation of solid nylon-6 fiber resulted in the formation of 3 to 4 percent methoxyl (depending on the experimental conditions used) which corresponds to an amide substitution in the polymer of approximately 11 to 15 percent. X-ray diffraction patterns of the *N*-methoxymethylated and unmodified fibers show no change of crystallinity, indicating that most likely only the amorphous regions are penetrated by the reagents. Since nylon-6 fiber is about 50 percent crystalline, 22 to 30 percent of the amide groups in the amorphous regions of the polymer were methoxymethylated.

Steps B and C involve the reaction of the methoxymethylated fiber with thiourea in the presence of strong acids and subsequent treatment with alkali to yield the sulfhydril product (IV). These reactions are analogous to the preparation of methylmercaptans from thiourea and alkyl halides (6):

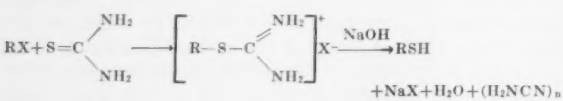

To determine the effect of the reaction medium on the extent of reactions A, B, and C, experiments were carried out both in water and in methyl alcohol, respectively, since the latter is a plasticizer for *N*-methoxymethylated polycaprolactams. In case of the experiments in water, methoxymethylated nylon-6 fibers were treated with thiourea and hydrochloric acid under various conditions, and then reacted with potassium hydroxide with concurrent air oxidation. Thus, the final structure contained both sulfhydril groups and disulfide crosslinks. Table 1 (samples 1 to 4) summarizes the pertinent analytical data. The percent of sulfur represents the combined quantities of sulfhydril groups and disulfide crosslinkages. The sulfur content of the samples varied from about one to two percent, depending on the conditions used.

The extent of crosslinking could also be estimated by equilibrium volume swelling measurements developed by Bruck [7] using a solvent (such as *m*-cresol) that could dissolve the uncrosslinked fiber. The symbol q_m represents the ratio of the volumes of the swollen to the unswollen structures, V/V_o at equilibrium [8]. The observed q_m values (table 1) are rather large indicating relatively few crosslinkages; this could be expected from the sulfur analyses, and from the mild air-oxidation treatment.

Although only a moderate number of crosslinks were present, cross sections of these fibers indicated that the intermolecular disulfide crosslinkages are not confined to the surface of the fiber but extend throughout the entire structure [9]. It is quite possible, however, that a larger number of crosslinks are located nearer to the surface than towards the center of the filaments. The significance of this will be discussed in a later section of this paper.

TABLE 1. *Analytical data on structurally modified nylon-6 fibers* [1]

No. [2]	Total S [3]	Reaction medium	Amide substitution	Swelling ratio, q_m [4]	Comments	
					Dry or wet	*m*-cresol
	%		%			
1	2.1	Water	7.4	11.7	Very few crimps.	Helix
2	1.0	...do.....	3.6	14.4	.....do.....	Do.
3	1.3	...do.....	4.8	6.9	.....do.....	Do.
4	1.0	...do.....	3.6	8.5	.....do.....	Do.
5	2.9	Methanol.	10.3	6.7	Highly crimped.	Helix
6	3.5	...do.....	12.4	4.3	.....do.....	Do.
7	2.7	...do.....	9.5	4.3	.....do.....	Do.

[1] *N*-methoxymethylated nylon-6: 3.4% methoxyl groups.
[2] For reaction conditions refer to Experimental section.
[3] Total sulfur includes both sulfhydril groups and disulfide crosslinkages.
[4] Measured photomicrographically after 24 hr air-oxidation $q_m = V/V_o$ where V=volume of network at equilibrium swelling, V_o=volume of network before swelling. Swelling agent: *m*-cresol.

In another series of experiments methyl alcohol was used as the reaction medium. The plasticizing effect of this solvent on *N*-methoxymethylated polycaprolactams facilitates the opening of the amorphous regions with some decrease in the crystallinity of the fiber. The experiments were carried out at room temperature since hot methyl alcohol partially dissolves the methoxymethylated fiber. Table 1 (samples 5 to 7) summarizes the results. The total quantities of sulfur (representing sulfhydril groups as well as disulfide crosslinkages) varied from 2.7 to 3.5 percent depending on the conditions used, a substantial increase over the reactions that had been carried out in water. Increased crosslinking is reflected by the decreased q_m values.

Birefringence measurements which were carried out on unmodified, and on methoxymethylated nylon-6 fibers (using a slot compensator and sodium D light) disclosed only small variations along a given fiber axis of approximately 2″ length. Birefringence $=(n_1-n_2)=R/t$, where n_1 and n_2 are the refractive indices along and across the fiber axis, respectively, R=retardation in millimicrons (measured

with the compensator), and t=thickness of the fiber in millimicrons. The birefringence values of these samples varied between +0.055 and +0.060. Furthermore, X-ray diffraction patterns showed no appreciable changes in the total crystallinity of these samples, a good indication that the *N*-methoxymethylation reaction is confined largely to the amorphous areas of the fiber [10]. Birefringence measurements on the disulfide-crosslinked structures that had been treated in water showed only small fluctuations along a given fiber axis, unlike those samples that had been treated in methanol. These latter samples showed birefringence values that ranged from +0.028 to +0.049 for five measurements along approximately 2″ length specimens. The reason for this may be the partial disruption of the crystallites due to the plasticizing effect of methyl alcohol and the structural strain caused by the intermolecular crosslinks.

In order to determine the effect of oxidizing agents other than air on the formation of disulfide crosslinks from sulfhydril groups, hydrogen peroxide and iodine (both well-known oxidizing agents for sulfhydril groups) were investigated. The samples described in table 1 were further subjected to oxidation by H_2O_2. When dilute solutions of the peroxide were used for 30 min, additional crosslinkages appeared in the polymers over those already introduced by air oxidation. This was evidenced by decreased q_m values as summarized in table 2. On the other hand, more concentrated solutions of H_2O_2 (or I_2) caused injury to the fibers which is not surprising considering the general sensitivity of nylons to prolonged exposure to strong oxidizing agents.

TABLE 2. *Equilibrium volume swelling ratios*[1] *of samples oxidized by air and hydrogen peroxide*

Sample No.	Oxidized by air—24 hr	Oxidized by H_2O_2—30 min	Oxidized by H_2O_2—4 hr
	q_m	q_m	q_m
5	6.7	5.9	5.5
6	4.3	3.9	3.5
7	4.3	4.1	3.9

[1] Measured photomicrographically, $q_m = V/V_0$, where V=volume of network at equilibrium swelling, V_0=volume of network before swelling. Swelling agent: *m*-cresol.

3. Crimping of the Disulfide-Crosslinked Fibers

The disulfide-crosslinked nylon-6 fibers exhibited unexpected three-dimensional wavy crimping of uneven distribution and dimensions, both in the wet and dry states, similar to wool. This crimping was especially pronounced in those fibers that had been treated in the presence of methyl alcohol and crosslinked by either air oxidation or by dilute solutions of H_2O_2 for 30 min. Figure 1 is a photograph of these fibers. Much reduced, but still noticeable crimping was also exhibited by those samples that had been crosslinked in the presence of water instead of methyl alcohol. On the other hand, helical

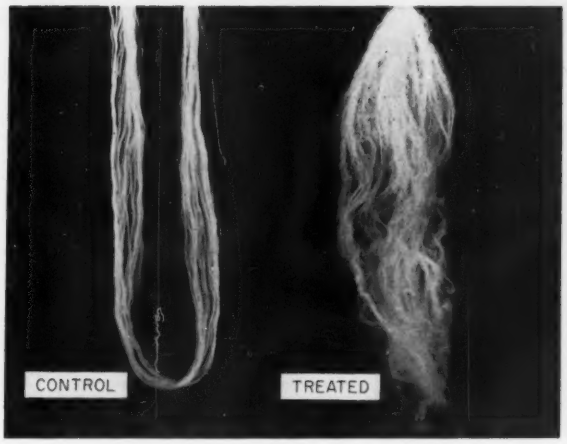

FIGURE 1. *Unmodified and disulfide- crosslinked nylon-6 fibers.*

coiling was produced by either series of fibers when they were treated with *m*-cresol which destroyed the remaining crystallites, thus removing the opposing force to coiling. Figures 2 and 3 are photographs of the helical coils produced after swelling in *m*-cresol. Corresponding phase-photomicrographs are illustrated by figures 4 and 5 before and after swelling, respectively (fibers under restraint), under identical magnifications.

As noted earlier, the formation of three-dimensional crimping and helical coiling has not been previously observed with round cross-section (symmetrical) synthetic homofibers, such as nylon-6. Thus, unlike wool, the homofiber has no "built-in" bilateral asymmetry. However, the observed crimping and coiling is undoubtedly due to some structural strain and asymmetry induced by the crosslinking process. Although the exact nature of this phenomenon is not clear at this time, a possible explanation will be attempted.

It was stated previously that the final oxidation step of sulfhydril groups to disulfide crosslinks was brought about by either air oxidation, or by relatively brief treatment (30 min) with dilute solutions of hydrogen peroxide. It is reasonable to assume that during this treatment those sylfhydril groups that are located nearer to the surface of the fiber will be oxidized to a greater extent than those situated towards the center. Furthermore the onset of the oxidation reaction will be accelerated at points along the fiber axis that are easily penetrated. As discussed already, step A in the chemical reaction series was carried out in the presence of hydrochloric acid which could cause structural nonuniformity in the fiber with the result that crosslinking agents will be able to penetrate certain regions more easily than others. Thus asymmetry should result within the round fibers by virtue of the varying crosslinking density across the fiber cross section. Although the fiber is crosslinked throughout, it might have an asymmetrical outer portion with a higher

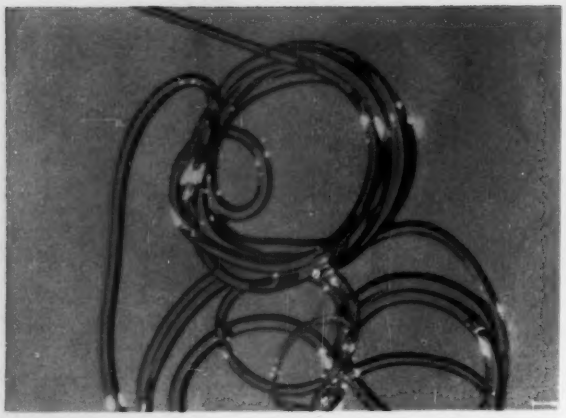

FIGURE 2. *Helical coiling of disulfide- crosslinked nylon-6 fiber.*

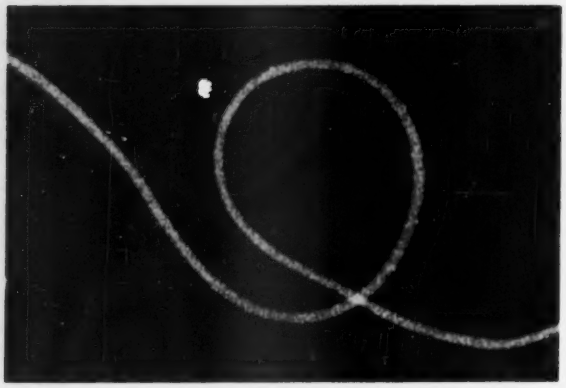

FIGURE 3. *A single helical coil of disulfide- crosslinked nylon-6 fiber.*

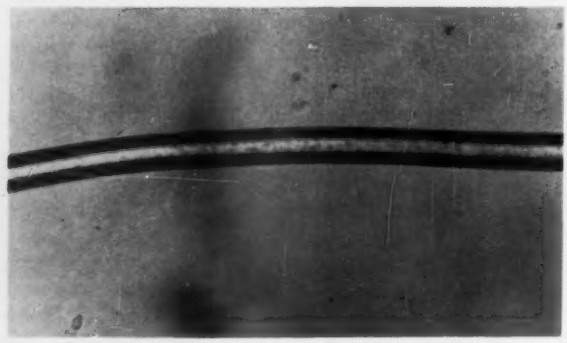

FIGURE 4. *Photomicrograph of unswollen disulfide- crosslinked nylon-6 fiber (under restraint).*

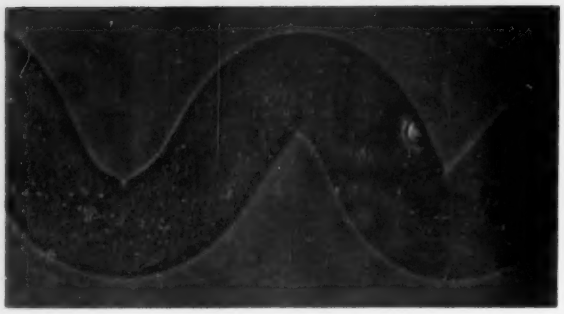

FIGURE 5. *Phase-photomicrograph of swollen (m-cresol) disulfide- crosslinked nylon-6 fiber (under restraint).*

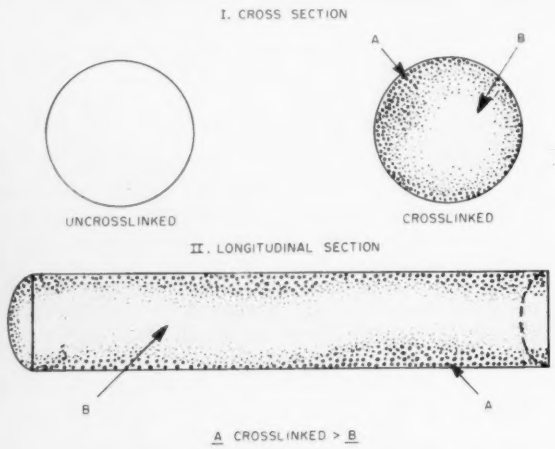

FIGURE 6. *Schematic illustrations of the crosslinked fibers.*

degree of crosslinking, and an inside asymmetrical portion with fewer crosslinks. A schematic illustration of this situation is given in figure 6. During swelling in water, the inner, less crosslinked parts will swell more than the outer more crosslinked portions. Water, which is a poor swelling agent, penetrates primarily the amorphous portions of the fiber and hence a counterforce is maintained as long as the crystallites remain intact. The relatively small differential swelling in water therefore is insufficient to overcome the masking effect of the crystallites which remain dominant, especially in view of the fact that the original fiber was approximately 50 percent crystalline. Under such conditions only crimping but no coiling is observed. During swelling in *m*-cresol, which completely destroys the crystallites, the differential swelling caused by the differential crosslinking density is no longer masked by the crystallites and this results in helical coiling of the fiber.

The fact that the fibers are crosslinked throughout and not just near the surface is of utmost importance. Fibers in which a different type of crosslinking was restricted to near the surface produced a hole in the

middle of the fiber when cross sections were treated with swelling agents capable of dissolving the uncrosslinked structure [9]. In such fibers there is no differential swelling process and hence no crimping and coiling are observed.

The critical importance of the differential swelling of the disulfide crosslinked fiber as the result of varying crosslinking density may also be demonstrated as follows. When those crosslinked fibers in which the final oxidation step was carried out with air or with dilute hydrogen peroxide solutions for 30 min were later subjected to additional, more prolonged oxidation by dilute H_2O_2, they exhibited greatly diminished crimping and coiling tendencies. This is most likely due to the more uniform distribution of crosslinks throughout the fiber as the result of better penetration by the oxidizing agent.

It may be desirable to stabilize the system to prevent any possible gradual slow oxidation throughout the fiber by air which could eventually negate the crimping and coiling effects. One possible way to avoid this is to treat the crosslinked and partially oxidized fiber with $AgNO_3$, according to the following equation [11]:

$$\underset{\text{I}}{-SH} + Ag^+ \longrightarrow \underset{\text{II}}{-SAg}$$

Product II is thus blocked from further oxidation and the fiber structure is "frozen" in the desired state.

Although in this work *m*-cresol was used to effect the complete destruction of the crystallites and hence produce maximum helical coiling, the judicious use of other swelling agents alone or in combination could result in various degrees of helical coiling depending on the extent of crystallinity of the fiber.

4. Experimental Procedure

All work was carried out with 7.8 Tex (60 denier)/32 filament nylon-6 fiber, polymer molecular weight 14,000 (end group analysis).

4.1. *N*-methoxymethylation[13]: Step A

A small skein of nylon-6 fiber, weighing approximately 0.1 to 0.2 g was scoured for 30 min in water containing 1 to 2 percent Na_3PO_4, washed in distilled water, and dried.

A solution was prepared containing 500 g paraformaldehyde and 500 g (625 ml) methyl alcohol by heating the solution to 60 °C and adding 3 to 4 pellets of KOH. The solution was stirred at this temperature until all paraformaldehyde dissolved (approx. 15 min) and then it was allowed to cool to room temperature. The *p*H of the solution was then adjusted to 0.6 to 0.7 with anhydrous oxalic acid (approx. 40 g). The skein was soaked in this solution for 12 hr at room temperature after which it was removed from the bath and heated at 120 ° C in a closed oven for 1 min, rinsed in methylalcohol followed by water, and dried. Methoxyl analysis [12]: 3.4%.

4.2. Introduction of Sulfhydril Group and Oxidation to Disulfide Crosslinks: Steps B, C, and D

Exp. No. 1. The *N*-methoxymethylated nylon-6 fiber was soaked in a solution containing 38.0 g thiourea (0.5 mole), 700 ml distilled water, and 35 ml conc. HCl (0.42 mole) at room temperature for 12 hr. After this period 28.0 g (0.5 mole) KOH was added in 100 ml distilled water and the fiber was permitted to soak at room temperature for 12 hr with concurrent air oxidation from a porous-disk bubbler. Next, the fiber was removed from the solution, thoroughly washed with distilled water, and dried. S=2.1%.

Exp. No. 2. Same as above, except that fiber was soaked for 1 hr in the thiourea, H_2O, and HCl mixture and for 1 hr in KOH. S=1.0%.

Exp. No. 3. The *N*-methoxymethylated nylon-6 fiber was soaked in a solution containing 38.0 g thiourea (0.5 mole) and 700 ml distilled water for 12 hr at room temperature. Next, 35 ml conc. HCl (0.42 mole) was added and the fiber soaked for 1 hr at room temperature. After this period 28.0 g (0.5 mole) KOH was added in 100 ml distilled water and the fiber was permitted to soak at room temperature for 1 hr with concurrent air oxidation from a porous-disk bubbler. The fiber was then washed with distilled water and dried. S=1.3%.

Exp. No. 4. The *N*-methoxymethylated nylon-6 fiber was soaked in a solution containing 38.0 g thiourea (0.5 mole) and 700 ml distilled water for 2 hr at 60 ° C. The solution was cooled to room temperature and 28.0 g (0.5 mole) KOH was added in 100 ml distilled water; the fiber was soaked in this solution for 1 hr at room temperature with concurrent air oxidation from a porous-disk bubbler. The fiber was then washed with distilled water and dried. S=1.0%.

Exp. No. 5. Same as Exp. No. 1, except that methyl alcohol was used instead of water as the reaction medium. S=2.9%.

Exp. No. 6. Same as Exp. No. 2, except that methyl alcohol was used instead of water as the reaction medium. S=3.5%.

Exp. No. 7. Same as Exp. No. 3, except that methyl alcohol was used instead of water as the reaction medium. S=2.7%.

Oxidation of Sulfhydril Groups to Disulfide Linkages with H_2O_2

The skeins from Exp. 1 to 7, respectively, were soaked at room temperature in a solution consisting of 250 ml distilled water, 2 pellets of KOH, and 10 ml of 3 percent H_2O_2 for 30 min to 4 hr, depending on the particular experiment.

The author wishes to thank R. A. Paulson, Applied Analytical Research Section, National Bureau of Standards, for the sulfur analyses, Sylvia M. Bailey for technical assistance in some phases of this work, and Mrs. Margaret Furst for the methoxyl analyses.

5. References

[1] W. A. Sisson and F. F. Morehead, Textile Research J. **23,** 152 (1953).
[2] M. Horio and T. Kondo, ibid. **23,** 373 (1953).
[3] M. Horio and T. Kondo, ibid. **23,** 137 (1953).
[4] T. L. Cairns, H. D. Foster, A. W. Larchar, A. K. Schneider, and R. S. Schreiber, J. Am. Chem. Soc. **71,** 651 (1949).
[5] T. L. Cairns, H. W. Gray, A. K. Schneider, and R. S. Schreiber, ibid. **71,** 655 (1949).
[6] R. Connor, Organic Chem., p. 841, ed. H. Gilman (John Wiley & Sons, Inc., New York, 1943).
[7] S. D. Bruck, J. Polymer Sci. (In press).
[8] P. J. Flory, Principles of Polymer Chemistry (Cornell University Press, Ithaca, N.Y., 1953).
[9] S. D. Bruck, unpublished data.
[10] Private communication from Dr. Aaron Posner, Dental Research Section, Organic and Fibrous Materials Division, NBS.
[11] R. Connor, Organic Chem., ed. H. Gilman, p. 835 (John Wiley & Sons, Inc., New York, 1943).
[12] Sidney Siggia, Quantitative Organic Analysis via Functional Groups, p. 27, Combined Methods of Elek and Samsel, et al. (John Wiley & Sons, Inc., New York, 1949).
[13] W. R. Sorensen and T. W. Campbell, Preparative Methods of Polymer Chemistry, p. 64 (Interscience Publ., Inc., New York, 1961).

(Paper 65A6–131)

JOURNAL OF RESEARCH of the National Bureau of Standards—A. Physics and Chemistry
Vol. 65A, No. 6, November–December 1961

Acidity Functions. Values of the Quantity $p(a_H\gamma_{Cl})$ for Buffer Solutions From 0 to 95 °C

Roger G. Bates and R. Gary

(August 7, 1961)

The thermodynamically defined quantity $p(a_H\gamma_{Cl})$ is a useful acidity function for measuring the acidic or basic character of electrolytic solutions. This function can be evaluated from electromotive force data (E) for cells without liquid junction consisting of one electrode reversible to hydrogen ions and one electrode reversible to chloride ions. The function is given by

$$p(a_H\gamma_{Cl})=\frac{E-E^\circ}{2.30259RT/F}+\log m_{Cl}.$$

Summarized in 20 tables, the function has been calculated from emf data recorded in the literature for the hydrogen-silver chloride cell. A consistent set of standard potentials (E°) and currently accepted values of the natural constants were used. The tables cover a range of $p(a_H\gamma_{Cl})$ from 1.6 to 12.5 and a range of temperature from 0 to 95° C. Included are buffer solutions of three different charge types. Ionic strengths vary in the range 0.01 to 0.20. Properties and uses of the acidity function are discussed.

1. Introduction

A measure of the acidity or basicity of a solution, applicable in a general way to solutions in all solvent media, has long been sought. Some years ago, Brønsted [1][1] suggested that the so-called "proton activity" might constitute a measure of the acidity of one solution relative to another. The concept of acidity is then directly related to the availability of protons for reaction with any base that may be introduced into the solution. It should be emphasized, however, that a high acidity does not indicate an appreciable concentration of free protons, which because of their extremely small size possess intense electrostatic fields and, consequently, can rarely exist uncombined in any liquid medium [2]. The concept of high proton activity therefore implies a relatively loose binding of protons to the basic species present in the solution. In such a solution, the potential of the hydrogen electrode is shifted toward positive values, and the *acidity potential* or *proton energy level* is said to be high [3].

The Brønsted concept of generalized acidity has proved pedagogically important and has facilitated greatly the visualization and interpretation of acid-base reactions where a proton-transfer mechanism is involved. Unfortunately, it is impossible, however, to compare experimentally the proton activities or energy levels in two different media [4]. All attempts to do so are doomed to failure because of the indeterminate character of the liquid-junction potential.

When the composition of the solvent itself is held constant, however, it appears that the acidity or basicity of the solution can be varied over rather wide ranges without changing the liquid-junction potentials appreciably. Consequently, it is often possible to obtain a useful measure of the *relative* acidity of different solutions, provided only that the composition of the solvent is unchanged. Thus a useful experimental pH scale exists for aqueous media, and other similar scales could be established for a number of partially aqueous or water-like solvents [4a]. Nevertheless, the acidity numbers would have no exact meaning when compared with those in another solvent or with the water scale.

Although the proton activity cannot be evaluated thermodynamically, the pH value of aqueous solutions derives some fundamental meaning from the arbitrary convention on which the numerical values of pH are based [5]. If one wishes to estimate thermodynamic equilibrium data through measurements of acidity, the individual *activity* of the proton or hydrogen ion would be much less useful than the hydrogen ion *concentration* or certain other related functions [6]. The simplest "acidity function" is therefore probably m_H, the hydrogen ion concentration, or its negative logarithm, which has been termed pcH [7].

The term "acidity function" as used here will signify a useful experimental or operational quantity with exact thermodynamic meaning, the value of which is a function of the acidity of the medium. Acidity functions are usually defined, as is the pH value, as the negative logarithm of the concentration of hydrogen ions (protons) multiplied by an appropriate combination of activity coefficients. A given acidity function customarily relates to a particular experimental arrangement or method, perhaps the electromotive force of a particular cell or the spectral absorption of a selected series of suitable indicators. Unlike the pH value, these acidity functions derive their usefulness from the unambiguous role that they play in specified chemical equilibria. A good example is provided by the Hammett acidity functions H_0 and H_-, which owe their validity to the regularities displayed in the behavior of certain indicators

[1] Figures in brackets indicate the literature references at the end of this paper.

in strongly acid media and in certain other solutions [8, 9].

In 1930, Guggenheim [6] pointed out that an experimental measure of the quantity $-\log(m_H\gamma_\pm)$ or $-\log(m_H\gamma_H\gamma_X)$ where X is a univalent anion, would be more useful than $-\log(m_H\gamma_H)$, even if the latter could be determined exactly. In 1936, Hitchcock [10] suggested the use of $-\log(m_H\gamma_H\gamma_{Cl})$, that is, $-\log(a_H\gamma_{Cl})$, as a useful acidity function of this type, pointing out that cells with hydrogen and silver-silver chloride electrodes (without a liquid junction) were capable of furnishing very precise values of this quantity in aqueous solutions over a wide range of compositions. This quantity was later termed *pw*H by one of the present authors [7]. Measurements of this function have formed the basis for the establishment of the NBS primary standards of *p*H and for the calculation of the dissociation constants of a number of weak acids and bases in this laboratory. It is likewise implicit in a method suggested by Hamer [11, 12] for the experimental measurement of hydrogen ion concentration or activity.

In 1954, Bates and Schwarzenbach [13] showed how the acidity function *pw*H could be used in combination with spectrophotometric measurements to facilitate greatly the determination of accurate values of the dissociation constants of many uncharged acids with appropriate spectral behavior. This method has been applied successfully to the determination of dissociation constants in aqueous solutions [14] and recently in ethanol-water mixtures [15].

It is the purpose of this paper to summarize in convenient form the most useful data available for the acidity function $-\log(m_H\gamma_H\gamma_{Cl})$. In accordance with a recent suggestion [16], this acidity function is now termed $p(a_H\gamma_{Cl})$ instead of *pw*H:

$$p(a_H\gamma_{Cl}) \equiv -\log(m_H\gamma_H\gamma_{Cl}). \quad (1)$$

The acidity functions have been calculated from emf measurements for various buffer solutions over a range of temperature, as recorded in the literature. The tabulated values of $p(a_H\gamma_{Cl})$ cover the range 1.64 to 12.5 at 25 °C. The range of temperatures extends from 0 to 50 °C, in some instances to 60 or 95 °C.

The original emf data were first converted, where necessary, to absolute volts. The acidity function was then calculated with the use of the most recent values of the standard potential of the cell and with a single, consistent set of the natural constants. In many instances, the functions have been plotted on a large scale and the acidity function interpolated at even values of the ionic strength.

2. Procedures

The acidity function $p(a_H\gamma_{Cl})$ was calculated from the electromotive force of cells of the type

$$Pt;H_2\ (g, 1\ atm),\ buffer\ solution\ containing\ soluble\ chloride,\ AgCl;Ag.$$

The calculation was made by the equation

$$p(a_H\gamma_{Cl}) = \frac{E - E^\circ}{2.30259RT/F} + \log m_{Cl}. \quad (2)$$

In eq (2), E is the electromotive force of the above cell, E° is the standard potential of this cell [17], R is the gas constant (8.31467 j deg^{-1} mole^{-1} [18]), T is the absolute temperature in degrees Kelvin (t °C+273.150), and F is the faraday (96,495.4 coulombs equiv.$^{-1}$ [18]). The values of E° and $2.30259RT/F$ (in abs v) used in deriving the acidity functions given in the tables below are summarized in table 1.[2] Electromotive force data published prior to January 1, 1948, were customarily given in international volts; these values have been converted to absolute volts by multiplying them by the factor 1.00033 [19].

TABLE 1. *Summary of the values of E° and $2.30259RT/F$ used to compute the acidity function $p(a_H\gamma_{Cl})$*

t	E°	$2.30259RT/F$
°C	abs v	abs v
0	0.23655	0.054195
5	.23413	.055187
10	.23142	.056183
15	.22857	.057171
20	.22557	.058163
25	.22234	.059155
30	.21904	.060147
35	.21565	.061139
38	.21352	.061734
40	.21208	.062131
45	.20835	.063123
50	.20449	.064115
55	.20056	.065107
60	.19649	.066099
70	.18782	.068083
80	.17873	.070067
90	.16952	.072051
95	.16511	.073043

In the use of $p(a_H\gamma_{Cl})$ for the determination of thermodynamic data, it is usually necessary to know the ionic strength (I) of the buffer solution used and to vary the ionic strength in such a way that an extrapolation to $I=0$ is possible. For this reason, values of $p(a_H\gamma_{Cl})$ over a range of ionic strength are needed. For a description of the method of calculating the ionic strength of each buffer system, the reader is referred to the original papers.

When $p(a_H\gamma_{Cl})$ was less than 2 and greater than 12, the ionic strength was different at each temperature because of the variation of m_H (or m_{OH}). In these cases, solutions of constant stoichiometric concentration were chosen, and the ionic strength at each temperature has been indicated.

In selected instances, it has been possible to give values of the acidity function for chloride-free buffer solutions. These values have been obtained by extrapolation (to the limit of zero concentration of chloride) of data for buffer solutions containing three or more small concentrations of soluble chloride.

[2] The planned change to the C-12 scale of atomic weights will affect both R and F in equal proportion and, hence, will not change the values of $2.30259RT/F$.

3. Results

Values of $p(a_H\gamma_{Cl})$ over a range of ionic strength and temperature are given in tables 2 to 20 of the appendix (section 6). In general, the maximum uncertainty in $p(a_H\gamma_{Cl})$ may be taken to be ± 0.004 at 0 to 60 °C. Above 60 °C, the values are probably accurate to ± 0.01 unit.

In those cases where the original data were plotted to yield values of $p(a_H\gamma_{Cl})$ at round values of ionic strength, or at nearly equally spaced intervals along the ionic strength axis, some smoothing of the original data has naturally occurred. However, no attempt was made to smooth the variation of $p(a_H\gamma_{Cl})$ with temperature, and some minor nonuniformities which have their source in the original experimental data may be noted. If it is necessary to obtain $p(a_H\gamma_{Cl})$ at temperatures other than those given (or if a smoothed set of data over a range of temperature is desired) the user will probably wish to smooth the data in some way.

Many of the tables show values of $-\log K$ over a range of temperature. These values have been corrected, where necessary, for changes in $E°$ and the natural constants. In the case of formic acid and acetic acid, values of $-\log K$ are as given in the original papers.

Details concerning the tabulated data for each buffer system are given below. The charge type of the principal acid-base equilibrium responsible for the buffering effect is designated by the charge borne by the base. A buffer composed of HA and A^-, for example,[3] is of the charge type -1, whereas buffers of the type HA^-, $A^=$ and HB^+, B are of charge type -2 and 0, respectively.

$KH_3(C_2O_4)_2$ (m) [20] (table 2). Buffer system: $H_2C_2O_4$, $HC_2O_4^-$. Charge type: -1. Ionic strength: $m+m_H$.

KH_2PO_4(m_1), HCl (m_2) [21] (table 3). Buffer system: H_3PO_4, $H_2PO_4^-$. Charge type: -1. Ionic strength: m_1+m_H.

HCOOH (m_1), HCOOK (m_2), KCl (m_3) [22] (table 4). Buffer system: HCOOH, $HCOO^-$. Charge type: -1. Ionic strength: $m_2+m_3+m_H$.

NaH succinate (m_1), HCl (m_2) [23] (table 5). Buffer system: H_2Suc, $HSuc^-$ (where Suc=succinate). Charge type: -1. Ionic strength: $m_1+m_H+m_{Suc^=}$.

KH phthalate (0.05m) [24] (table 6). Buffer systems: H_2Ph,HPh^- and HPh^-, $Ph^=$ (where Ph=phthalate). Charge types: -1 and -2. Ionic strength: 0.0533.

CH_3COOH (m_1), CH_3COONa (m_2), NaCl (m_3) [25] (table 7a). Buffer system: CH_3COOH, CH_3COO^-. Charge type: -1. Ionic strength: $m_2+m_3+m_H$.

CH_3COOH (m), CH_3COONa (m), NaCl (m) [26] (table 7b). Buffer system: CH_3COOH, CH_3COO^-. Charge type: -1. Ionic strength: $2m+m_H$.

NaH succinate (m), NaCl (m) [27] (table 8). Buffer systems: H_2Suc, $HSuc^-$ and $HSuc^-$, $Suc^=$, (where Suc=succinate). Charge types: -1 and -2. Ionic strength: $2m+2m_H+m_{H_2Suc}$.

KH phthalate (m_1), K_2 phthalate (m_2), KCl (m_3) [28] (table 9). Buffer systems: HPh^-, $Ph^=$ (where Ph=phthalate). Charge type: -2. Ionic strength: $m_1+3m_2+m_3+2m_H$.

NaH succinate (m), Na_2 succinate (m) [29] (table 10). Buffer system: $HSuc^-$ $Suc^=$ (where Suc=succinate). Charge type: -2. Ionic strength: $4m+2m_H+m_{H_2Suc}$.

KH_2PO_4 (m), Na_2HPO_4 (m) [30] (table 11). Buffer system: $H_2PO_4^-$, $HPO_4^=$. Charge type: -2. Ionic strength: $4m$.

KH p-phenolsulfonate (m_1), KNa p-phenolatesulfonate (m_2), NaCl (m_3) [31] (table 12). Buffer system: HPs^-, $Ps^=$ (where Ps=p-phenolatesulfonate). Charge type: -2. Ionic strength: $m_1+3m_2+m_3-m_{OH}$.

$Na_2B_4O_7$ (m_1), NaCl (m_2) [32] (table 13). Buffer system: H_3BO_3,BO_2^-. Charge type: -1. Ionic strength: $2m_1+m_2-m_{OH}$.

Triethanolamine (m_1), HCl (m_2) [33] (table 14). Buffer system: $(HOC_2H_4)_3NH^+$, $(HOC_2H_4)_3N$. Charge type: 0. Ionic strength: m_2.

Tris(hydroxymethyl)aminomethane (m_1), HCl (m_2) [34] (table 15). Buffer system: $(HOCH_2)_3CNH_3^+$, $(HOCH_2)_3CNH_2$. Charge type: 0. Ionic strength: m_2.

4-Aminopyridine (m_1), HCl (m_2) [35] (table 16). Buffer system: $H_2NC_5H_4NH^+$, $H_2NC_5H_4N$. Charge type: 0. Ionic strength: m_2.

Monoethanolamine (m_1), HCl (m_2) [36] (table 17). Buffer system: $HOC_2H_4NH_3^+$, $HOC_2H_4NH_2$. Charge type: 0. Ionic strength: m_2+m_{OH}.

Piperidine (m_1), HCl (m_2) [37] (table 18). Buffer system: $C_5H_{10}NH_2^+$, $C_5H_{10}NH$. Charge type: 0. Ionic strength: m_2+m_{OH}.

Calcium hydroxide (m) [38] (table 19). Buffer system: $CaOH^+$, Ca^{++}. Ionic strength: $2m_{OH}-m$.

$p(a_H\gamma_{Cl})$ in some solutions at 60 to 95° C [39] (table 20). Charge types: -1 (tetroxalate); -1, -2 (tartrate); -1, -2 (phthalate); -2 (phosphate); -1 (borax). Ionic strength: 0.073 (tetroxalate); 0.04 (tartrate); 0.053 (phthalate); 0.1 (phosphate); 0.02 (borax).

4. Uses of $p(a_H\gamma_{Cl})$

4.1. Hydrogen Ion Concentrations

From the definition of the acidity function $p(a_H\gamma_{Cl})$ given in eq (1), it is evident that the hydrogen ion concentration (m_H) is formally related to the acidity function as follows:

$$-\log m_H = p(a_H\gamma_{Cl}) + \log(\gamma_H\gamma_{Cl})$$

$$= p(a_H\gamma_{Cl}) + 2\log\gamma_{\pm}. \quad (3)$$

In this equation, $\gamma_{\pm}$ is the mean ionic activity coefficient of hydrochloric acid in the buffer solution for which the acidity function has been obtained.

[3] In these examples, A^-, $A^=$, and B are all bases in the Brønsted sense, in that they are able to accept protons.

606329—61——3

Although each of the terms in eq (3) is thermodynamically defined, the mean activity coefficients of hydrochloric acid in buffer solutions have not often been determined. Largely as a result of the fact that the concentration of hydrogen ion in buffer solutions is rarely known, the determinations of these mean activity coefficients is not usually a simple matter. It is possible, nonetheless, to derive approximate hydrogen ion concentrations from the acidity function when the ionic strength does not exceed 0.1. Perhaps the best procedure is to utilize the Davies equation [40], as modified by Robinson [41], to compute $\gamma_{\pm}$:

$$-\log \gamma_{\pm}=\frac{A\sqrt{I}}{1+\sqrt{I}}-0.2\ I, \tag{4}$$

where A, the Debye-Hückel slope, is a function of temperature. Values of A have been tabulated by Robinson and Stokes [42]. This equation reproduces rather satisfactorily the known mean activity coefficients of hydrochloric acid in the pure aqueous solution or in the presence of alkali halides in the low range of ionic strengths.

4.2. Hydroxide Ion Concentrations

A useful application of $p(a_{\mathrm{H}}\gamma_{\mathrm{Cl}})$ has been suggested by Bates, Siegel, and Acree [43]. According to this proposal, hydroxide ion concentrations in buffer solutions can be calculated by combining the acidity function with the ion-product constant, K_w, for water, values of which are listed by Harned and Owen [44]. Thus,

$$-\log K_w'-p(a_{\mathrm{H}}\gamma_{\mathrm{Cl}})=-\log m_{\mathrm{OH}}$$

$$+\log a_{\mathrm{H_2O}}\gamma_{\mathrm{Cl}}/\gamma_{\mathrm{OH}}\approx-\log m_{\mathrm{OH}}. \tag{5}$$

The activity of water, $a_{\mathrm{H_2O}}$, does not depart greatly from unity in dilute solutions; furthermore, both the hydroxide and chloride ions bear the same charge, and the ratio of their activity coefficients is likewise nearly unity when the ionic strength is less than 0.1. Electromotive force data in the literature show that the second term on the right of eq (5) amounts to only 0.013 in a mixture of potassium hydroxide (0.01 m) and potassium chloride (0.1 m) [45], and to only 0.003 in a mixture of sodium hydroxide (0.01 m) and sodium chloride (0.1 m) [46]. The ionic strength of both of these solutions is 0.11. It follows, therefore, that the left side of eq (5) is very often a useful approximation to $-\log m_{\mathrm{OH}}$.

4.3. Activity Coefficients

By combining acidity potentials with the dissociation constants for the buffer acids or bases, one can derive certain useful thermodynamic combinations of activity coefficients for the respective buffer systems. If HB and B represent, respectively, the weak acid and its conjugate base, which together are responsible for the buffering effect, one obtains

$$-\log \frac{\gamma_{\mathrm{Cl}}\gamma_{\mathrm{HB}}}{\gamma_{\mathrm{B}}}=p(a_{\mathrm{H}}\gamma_{\mathrm{Cl}})+\log K+\log \frac{m_{\mathrm{HB}}}{m_{\mathrm{B}}}, \tag{6}$$

where K is the dissociation constant of the buffer acid given in the appended tables. For the various buffers listed in the tables, the buffer pair HB, B may have the following charges: HB^+, B; HB, B^-; or HB^-, $B^=$.

In order to utilize eq (6) for the calculation of activity coefficients, it is evidently necessary to know the ratio of the concentrations of the buffer species in the solution. When the value of $p(a_{\mathrm{H}}\gamma_{\mathrm{Cl}})$ lies between 4 and 10, it is usually possible to use directly the stoichiometric ratio of molalities given in the tables. For dilute solutions of low and high acidity, however, the hydrolysis of HB or B may be sufficiently extensive that the stoichiometric ratio must be corrected accordingly. This is easily accomplished with the aid of hydrogen ion concentrations or hydroxyl ion concentrations estimated as indicated in the above paragraphs. Thus,

$$\frac{m_{\mathrm{HB}}}{m_{\mathrm{B}}}=\frac{m^{\circ}_{\mathrm{HB}}-m_{\mathrm{H}}+m_{\mathrm{OH}}}{m^{\circ}_{\mathrm{B}}+m_{\mathrm{H}}-m_{\mathrm{OH}}} \tag{7}$$

where m°_{HB} and m°_{B} represent the stoichiometric molalities of the two species.

4.4. pa_{H} Values

The acidity function $p(a_{\mathrm{H}}\gamma_{\mathrm{Cl}})$ can be used to estimate—$\log a_{\mathrm{H}}$ when values of this quantity are needed. Indeed, the standard reference values for the buffer solutions used by the National Bureau of Standards to define the pH scale are derived in this way. They are designated $p\mathrm{H_S}$ or pa_{H} and are computed by the following equation:

$$p\mathrm{H_S}=p(a_{\mathrm{H}}\gamma_{\mathrm{Cl}})+\log \gamma_{\mathrm{Cl}} \tag{8}$$

$$=p(a_{\mathrm{H}}\gamma_{\mathrm{Cl}})-\frac{\mathrm{A}\sqrt{I}}{1+1.5\sqrt{I}}, \tag{8a}$$

where A is again the Debye-Hückel slope. The activity coefficient of a single ionic species such as chloride is, of course, not thermodynamically defined. The convention used to evaluate this coefficient for the determination of standard pH values by eq (8a) is that recently proposed to International Union of Pure and Applied Chemistry by Bates and Guggenheim [16].

4.5. Dissociation Constants

Perhaps the most fruitful use of the acidity function $p(a_{\mathrm{H}}\gamma_{\mathrm{Cl}})$ is in the determination of the dissociation constants of uncharged acids by means of spectrophotometric measurements, when the spectral absorptions of the conjugate acid and base species differ sufficiently to permit the ratio of the concentrations of these forms in the solution to be established accurately by absorption spectrophotometry [13]. The acid-base system will be written HIn,In^- to designate its indicator properties. The acid HIn and its conjugate base In^- are added to suitable "regulating" buffer solutions (HB,B) in quantities so small that

the acidity function of the buffer is unaffected by their presence. The buffers selected must (a) have acidity functions that differ no more than about 1 unit from $-\log K_{\mathrm{HIn}}$ for best results, and (b) must not absorb light in the wavelength region where the useful absorption bands of In^- or HIn are located. The dissociation constant is then calculated by the expression

$$-\log K_{\mathrm{HIn}}=p(a_{\mathrm{H}}\gamma_{\mathrm{Cl}})-\log\frac{m_{\mathrm{In}^-}}{m_{\mathrm{HIn}}}+\log\frac{\gamma_{\mathrm{HIn}}\gamma_{\mathrm{Cl}^-}}{\gamma_{\mathrm{In}^-}}. \quad (9)$$

It is well known that quantities such as the last term of eq (9) are not only small in magnitude but vary linearly with ionic strength in dilute solutions. For this reason, two or more buffer solutions of different ionic strengths are chosen, and the apparent values of $-\log K_{\mathrm{HIn}}$ are plotted as a function of ionic strength and extrapolated to infinite dilution. This method has been applied with success to the determination of dissociation constants of substituted phenols and substituted anilines in aqueous solution [13, 14] and to the determination of the dissociation constant of anisic acid in ethanol-water mixtures [15]. For the most refined measurements, corrections should be applied for the effect of the system HIn, In^- upon the acidity function, as Robinson and Biggs have shown [41].

From an examination of the last term in eq (9), it is evident that the acidity function $p(a_{\mathrm{H}}\gamma_{\mathrm{Cl}})$ is more suitable for determining the dissociation constants of uncharged indicator acids, HIn, than for those of acids of other charge types, because of the near equality of the activity coefficients of ions of like charge in the same solution. For indicator acids of other charge types, Bates and Schwarzenbach [13] suggested that the control buffer solution (HB,B) selected be of the same charge type as the indicator acid system (HIn,In). If, then, the equations are written in terms of the dissociation constant of the buffer acid HB (whatever its charge type) instead of the acidity function, the same advantage of a cancellation of the activity coefficients can be gained. Regardless of charge type, the applicable equation is

$$-\log K_{\mathrm{HIn}}=-\log K_{\mathrm{HB}}+\log\frac{m_{\mathrm{HIn}}}{m_{\mathrm{In}}}-\log\frac{m_{\mathrm{HB}}}{m_{\mathrm{B}}}+\log\frac{\gamma_{\mathrm{HIn}}\gamma_{\mathrm{B}}}{\gamma_{\mathrm{In}}\gamma_{\mathrm{HB}}}. \quad (10)$$

The last term is again small and varies linearly with ionic strength. The ratio of concentrations of HIn and In is determined spectrophotometrically, and that of HB and B is derived from the composition of the control buffer solution. Values of $-\log K_{\mathrm{HB}}$ are listed in the tables. These have been corrected, where necessary, to conform to the values of E° and $2.30259RT/F$ given in table 1.

4.6. Nonaqueous and Partially Aqueous Media

The Hammett acidity functions H_0 and H_- have been conspicuously successful in correlating proton levels with the extent of acid-base reactions and with reaction rates, particularly in concentrated aqueous solutions of the strong acids [8, 9]. These acidity functions are defined in terms of the spectral absorption of a series of selected indicators. They depend for their validity on the regularities shown by the ratio of activity coefficients, $\gamma_{\mathrm{HIn}}/\gamma_{\mathrm{In}}$, of these indicator forms in strongly acidic media. Unfortunately, however, the values of $\gamma_{\mathrm{HIn}}/\gamma_{\mathrm{In}}$ for different indicator acids of a given charge type cannot be expected to be equal in the same medium any more than are the values of $\gamma_{\mathrm{HA}}/\gamma_{\mathrm{A}}$ for other acids [47, 48]. In many media, indeed, indicator behavior displays even less regularity than it does in solutions of strong acids, it appears. Without specifying the charge type of the indicator, one may define the Hammett function as follows:

$$\mathrm{H}=-\log a_{\mathrm{H}}\frac{\gamma_{\mathrm{In}}}{\gamma_{\mathrm{HIn}}}. \quad (11)$$

The subscripts in the symbols H_0 and H_- signify that the base form of the indicator (In) is, respectively, either an uncharged molecule or a singly-charged anion.

It is apparent that the acidity function $p(a_{\mathrm{H}}\gamma_{\mathrm{Cl}})$ has very much the same form as the Hammett function H_-. It seems possible that $p(a_{\mathrm{H}}\gamma_{\mathrm{Cl}})$ may find use as a practical index of the acidity of a wide variety of media to which it has not as yet been applied. The Hammett functions derive their usefulness in part from the fact that the aqueous standard state is maintained throughout. The function therefore reflects, to a degree, the changes of acidity from one medium to another. To preserve this same utility, values of $p(a_{\mathrm{H}}\gamma_{\mathrm{Cl}})$ should likewise be based upon standard potentials for the hydrogen-silver chloride cell in water, no matter what the composition of the medium in which the measurement of electromotive force is made.

Even so, the changes in $p(a_{\mathrm{H}}\gamma_{\mathrm{Cl}})$ cannot be expected to parallel the changes in H_-. In the first place, it must be recognized that profound changes in the character of the solvent medium will affect γ_{Cl^-} and γ_{In^-} in different ways, depending upon the susceptibilities of these two ions to solvation in the medium concerned and the abilities of the ions to "sort out" the molecules of mixed solvents. Furthermore, γ_{HIn}, which occurs in the expression for H_-, is not unaffected by changes of solvent, even though the species HIn bears no charge. According to Kolthoff, Lingane, and Larson [49], the activity coefficients of uncharged buffer acids decrease from values near unity to values in the vicinity of 0.01 when the solvent composition passes from pure water to pure ethanol or pure methanol.

In addition, determinations of $p(a_{\mathrm{H}}\gamma_{\mathrm{Cl}})$ are, of course, limited to media in which the hydrogen electrode and the silver-silver chloride electrode give reproducible potentials. It is necessary, therefore, to add a small known concentration of soluble chloride to the medium whose acidity potential is to be determined. It is probably true, however, that the difficulties in determining $p(a_{\mathrm{H}}\gamma_{\mathrm{Cl}})$ are no more restrictive than those affecting the determination of the Hammett functions. The use of the thermodynamically defined quantity $p(a_{\mathrm{H}}\gamma_{\mathrm{Cl}})$ in a variety of media as an index of the proton availability (still experimentally inaccessible) therefore merits further study.

606329—61——4

5. References

[1] J. N. Brønsted, Z. angew. Chem. **43,** 229 (1930).
[2] R. P. Bell, The proton in chemistry, Ch 1 (Cornell Univ. Press, Ithaca, N.Y., 1959).
[3] R. W. Gurney, Ionic processes in solution, Chs 7 and 14 (McGraw-Hill Book Co., Inc., New York, N.Y., 1953).
[4] G. Schwarzenbach, Helv. Chim. Acta **13,** 896 (1930); B. Gutbezahl and E. Grunwald, J. Am. Chem. Soc. **75,** 565 (1953).
[4a] C. L. deLigny, P. F. M. Luykx, M. Rehbach, and A. A. Wieneke, Rec. trav. chim. **79,** 699, 713 (1960).
[5] R. G. Bates, Electrometric *p*H determinations, Ch 4 (John Wiley and Sons, Inc., New York, N.Y., 1954).
[6] E. A. Guggenheim, J. Phys. Chem. **34,** 1758 (1930).
[7] R. G. Bates, Chem. Revs. **42,** 1 (1948).
[8] L. P. Hammett and A. J. Deyrup, J. Am. Chem. Soc. **54,** 2721, 4239 (1932); L. P. Hammett, Chem. Revs. **13,** 61 (1933).
[9] M. A. Paul and F. A. Long, Chem. Revs. **57,** 1 (1957); F. A. Long and M. A. Paul, Chem. Revs. **57,** 935 (1957).
[10] D. I. Hitchcock, J. Am. Chem. Soc. **58,** 855 (1936).
[11] W. J. Hamer, Trans. Electrochem. Soc. **72,** 45 (1937).
[12] W. J. Hamer and S. F. Acree, J. Research NBS **23,** 647 (1939) RP1261.
[13] R. G. Bates and G. Schwarzenbach, Helv. Chim. Acta **37,** 1069 (1954).
[14] R. A. Robinson, in W. J. Hamer, Ed., The structure of electrolytic solutions, p. 253 (John Wiley and Sons, Inc., New York, N.Y., 1959).
[15] E. E. Sager and V. E. Bower, J. Research NBS **64A,** 351 (1960).
[16] R. G. Bates and E. A. Guggenheim, Pure and Appl. Chem. **1,** 163 (1960).
[17] R. G. Bates and V. E. Bower, J. Research NBS **53,** 283 (1954) RP2546.
[18] E. R. Cohen, K. M. Crowe, and J. W. M. DuMond, Fundamental constants of physics, Ch 8 (Interscience Publishers, New York, N.Y., 1957).
[19] Announcement of changes in electrical and photometric units, NBS Cir. **C459** (May 15, 1947).
[20] V. E. Bower, R. G. Bates, and E. R. Smith, J. Research NBS **51,** 189 (1953) RP2450.
[21] R. G. Bates, J. Research NBS **47,** 127 (1951) RP2236.
[22] H. S. Harned and N. D. Embree, J. Am. Chem. Soc. **56,** 1042 (1934).
[23] G. D. Pinching and R. G. Bates, J. Research NBS **45,** 444 (1950).
[24] W. J. Hamer and S. F. Acree, J. Research NBS **32,** 215 (1944) RP1586.
[25] H. S. Harned and R. W. Ehlers, J. Am. Chem. Soc. **54,** 1350 (1932).
[26] H. S. Harned and R. W. Ehlers, J. Am. Chem. Soc. **55,** 652 (1933).
[27] G. D. Pinching and R. G. Bates, J. Research NBS **45,** 322 (1950) RP2142.
[28] W. J. Hamer and S. F. Acree, J. Research NBS **35,** 381 (1945) RP1678.
[29] R. G. Bates, G. D. Pinching, and E. R. Smith, J. Research NBS **45,** 418 (1950) RP2153.
[30] R. G. Bates and S. F. Acree, J. Research NBS **34,** 373 (1945) RP1648.
[31] R. G. Bates, G. L. Siegel, and S. F. Acree, J. Research NBS **31,** 205 (1943) RP1559.
[32] G. G. Manov, N. J. DeLollis, and S. F. Acree, J. Research NBS **33,** 287 (1944) RP1609.
[33] R. G. Bates and G. F. Allen, J. Research NBS **64A,** 343 (1960).
[34] R. G. Bates and H. B. Hetzer, J. Phys. Chem. **65,** 667 (1961).
[35] R. G. Bates and H. B. Hetzer, J. Research NBS **64A,** 427 (1960).
[36] R. G. Bates and G. D. Pinching, J. Research NBS **46,** 349 (1951) RP2205.
[37] R. G. Bates and V. E. Bower, J. Research NBS **57,** 153 (1956) RP2705.
[38] R. G. Bates, V. E. Bower, and E. R. Smith, J. Research NBS **56,** 305 (1956) RP2680.
[36] V. E. Bower and R. G. Bates, J. Research NBS **59,** 261 (1957) RP2797.
[40] C. W. Davies, J. Chem. Soc., **1938,** 2093.
[41] R. A. Robinson and A. I. Biggs, Trans. Faraday Soc. **51,** 901 (1955).
[42] R. A. Robinson and R. H. Stokes, Electrolyte Solutions, 2d ed., appendix 7.1 (Academic Press, New York, N.Y., 1959).
[43] R. G. Bates, G. L. Siegel, and S. F. Acree, J. Research NBS **31,** 205 (1943) RP1559.
[44] H. S. Harned and B. B. Owen, The physical chemistry of electrolytic solutions, 3d ed., ch. 15 (Reinhold Publishing Corp., New York, N.Y., 1958).
[45] H. S. Harned and W. J. Hamer, J. Am. Chem. Soc. **55,** 2194 (1933).
[46] H. S. Harned and G. E. Mannweiler, J. Am. Chem. Soc. **57,** 1873 (1935).
[47] E. Grunwald and B. J. Berkowitz, J. Am. Chem. Soc. **73,** 4939 (1951).
[48] B. Gutbezahl and E. Grunwald, J. Am. Chem. Soc. **75,** 559 (1953).
[49] I. M. Kolthoff, J. J. Lingane, and W. D. Larson, J. Am. Chem. Soc. **60,** 2512 (1938).

6. Appendix. Tables of Data

TABLE 2. *$p(a_{HYCl})$ in solutions of potassium textroxalate* (m)

t	m=0.01000		0.02500		0.05000		0.10000	
	I	$p(a_{HYCl})$	I	$p(a_{HYCl})$	I	$p(a_{HYCl})$	I	$p(a_{HYCl})$
°C								
0	0.0181	2.206	0.0417	1.932	0.0772	1.765		
5	.0181	2.202	.0416	1.934	.0770	1.764		
10	.0181	2.207	.0416	1.938	.0767	1.765		
15	.0181	2.210	.0415	1.940	.0765	1.769	0.1409	1.623
20	.0180	2.212	.0414	1.942	.0763	1.773	.1404	1.627
25	.0180	2.214	.0413	1.947	.0760	1.780	.1400	1.640
30	.0180	2.218	.0412	1.952	.0758	1.785	.1396	1.643
35	.0179	2.221	.0410	1.957	.0755	1.792	.1394	1.651
40	.0179	2.220	.0408	1.962	.0753	1.797	.1391	1.660
45	.0178	2.230	.0407	1.968	.0751	1.803	.1389	1.670
50	.0177	2.234	.0405	1.970	.0749	1.811	.1387	1.681
55	.0176	2.238	.0403	1.981	.0747	1.819	.1385	1.692
60	.0175	2.239	.0401	1.987	.0744	1.824	.1383	1.702

TABLE 3. *(pa_{HYCl}) in solutions containing potassium dihydrogen phosphate (m_1) and hydrochloric acid (m_2); $m_2 = 0.8055 m_1$*

t	$-\log K_1$	m_1=0.02600		0.03010		0.03841		0.04684		0.05533		0.06386		0.07249		0.08124	
		I	$p(a_{HYCl})$	I	$p(a_{HYCl})$	I	$p(a_{HYCl})$	I	$p(a_{HYCl})$	I	$p(a_{HYCl})$	I	$p(a_{HYCl})$	I	$p(a_{HYCl})$	I	$p(a_{HYCl})$
°C																	
0	2.056	0.0359	2.156	0.0410	2.120	0.0512	2.065	0.0614	2.022	0.0716	1.986	0.0818	1.954	0.0920	1.928	0.1023	1.904
5	2.070	.0357	2.164	.0408	2.129	.0510	2.074	.0611	2.030	.0713	1.994	.0815	1.963	.0916	1.937	.1018	1.913
10	2.088	.0355	2.172	.0406	2.137	.0507	2.083	.0609	2.040	.0710	2.003	.0811	1.973	.0912	1.947	.1013	1.923
15	2.106	.0353	2.180	.0404	2.146	.0506	2.092	.0606	2.049	.0707	2.013	.0807	1.983	.0908	1.957	.1009	1.934
20	2.127	.0352	2.189	.0402	2.156	.0503	2.102	.0603	2.059	.0703	2.024	.0804	1.994	.0904	1.968	.1004	1.945
25	2.150	.0350	2.201	.0400	2.166	.0500	2.115	.0600	2.071	.0700	2.036	.0800	2.006	.0900	1.982	.1000	1.958
30	2.169	.0348	2.212	.0398	2.178	.0497	2.127	.0597	2.083	.0696	2.049	.0796	2.019	.0895	1.995	.0995	1.971
35	2.195	.0346	2.223	.0395	2.190	.0494	2.139	.0593	2.097	.0692	2.062	.0791	2.032	.0890	2.008	.0989	1.985
40	2.223	.0344	2.234	.0393	2.202	.0491	2.151	.0590	2.109	.0688	2.074	.0787	2.045	.0885	2.020	.0984	1.998
45	2.249	.0341	2.246	.0390	2.215	.0488	2.164	.0586	2.122	.0685	2.088	.0782	2.058	.0881	2.034	.0979	2.012
50	2.276	.0339	2.258	.0388	2.228	.0485	2.177	.0583	2.136	.0681	2.102	.0778	2.073	.0876	2.049	.0973	2.028
55	2.305	.0337	2.271	.0385	2.241	.0482	2.191	.0580	2.150	.0677	2.117	.0774	2.089	.0871	2.065	.0968	2.046
60	2.335	.0335	2.285	.0383	2.255	.0479	2.205	.0576	2.165	.0673	2.133	.0769	2.106	.0866	2.082	.0963	2.064

TABLE 4. *$p(a_{HYCl})$ in solutions containing formic acid (m_1), potassium formate (m_2), and potassium chloride (m_3); $m_2 = 1.2467\ m_1$; $m_3 = 1.0789\ m_1$*

t	$-\log K$	I=0.02	0.03	0.04	0.05	0.06	0.07	0.08	0.10	0.12	0.15
		m_1=0.008544	0.012840	0.017136	0.02143	0.02573	0.03004	0.03434	0.04294	0.05154	0.06444
°C											
0	3.786	3.894	3.892	3.891	3.891	3.891	3.891	3.892	3.893	3.895	3.898
5	3.772	3.882	3.879	3.878	3.878	3.878	3.878	3.879	3.880	3.881	3.883
10	3.762	3.875	3.871	3.870	3.869	3.869	3.870	3.870	3.872	3.873	3.875
15	3.757	3.870	3.867	3.865	3.864	3.864	3.864	3.865	3.866	3.867	3.869
20	3.753	3.866	3.864	3.862	3.862	3.862	3.862	3.862	3.863	3.864	3.866
25	3.752	3.867	3.864	3.862	3.861	3.861	3.862	3.862	3.863	3.864	3.866
30	3.752	3.868	3.865	3.863	3.862	3.862	3.863	3.863	3.865	3.866	3.868
35	3.758	3.871	3.868	3.867	3.866	3.866	3.866	3.866	3.867	3.868	3.870
40	3.766	3.886	3.875	3.872	3.872	3.871	3.871	3.872	3.872	3.873	3.875
45	3.773	3.885	3.881	3.880	3.879	3.878	3.878	3.878	3.878	3.879	3.880
50	3.782	3.894	3.890	3.888	3.887	3.887	3.887	3.888	3.888	3.889	3.890
55	3.794	3.904	3.900	3.898	3.897	3.897	3.898	3.898	3.899	3.900	3.901
60	3.809	3.917	3.913	3.911	3.910	3.910	3.910	3.910	3.911	3.912	3.913

TABLE 5. *$p(a_{HYCl})$ in solutions containing sodium hydrogen succinate (m_1) and hydrochloric acid (m_2); $m_2 = 0.6667\ m_1$*

t	$-\log K_1$	I=0.01516	0.02017	0.02517	0.03018	0.04019	0.05019	0.06020	0.07020	0.08021	0.10021
		m_1=0.015000	0.02000	0.02500	0.03000	0.04000	0.05000	0.06000	0.07000	0.08000	0.10000
°C											
0	4.284	3.970	3.967	3.964	3.962	3.958	3.955	3.953	3.952	3.950	3.948
5	4.261	3.950	3.947	3.945	3.942	3.938	3.935	3.933	3.931	3.929	3.925
10	4.245	3.933	3.930	3.927	3.925	3.921	3.918	3.916	3.914	3.913	3.909
15	4.231	3.920	3.917	3.914	3.912	3.908	3.905	3.902	3.900	3.898	3.895
20	4.218	3.909	3.905	3.902	3.899	3.895	3.893	3.890	3.888	3.886	3.883
25	4.209	3.902	3.898	3.895	3.892	3.887	3.884	3.882	3.880	3.878	3.875
30	4.200	3.894	3.890	3.886	3.884	3.880	3.877	3.874	3.872	3.871	3.867
35	4.192	3.888	3.884	3.881	3.878	3.873	3.870	3.868	3.866	3.864	3.861
40	4.189	3.885	3.881	3.878	3.875	3.870	3.867	3.865	3.863	3.861	3.858
45	4.186	3.884	3.880	3.876	3.873	3.868	3.865	3.862	3.860	3.858	3.855
50	4.185	3.882	3.878	3.874	3.871	3.867	3.864	3.861	3.859	3.857	3.853

TABLE 6. *$p(a_{HYCl})$ in solutions containing* 0.05-m *potassium hydrogen phthalate* ($I=0.0533$)

t	$p(a_{HYCl})$
°C	
0	4.090
5	4.084
10	4.082
15	4.083
20	4.087
25	4.096
30	4.104
35	4.113
40	4.125
45	4.138
50	4.155

TABLE 7a. *$p(a_{HYCl})$ in solutions containing acetic acid* (m_1), *sodium acetate* (m_2), *and sodium chloride* (m_3); $m_2=0.9624\ m_1$; $m_3=1.0243\ m_1$

t	$-\log K$	I=0.01	0.02	0.03	0.04	0.05	0.06	0.07	0.08	0.09	0.10
		m_1=0.005034	0.010067	0.015100	0.02013	0.02517	0.03020	0.03523	0.04027	0.04530	0.05034
°C											
0	4.781	4.768	4.769	4.770	4.771	4.772	4.773	4.773	4.774	4.774	4.775
5	4.770	4.757	4.758	4.758	4.759	4.759	4.760	4.761	4.761	4.762	4.762
10	4.762	4.750	4.751	4.752	4.752	4.753	4.753	4.754	4.754	4.755	4.756
15	4.758	4.746	4.747	4.747	4.748	4.748	4.748	4.749	4.749	4.750	4.750
20	4.756	4.746	4.747	4.747	4.747	4.747	4.747	4.747	4.747	4.748	4.748
25	4.756	4.746	4.747	4.747	4.747	4.747	4.747	4.748	4.748	4.748	4.748
30	4.757	4.748	4.748	4.748	4.748	4.749	4.749	4.749	4.749	4.749	4.750
35	4.762	4.752	4.752	4.752	4.752	4.752	4.752	4.752	4.752	4.752	4.752

TABLE 7b. *$p(a_{HYCl})$ in solutions containing acetic acid* (m), *sodium acetate* (m), *and sodium chloride* (m)

t	$-\log K$	I=0.01	0.02	0.03	0.04	0.05	0.06	0.07	0.08	0.09	0.10
		m=0.005000	0.01000	0.01500	0.02000	0.02500	0.03000	0.03500	0.04000	0.04500	0.05000
°C											
35	4.762	4.768	4.768	4.769	4.770	4.770	4.770	4.770	4.770	4.770	4.770
40	4.769	4.775	4.775	4.775	4.775	4.775	4.775	4.775	4.775	4.775	4.775
45	4.777	4.781	4.782	4.782	4.782	4.782	4.782	4.782	4.783	4.783	4.783
50	4.787	4.791	4.790	4.790	4.790	4.790	4.790	4.790	4.790	4.790	4.790
55	4.799	4.801	4.801	4.800	4.800	4.800	4.800	4.800	4.800	4.800	4.800
60	4.812	4.813	4.813	4.812	4.812	4.812	4.812	4.812	4.811	4.811	4.811

TABLE 8. *$p(a_{HYCl})$ in solutions containing sodium acid succinate* (m) *and sodium chloride* (m)

t	I=0.0418	0.0681	0.108	0.158	0.217
	m=0.019390	0.03155	0.05012	0.07296	0.10000
°C					
0	4.915	4.901	4.887	4.877	4.867
5	4.894	4.879	4.866	4.855	4.845
10	4.880	4.864	4.851	4.839	4.829
15	4.868	4.853	4.838	4.827	4.817
20	4.861	4.847	4.831	4.817	4.809
25	4.853	4.838	4.826	4.814	4.802
30	4.852	4.839	4.822	4.809	4.798
35	4.850	4.837	4.820	4.805	4.796
40	4.851	4.838	4.821	4.806	4.796
45	4.855	4.842	4.823	4.810	4.799
50	4.860	4.848	4.827	4.815	4.804

TABLE 9.—$p(a_H\gamma_{Cl})$ *in solutions containing potassium hydrogen phthalate* (m_1), *dipotassium phthalate* (m_2), *and potassium chloride* (m_3); $m_2 = 1.0057\ m_1$ and $m_3 = 1.0014\ m_1$

t	$-\log K_2$	I=0.01	0.02	0.03	0.04	0.05	0.06	0.07	0.08	0.09	0.10
		m_1=0.002007	0.004015	0.006022	0.008031	0.010037	0.012044	0.014052	0.016059	0.018067	0.022007
°C											
0	5.432	5.349	5.316	5.295	5.279	5.265	5.253	5.242	5.232	5.223	5.216
5	5.417	5.331	5.300	5.278	5.262	5.248	5.236	5.225	5.215	5.206	5.199
10	5.408	5.322	5.292	5.270	5.253	5.240	5.227	5.216	5.206	5.197	5.190
15	5.404	5.317	5.286	5.264	5.246	5.232	5.220	5.209	5.200	5.191	5.183
20	5.404	5.316	5.284	5.262	5.245	5.230	5.218	5.207	5.197	5.188	5.180
25	5.411	5.323	5.290	5.268	5.251	5.237	5.224	5.212	5.202	5.192	5.184
30	5.419	5.329	5.297	5.275	5.257	5.242	5.229	5.218	5.208	5.199	5.190
35	5.428	5.338	5.305	5.281	5.262	5.247	5.235	5.224	5.214	5.205	5.197
40	5.443	5.352	5.319	5.296	5.278	5.263	5.250	5.239	5.228	5.218	5.209
45	5.462	5.368	5.335	5.312	5.293	5.278	5.265	5.253	5.243	5.233	5.225
50	5.484	5.390	5.356	5.333	5.314	5.299	5.285	5.274	5.263	5.253	5.244
55	5.510	5.415	5.382	5.357	5.338	5.322	5.309	5.298	5.287	5.278	5.269
60	5.538	5.444	5.409	5.384	5.365	5.349	5.335	5.324	5.314	5.305	5.296

TABLE 10.—$p(a_H\gamma_{Cl})$ *in solutions containing sodium hydrogen succinate* (m) *and disodium succinate* (m)

t	$-\log K_2$	I=0.041	0.101	0.202
		m=0.01000	0.02500	0.05000
°C				
0	5.675	5.599	5.560	5.531
5	5.660	5.582	5.542	5.513
10	5.649	5.569	5.528	5.498
15	5.642	5.561	5.519	5.488
20	5.638	5.555	5.513	5.481
25	5.638	5.553	5.511	5.477
30	5.641	5.553	5.511	5.476
35	5.647	5.556	5.514	5.477
38	5.652	5.559	5.517	5.479
40	5.656	5.562	5.520	5.481

TABLE 11.—$p(a_H\gamma_{Cl})$ *in solutions containing potassium dihydrogen phosphate* (m) *and disodium hydrogen phosphate* (m)

t	$-\log K_2$	I=0.01	0.02	0.03	0.04	0.05	0.06	0.08	0.10	0.12	0.15	0.20
		m=0.002500	0.004000	0.007500	0.01000	0.01250	0.01500	0.02000	0.02500	0.03000	0.03750	0.05000
°C												
0	7.313	7.226	7.196	7.174	7.157	7.143	7.130	7.109	7.091	7.076	7.056	7.029
5	7.280	7.193	7.162	7.141	7.123	7.109	7.096	7.075	7.057	7.042	7.022	6.995
10	7.253	7.165	7.134	7.112	7.095	7.081	7.068	7.047	7.029	7.014	6.994	6.969
15	7.230	7.142	7.111	7.089	7.072	7.057	7.045	7.024	7.006	6.992	6.971	6.945
20	7.213	7.124	7.093	7.072	7.054	7.039	7.027	7.005	6.988	6.973	6.953	6.927
25	7.200	7.111	7.080	7.058	7.040	7.026	7.013	6.992	6.974	6.959	6.940	6.912
30	7.192	7.102	7.070	7.048	7.031	7.016	7.003	6.982	6.964	6.949	6.929	6.902
35	7.186	7.095	7.064	7.041	7.024	7.009	6.996	6.974	6.956	6.941	6.921	6.894
40	7.182	7.090	7.059	7.036	7.019	7.004	6.991	6.969	6.951	6.936	6.917	6.890
45	7.181	7.089	7.057	7.034	7.016	7.001	6.989	6.967	6.949	6.934	6.914	6.886
50	7.182	7.089	7.057	7.034	7.016	7.001	6.988	6.966	6.948	6.933	6.913	6.885
55	7.185	7.091	7.059	7.036	7.018	7.003	6.990	6.968	6.950	6.935	6.915	6.888
60	7.191	7.096	7.064	7.041	7.023	7.008	6.995	6.973	6.954	6.939	6.919	6.892

TABLE 12. *$p(a_{HYCl})$ in solutions containing potassium* p-*phenolsulfonate* (m_1), *potassium sodium* p-*phenolatesulfonate* (m_2), *and sodium chloride* (m_3); $m_2 = 1.0120\ m_1$ *and* $m_3 = 0.9994\ m_1$

t	$-\log K_1$	I=0.02	0.03	0.04	0.05	0.06	0.07	0.08	0.09	0.10
		m_1=0.003972	0.005958	0.007943	0.009929	0.011915	0.013901	0.015887	0.017873	0.019858
°C										
0	9.352	9.258	9.244	9.232	9.223	9.216	9.208	9.203	9.198	9.194
5	9.282	9.189	9.176	9.164	9.154	9.146	9.139	9.134	9.129	9.124
10	9.219	9.124	9.111	9.099	9.090	9.082	9.075	9.069	9.064	9.059
15	9.159	9.063	9.050	9.040	9.030	9.022	9.015	9.009	9.004	8.999
20	9.105	9.007	8.994	8.982	8.972	8.964	8.958	8.952	8.946	8.942
25	9.055	8.957	8.944	8.932	8.922	8.914	8.907	8.901	8.896	8.891
30	9.008	8.908	8.895	8.884	8.874	8.865	8.857	8.851	8.845	8.840
35	8.962	8.861	8.848	8.836	8.827	8.818	8.810	8.804	8.798	8.793
40	8.922	8.818	8.804	8.793	8.784	8.776	8.768	8.761	8.755	8.750
45	8.883	8.778	8.766	8.754	8.744	8.735	8.727	8.721	8.715	8.710
50	8.848	8.740	8.729	8.717	8.707	8.698	8.690	8.684	8.678	8.674
55	8.814	8.702	8.692	8.681	8.671	8.662	8.654	8.648	8.642	8.638
60	8.784	8.669	8.658	8.648	8.638	8.629	8.620	8.614	8.609	8.605

TABLE 13. *$p(a_{HYCl})$ in solutions containing borax* ($Na_2B_4O_7$) (m_1) *and sodium chloride* (m_2); $m_2 = 1.8548\ m_1$

t	$-\log K$	I=0.010	0.015	0.020	0.025	0.030	0.035	0.040
		m_1=0.002594	0.003891	0.005190	0.006485	0.007780	0.009080	0.01038
°C								
0	9.508	9.514	9.515	9.515	9.516	9.516	9.516	9.516
5	9.436	9.435	9.438	9.440	9.441	9.442	9.443	9.443
10	9.377	9.377	9.380	9.382	9.382	9.382	9.383	9.383
15	9.325	9.324	9.327	9.328	9.329	9.329	9.330	9.330
20	9.278	9.276	9.280	9.281	9.281	9.282	9.282	9.282
25	9.237	9.234	9.237	9.237	9.238	9.239	9.239	9.239
30	9.199	9.192	9.196	9.198	9.199	9.199	9.199	9.199
35	9.162	9.154	9.157	9.159	9.160	9.161	9.162	9.162
40	9.129	9.121	9.126	9.128	9.129	9.130	9.130	9.130
45	9.101	9.089	9.095	9.098	9.100	9.101	9.101	9.102
50	9.076	9.062	9.069	9.072	9.074	9.075	9.076	9.076
55	9.052	9.035	9.042	9.047	9.049	9.051	9.052	9.052
60	9.028	9.008	9.018	9.023	9.026	9.027	9.028	9.029

TABLE 14. *$p(a_{HYCl})$ in solutions composed of triethanolamine* (m_1) *and hydrochloric acid* (m_2); $m_2 = 0.4860\ m_1$

t	$-\log K_{bh}$	I=0.010	0.015	0.020	0.030	0.040	0.050	0.060	0.080	0.100
		m_1=0.02058	0.03087	0.04116	0.06173	0.08231	0.10289	0.12247	0.16462	0.2058
°C										
0	8.291	8.407	8.430	8.449	8.475	8.493	8.510	8.525	8.552	8.577
5	8.173	8.291	8.315	8.335	8.361	8.378	8.394	8.409	8.437	8.462
10	8.067	8.186	8.209	8.227	8.253	8.272	8.288	8.303	8.330	8.358
15	7.963	8.081	8.105	8.125	8.152	8.168	8.183	8.198	8.226	8.249
20	7.861	7.979	8.002	8.022	8.050	8.067	8.082	8.096	8.123	8.146
25	7.762	7.883	7.907	7.926	7.951	7.968	7.984	7.998	8.026	8.048
30	7.666	7.786	7.809	7.827	7.853	7.870	7.885	7.899	7.927	7.952
35	7.571	7.692	7.715	7.732	7.758	7.775	7.790	7.805	7.832	7.856
40	7.477	7.601	7.623	7.641	7.664	7.681	7.699	7.714	7.739	7.761
45	7.387	7.511	7.534	7.551	7.575	7.593	7.607	7.622	7.649	7.673
50	7.299	7.423	7.446	7.463	7.488	7.506	7.521	7.536	7.562	7.584

TABLE 15. *$p(a_{HYCl})$ in solutions composed of tris (hydroxymethyl) aminomethane* (m_1) *and hydrochloric acid* (m_2); $m_2 = 0.4961\ m_1$

	$-\log K_{bh}$	I=0.01	0.02	0.03	0.04	0.05	0.06	0.07	0.08	0.09	0.10
		m_1=0.02016	0.04032	0.06047	0.08063	0.10079	0.12094	0.14110	0.16026	0.18142	0.2016
°C											
0	8.850	8.946	8.981	9.004	9.021	9.035	9.049	9.061	9.071	9.081	9.090
5	8.677	8.777	8.809	8.834	8.851	8.864	8.877	8.890	8.901	8.911	8.922
10	8.516	8.614	8.649	8.673	8.690	8.704	8.718	8.730	8.741	8.752	8.762
15	8.362	8.461	8.493	8.518	8.537	8.552	8.566	8.578	8.588	8.598	8.607
20	8.214	8.315	8.345	8.370	8.390	8.405	8.419	8.431	8.441	8.451	8.460
25	8.075	8.176	8.207	8.232	8.251	8.266	8.280	8.292	8.302	8.312	8.321
30	7.934	8.037	8.069	8.095	8.114	8.129	8.142	8.153	8.164	8.175	8.186
35	7.803	7.907	7.936	7.961	7.982	7.998	8.012	8.023	8.035	8.046	8.056
40	7.677	7.781	7.811	7.836	7.857	7.872	7.885	7.896	7.908	7.920	7.931
45	7.554	7.660	7.691	7.715	7.735	7.750	7.764	7.776	7.788	7.800	7.811
50	7.437	7.543	7.574	7.599	7.618	7.633	7.647	7.660	7.672	7.684	7.694

TABLE 16. *$p(a_{H\gamma Cl})$ in solutions composed of 4-aminopyridine (m_1) and hydrochloric acid (m_2); $m_2=0.4962\ m_1$*

t	$-\log K_{ba}$	I=0.02	0.03	0.04	0.05	0.06	0.07	0.08	0.09	0.10
		m_1=0.04031	0.06046	0.08061	0.10077	0.12092	0.14107	0.16122	0.18138	0.2015
°C										
0	9.873	9.992	10.016	10.037	10.056	10.072	10.085	10.096	10.107	10.118
5	9.704	9.825	9.850	9.872	9.890	9.906	9.919	9.931	9.942	9.953
10	9.549	9.668	9.694	9.716	9.735	9.750	9.763	9.774	9.785	9.796
15	9.398	9.519	9.543	9.565	9.582	9.597	9.610	9.623	9.634	9.645
20	9.252	9.375	9.399	9.419	9.437	9.453	9.466	9.477	9.488	9.499
25	9.114	9.236	9.259	9.279	9.297	9.313	9.326	9.338	9.348	9.358
30	8.978	9.103	9.125	9.145	9.162	9.177	9.190	9.202	9.212	9.223
35	8.845	8.970	8.993	9.013	9.031	9.046	9.058	9.070	9.081	9.091
40	8.717	8.842	8.864	8.885	8.904	8.920	8.933	8.945	8.955	8.964
45	8.594	8.717	8.741	8.763	8.783	8.799	8.813	8.824	8.834	8.844
50	8.477	8.603	8.624	8.646	8.666	8.682	8.694	8.705	8.716	8.727

TABLE 17. *$p(a_{H\gamma Cl})$ in solutions containing monoethanolamine (m_1) and hydrochloric acid (m_2); $m_2=0.5000\ m_1$*

t	$-\log K_{ba}$	I=0.010	0.015	0.020	0.025	0.030	0.040	0.050	0.060	0.070	0.080
		m_1=0.02000	0.03000	0.04000	0.05000	0.06000	0.08000	0.10000	0.12000	0.14000	0.16000
°C											
0	10.306	10.390	10.412	10.429	10.443	10.456	10.476	10.492	10.506	10.519	10.531
5	10.133	10.219	10.241	10.258	10.272	10.283	10.301	10.318	10.333	10.345	10.357
10	9.965	10.054	10.074	10.091	10.105	10.117	10.137	10.153	10.167	10.179	10.191
15	9.803	9.892	9.911	9.928	9.943	9.955	9.976	9.992	10.005	10.017	10.029
20	9.647	9.735	9.756	9.775	9.790	9.802	9.821	9.836	9.850	9.861	9.872
25	9.500	9.590	9.612	9.629	9.643	9.654	9.673	9.690	9.704	9.717	9.729
30	9.351	9.441	9.461	9.480	9.495	9.507	9.527	9.544	9.558	9.570	9.580
35	9.209	9.300	9.320	9.338	9.353	9.366	9.387	9.404	9.418	9.429	9.439
40	9.071	9.163	9.182	9.199	9.215	9.229	9.251	9.268	9.282	9.294	9.303
45	8.939	9.033	9.052	9.067	9.082	9.096	9.119	9.138	9.151	9.162	9.173
50	8.811	8.903	8.920	8.937	8.953	8.969	8.993	9.010	9.023	9.034	9.045

TABLE 18. *$p(a_{H\gamma Cl})$ in solutions containing piperidine (m_1) and hydrochloric acid (m_2); $m_2=0.5003\ m_1$*

t	$-\log K_{ba}$	I=0.0265	0.0315	0.0365	0.0416	0.0516	0.0617	0.0717	0.0818	0.0918	0.1019
		m_1=0.04997	0.05996	0.06995	0.07995	0.09993	0.11992	0.13991	0.15990	0.17988	0.19987
°C											
0	11.963	12.050	12.066	12.080	12.092	12.110	12.124	12.137	12.148	12.158	12.168
5	11.786	11.865	11.882	11.896	11.910	11.929	11.944	11.958	11.970	11.980	11.990
10	11.613	11.691	11.708	11.723	11.736	11.756	11.771	11.784	11.796	11.807	11.818
15	11.443	11.521	11.538	11.553	11.566	11.587	11.602	11.615	11.627	11.638	11.649
20	11.280	11.356	11.373	11.388	11.402	11.423	11.439	11.452	11.464	11.475	11.486
25	11.123	11.198	11.216	11.232	11.245	11.266	11.281	11.294	11.306	11.318	11.329
30	10.974	11.043	11.061	11.077	11.090	11.109	11.123	11.137	11.150	11.162	11.174
35	10.818	10.890	10.907	10.923	10.936	10.955	10.969	10.981	10.994	11.006	11.018
40	10.670	10.742	10.760	10.776	10.790	10.811	10.826	10.839	10.850	10.860	10.870
45	10.526	10.598	10.616	10.632	10.645	10.665	10.678	10.690	10.702	10.714	10.725
50	10.384	10.452	10.467	10.481	10.493	10.515	10.531	10.544	10.557	10.569	10.581

TABLE 19. *$p(a_{H\gamma Cl})$ in solutions of calcium hydroxide* (m)

t	m=0.01500		0.01750		0.02000		0.0203 (Satd. at 25 °C)	
	I	$p(a_{H\gamma Cl})$	I	$p(a_{H\gamma Cl})$	I	$p(a_{H\gamma Cl})$	I	$p(a_{HCl})$
°C								
0	0.040	13.386	0.047	13.449	0.053	13.504	0.054	13.510
5	.039	13.161	.046	13.226	.052	13.285	.053	13.291
10	.039	12.958	.045	13.024	.051	13.082	.051	13.088
15	.038	12.769	.045	12.832	.051	12.887	.050	12.893
20	.038	12.584	.044	12.649	.050	12.706	.050	12.712
25	.037	12.414	.043	12.477	.049	12.531	.049	12.537
30	.037	12.250	.043	12.317	.049	12.375	.049	12.381
35	.037	12.095	.043	12.158	.048	12.213	.048	12.219
40	.036	11.954	.042	12.012	.048	12.064	.048	12.070
45	.036	11.809	.042	11.871	.047	11.920	.048	11.926
50	.036	11.674	.042	11.735	.047	11.786	.047	11.790
55	.035	11.545	.041	11.603	.046	11.654	.047	11.661
60	.035	11.418	.041	11.480	.046	11.534	.047	11.540

TABLE 20. *$p(a_{H\gamma Cl})$ in some solutions at 60 to 95 °C*

Solution	t (°C)=60	70	80	90	95
0.05-*m* potassium tetroxalate	1.827	1.849	1.877	1.904	1.919
Potassium hydrogen tartrate, satd. at 25 °C	3.643	3.664	3.698	3.738	3.767
0.05-*m* potassium hydrogen phthalate	4.175	4.219	4.259	4.301	4.331
0.025-*m* potassium dihydrogen phosphate 0.025-*m* disodium hydrogen phosphate	6.948	6.962	6.979	7.001	7.014
0.01-*m* borax	9.026	8.990	8.953	8.920	8.899

(Paper 65A6—132)

JOURNAL OF RESEARCH of the National Bureau of Standards—A. Physics and Chemistry
Vol. 65A, No. 6, November–December 1961

2,3-*O*-Isopropylidene-α-D-lyxofuranose, the Monoacetone-D-lyxose of Levene and Tipson[1]

Robert Schaffer

(July 11, 1961)

A proof of structure is presented for the title compound, previously uncharacterized. In the course of the investigation, the crystalline 2,3-*O*-isopropylidene acetals of calcium D-lyxonate, D-lyxono-1,4-lactone, D-lyxitol, β-D-erythrofuranose, calcium D-erythronate, and D-erythrono-1,4-lactone were prepared. The diacetate and dibenzoate of 2,3-*O*-isopropylidene-D-lyxose were also synthesized.

1. Introduction

Among the acetals whose infrared absorption spectra were studied by Tipson, Isbell, and Stewart [1][2] was a crystalline mono-*O*-isopropylidene-D-lyxose (I) that Levene and Tipson [2] had prepared in 1936, but whose structure has not hitherto been determined. Interestingly, its infrared absorption spectrum was found [1] to contain bands that had previously been tentatively correlated with furanoid structures [3], but, as was pointed out [1], a furanoid ring could not be assigned from this evidence alone, because some nonfuranoid structures show many of these bands, too. In addition, however, since D-lyxose is in the same homomorphous series as D-mannose, which forms a furanose 2,3:5,6-di-*O*-isopropylidene acetal [4], the mono-*O*-isopropylidene-D-lyxose could be expected to possess, structural similarities to the di-*O*-isopropylidene-D-mannose. This consideration extended the possibility that compound I would prove to be a *reducing, furanoid*, sugar derivative. The scarcity of compounds having such structure, and our interest in the properties that it would exhibit, prompted this study of Levene and Tipson's compound.

2. Discussion

From its behavior with Fehling solution, it appeared that the lyxose derivative I is indeed a reducing sugar derivative, but the rate of reaction was so low that additional evidence was sought in order to make sure that this was simply a reaction indicative of an unsubstituted reducing group in the molecule. This was achieved by obtaining a quantitative oxidation of I with hypoiodite [5], and isolating a crystalline calcium *O*-isopropylidene-D-lyxonate dihydrate (II). Treatment of II with a cation-exchange resin [3] led to removal of the metal ion, and this was followed by crystallization of an *O*-isopropylidene-D-lyxonic lactone (III); the latter was also obtained directly from I by oxidation with bromine in a buffered solution [6]. Additional evidence for the presence of a free reducing group was found on treating I with sodium borohydride [7]; a crystalline *O*-isopropylidene-D-lyxitol (IV) was isolated. Thus, I exhibits the properties of an aldopentose that has been condensed with an equimolecular proportion of acetone at two of its four *alcoholic* hydroxyl groups.

The rather slow reaction that took place on treating I with sodium metaperiodate provided evidence for one of the points of attachment of the isopropylidene group. No acid was detected among the products after 40 hr of reaction (when 0.7 mole of periodate had been consumed per mole of I); this indicates that the hydroxyl group at C–2 is substituted, since otherwise formic acid would have been produced [8].

The location of the second point of attachment of the isopropylidene group was determined upon characterizing compound V, a crystalline product that resulted from interaction of IV and sodium metaperiodate. This compound (V) had the composition of an acetonated tetrose. Acid hydrolysis converted it to a sirupy compound, which was found by paper chromatography to behave identically with an authentic specimen of D-erythrose [9]. Compound V was further characterized by oxidation with hypoiodite to a crystalline calcium *O*-isopropylidenetetronate hemihydrate (VI); and from this salt (VI), a crystalline *O*-isopropylidenetetronic lactone (VII) was prepared. Bromine in buffered solution yielded the same lactone (VII) directly from V. Acid hydrolysis converted VII to D-erythronic lactone [10], which was identified by paper chromatography. Thus, V is an acetonated D-erythrose, and, from this conclusion, the location of the isopropylidene group of compounds I through VII can be deduced. As the isopropylidene-D-lyxitol (IV) can be degraded to a D-*erythro*-tetrose by glycol cleavage only at C–4 and C–5, and as the hydroxyl group at C–1 of compound IV is unsubstituted (from its origin), therefore the isopropylidene linkages are to the oxygen atoms at C–2 and C–3. These two carbon atoms become C–3

[1] Presented, in part, before the Division of Carbohydrate Chemistry of the American Chemical Society at the 138th National Meeting in New York, N.Y., September 12, 1960.
[2] Figures in brackets indicate the literature references at the end of this paper.
[3] Amberlite IR-120 (H^+), a product of Rohm and Haas Co., Philadelphia, Pa.

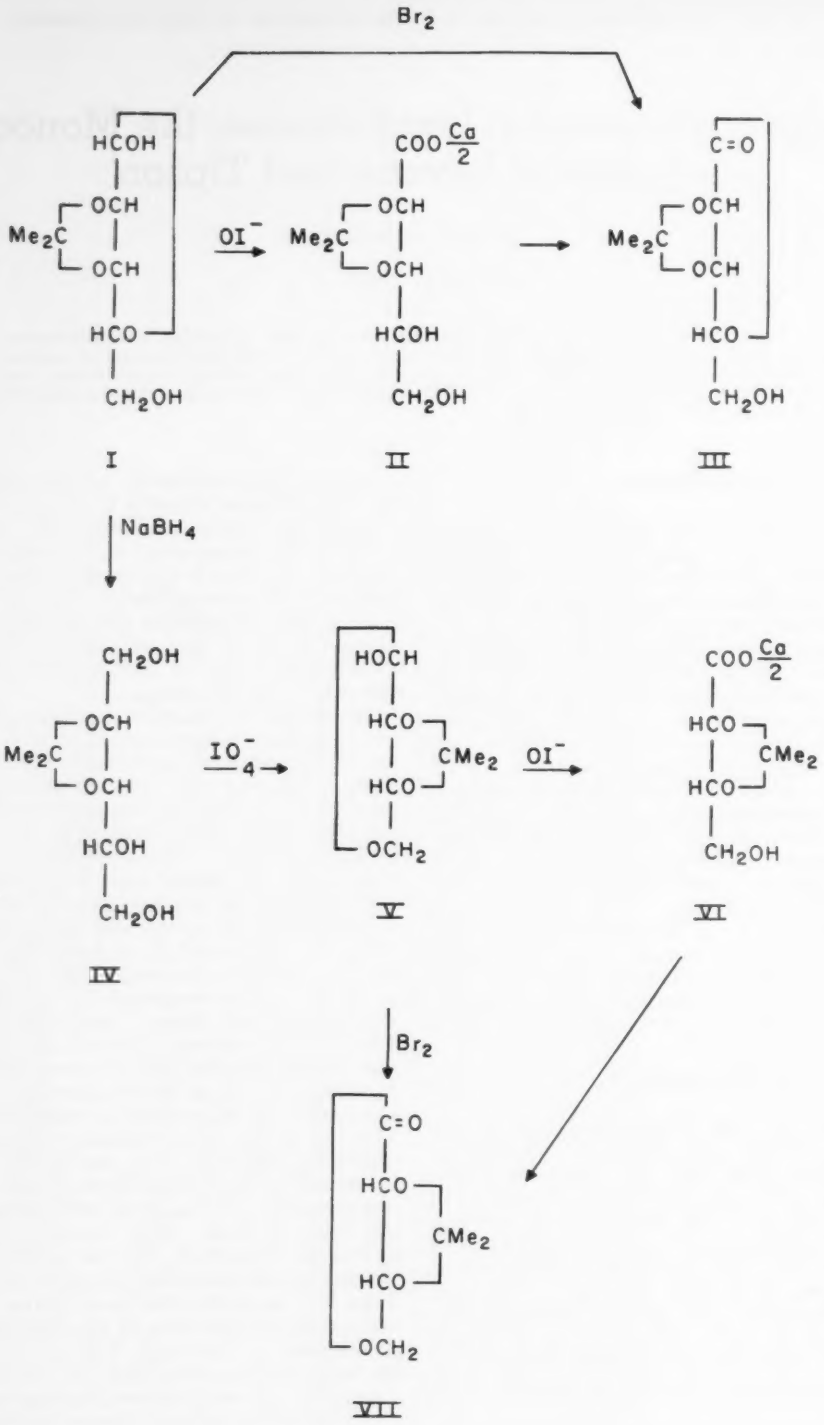
Br2
HCOH
OCH
Me2C
OCH
HCO
CH2OH
I
OI⁻
COO Ca/2
II
C=O
III
NaBH4
IV
IO4⁻
HOCH
HCO
CMe2
OCH2
V
VI
VII

and C–2, respectively, of the derived tetrose, but, due to the symmetry of the substituent, compounds I through VII are all 2,3-*O*-isopropylidene derivatives. Of these, compounds IV and V had previously been prepared but not crystallized [11], and the enantiomorph of V was recently crystallized by Baxter and Perlin [12].

Molecular models of 2,3-*O*-isopropylidene-D-lyxose show that the aldehyde group of the acyclic sugar can form either a furanose ring with the hydroxyl group at C–4, or a pyranose ring with the hydroxyl group at C–5, and that, for both rings, α and β anomers are possible [2]. Similarly, a model of 2,3-*O*-isopropylidene-D-erythrose shows that a furanose ring, which is the only possible sugar-ring form of this acetal, can readily be constructed, and that both an α or a β anomer are possible.

The actual hemiacetal-ring structures of the acetonated sugars were ascertained from the sizes of the lactone rings of the products obtained on oxidation under conditions that precluded expansion or contraction of the lactone rings produced. These conditions were provided by a buffer, in the oxidation medium, that served to neutralize any acid that might be formed by hydrolysis of lactone and might otherwise be transformed into a lactone of another ring size. This is the method of Isbell and Hudson, and of Isbell [6], who showed that, in the presence of buffer, a cyclic sugar is oxidized directly to a lactone of the same ring size. In the present study, evidence was educed to show that the bromine-oxidation product of each sugar is the lactone that was subsequently isolated. The ring structures of the isolated lactones, which are new compounds, were deduced [13] from their carbonyl stretching frequencies in the infrared. The carbonyl stretching frequencies given in the literature are in the range of 1,725 to 1,760 cm^{-1} for δ-lactones (and for esters) and in the range of 1,755 to 1,800 cm^{-1} for γ-lactones. Compound III, with an absorption maximum at 1,785 cm^{-1}, and compound VII, with a maximum at 1,770 cm^{-1}, fall in the latter range and are, therefore, γ-lactones. (The closely related 2,3:5,6-di-*O*-isopropylidene-D-mannono-1,4-lactone absorbs at 1,780 cm^{-1} [11].)

In determining the hemiacetal-ring form of compound I, a solution of the products obtained on reaction of I with bromine at 0° for 2.5 hr, when the oxidation was about complete, was found to have a specific optical rotation of +100°. A solution of the isolated oxidation product, compound III, had an initial specific rotation of +106°, and on allowing both of the above solutions to stand, their values decreased. In contrast, the free acid form of III and its calcium salt have values of −22 and −46.5°, respectively, and, on standing in solution, the rotation of the former becomes dextrorotatory. Thus, the optical rotatory properties of the oxidation mixture correspond closely to those of III, which was obtained in high yield simply by extracting the buffered oxidation mixture; and III is, therefore, the directly formed oxidation product. Compound III is 2,3-*O*-isopropylidene-D-lyxono-1,4-lactone and, consequently, compound I is a 2,3-*O*-isopropylidene-D-lyxofuranose. Compound I shows an initial $[\alpha]_D^{22}$ of +21.4° that changes in 10 min to +18.5°. From this mutarotation, an α configuration is assigned [14] to C–1 of I.

Starting with compound V, the specific optica rotation of the products, measured after about 2 hr of oxidation by bromine, was −103°; for a freshly prepared solution of VII, the isolated product, the value is −116°. With time, the rotations of both of these solutions become less levorotatory. On the other hand, the free acid form of VII and its calcium salt have specific optical rotations of +22.2 and +65.6°, respectively, and the rotation of the acid becomes levorotatory on standing in solution. Compound VII, which is isolated in very high yield by extraction of the reaction products, is clearly the direct product of oxidation of V. Compound VII is 2,3-*O*-isopropylidene-D-erythrono-1,4-lactone, and V, its precursor, is, therefore, a 2,3-*O*-isopropylidene-D-erythrofuranose. Although mutarotation was not detected for its enantiomorph [10], compound V *was found to mutarotate* from $[\alpha]_D^{22}$ −68 to −66° in water and from $[\alpha]_D^{24}$ −77.6 to −76.2° in methanol. Therefore, it is 2,3-*O*-isopropylidene-β-D-erythrofuranose [14].

A partial explanation of the relatively slow oxidation of I by periodate can be advanced, now that its structure is known. For the reaction to proceed, hydroxyl groups at C–4 and C–5 are needed, and both are present on tautomerization of the hemiacetal form to the open-chain form of I. These vicinal hydroxyl groups should be as reactive as the corresponding pair in compound IV, whose reaction with periodate was complete in less than 5 min. The much lower rate actually observed with I must, because of the observed mutarotation, be due to an exceedingly low equilibrium concentration of the open-chain form. This explanation for the diminished rate of periodate oxidation of I, because of the presence of a furanose ring, is in contrast, but not in conflict, with the acceleration of the periodate reaction that may accompany formation of a furanose ring, since the latter oxidation occurs with α,γ-dihydroxy aldehydes (where the bond between the anomeric hydroxyl group of the furanose ring formed and the α-hydroxyl group is oxidized [8]).

Two crystalline esters of 2,3-*O*-isopropylidene-D-lyxose were synthesized, namely, a diacetate and a dibenzoate. As they were obtained in high yield on treating pyridine solutions of I with acetic anhydride and with benzoyl chloride, respectively, it is assumed that they are 1,5-diesters. From steric considerations, the anomeric acyl groups are expected to be *exo*. Thus, they are tentatively formulated as 1,5-di-*O*-acyl-2,3-*O*-isopropylidene-α-D-lyxofuranoses.

As pointed out by Levene and Tipson [2], and confirmed in this laboratory, on slow distillation of I, there is formed a second volatile fraction, which distills at temperatures higher than does I. This as-yet-uncrystallized material is dextrorotatory [2] and nonreducing. Its constitution will be the subject of a future report.

3. Experimental Procedures

3.1. Acetonation of D-Lyxose to 2,3-*O*-Isopropylidene-α-D-lyxofuranose (I)

The procedure of Levene and Tipson [2] was modified by use of a magnetic stirrer for mixing 20 g of crystalline D-lyxose, 50 g of anhydrous cupric sulfate, and 0.5 ml of concentrated sulfuric acid in 500 ml of technical acetone in a stoppered Erlenmeyer flask. The heat from the stirrer kept the mixture at about 35° for the 5-day reaction time. The mixture was then filtered, the filtrate was passed through 40 ml of acetone-washed, anion-exchange resin,[4] and the effluent was evaporated to dryness under diminished pressure. The residue was distilled at 0.04 mm, and a fraction weighing 6.0 g was collected at 105 to 127°. Compound I crystallized from its solution in toluene; yield 4.3 g; mp 81.5–82.5°; $[\alpha]_D^{22}$+21.4° (extrapolated) →+18.5° in 10 min (*c*, 10; water). Compound I had been reported with bp 110° at 0.1 mm, mp 79 to 80°, and $[\alpha]_D^{22}$ +18.7° at equilibrium in water [2]. A second fraction, weighing 7.4 g, distilled between 170 and 180°; this higher-boiling fraction is a viscous sirup that does not reduce Fehling solution unless it is first hydrolyzed with dilute mineral acid.

Compound I, heated with Fehling solution, does not begin to show visible evidence of reaction until many minutes have elapsed. Cuprous oxide is then slowly precipitated, and its amount gradually increases over several hours.

A sample (0.020 g) of I, treated with 0.053 g of sodium metaperiodate in 10 ml of solution at room temperature, showed 0.1, 0.5, and 0.7 mole of periodate consumed per mole of I, in 2, 17, and 40 hr of reaction, respectively. On adding a droplet of ethylene glycol to a 1-ml aliquot of the mixture after 40 hr of reaction, one drop of 0.01 *N* sodium hydroxide brought the solution to the endpoint of bromothymol blue.

3.2. Calcium 2,3-*O*-Isopropylidene-D-lyxonate Dihydrate (II)

An aqueous solution of 0.95 g of I was treated alternately with 10 ml of 0.1 *N* iodine solution (0.25 *N* potassium iodide and 0.1 *N* iodine) and (dropwise) with 15 ml of 0.1 *N* sodium hydroxide, until a total of 110 ml of the former and 165 ml of the latter had been added. The additions required about 15 min, and, after 5 min additional, the mixture was cooled to 0° and passed through a column containing 60 ml of ice-cold, cation-exchange resin (see footnote 3). The effluent was collected in a stirred, aqueous slurry of 10 g of silver carbonate. After filtration of the suspension, the ice-cold filtrate was passed through an additional 10 ml of the resin. Neutralization of the effluent with calcium hydroxide was followed by concentration under diminished pressure and crystallization of II from 95-percent ethyl alcohol. The product was purified further by dissolution in absolute ethanol, filtration, evaporation, and recrystallization from 95-percent ethyl alcohol. Calcium 2,3-*O*-isopropylidene-D-lyxonate dihydrate was isolated in 80-percent yield; $[\alpha]_D^{22}$−46.5° (*c*,1; water).

Anal. Calculated for $C_{16}H_{26}CaO_{12}\cdot 2\,H_2O$: C, 39.5; H, 6.2; Ca, 8.2. Found: C, 39.2; H, 6.3; Ca, 8.2.

Acidification of a solution of 0.122 g of the salt with an equivalent proportion of hydrochloric acid changed the specific rotation to $[\alpha]_D^{22}$−22° (calculated as 2,3-*O*-isopropylidene-D-lyxonic acid), and no change in optical rotation was detected during the next 5 min. However, on addition of a second equivalent proportion of acid, the observed optical rotation[5] changed in several hours from −1.24 °S to values higher than +2.9 °S, then decreased slowly, and finally increased very slowly during the next 10 days to +2.6 °S.

3.3. 2,3-*O*-Isopropylidene-D-lyxono-1,4-lactone (III) From II

An ice-cold aqueous solution of 0.68 g of II was passed through a column containing 10 ml of ice-cold, cation-exchange resin (see footnote 3), and the effluent was freeze-dried. The dried residue was crystallized from benzene; yield, 90 percent; mp 99 to 100°; $[\alpha]_D^{22}$+106°, initially (*c*, 1.6; water). The initial observed rotation, +9.9 °S, decreased to +3.6 °S in 22 days.

Anal. Calculated for $C_8H_{12}O_5$: C, 51.0; H, 6.4. Found C, 51.1; H, 6.4.

3.4. Preparation of Compound III by Bromine Oxidation of I

A sample (0.19 g) of I, mixed with 1.2 g of barium carbonate, was treated at 0° with 20 ml of an ice-cold solution containing 1.2 g of barium bromide dihydrate, 0.4 ml of bromine, and 0.08 ml of concentrated hydrobromic acid. After 2.5 hr, ethylene was bubbled through the mixture, and the debrominated suspension was filtered. The specific optical rotation of the filtrate was about +100° and changed to +96° in the next 25 min. The filtrate was freeze-dried, and the residue, extracted with chloroform, gave, on evaporation of the extract, 0.16 g of crystalline III.

3.5. 2,3-*O*-Isopropylidene-D-lyxitol (IV)

To a stirred solution of 1.0 g of I in 5 ml of water at 0°, 0.175 g of sodium borohydride was added, and the solution was allowed to warm to room temperature. The next day, the solution was again cooled to 0°, treated with 5 ml of ice-cold, cation-exchange resin (see footnote 3), and then passed through a column containing an additional 5 ml of the ice-cold resin. The effluent was concentrated under diminished pressure (with absolute ethanol, to remove water), and the concentration was repeated

[4] Duolite A-4, a product of Chemical Process Co., Redwood City, Calif.

[5] Observed optical rotations, measured in a saccharimeter, are given in "degrees sugar" (°S). One degree circular equals 0.3462 times one degree sugar.

several times with methanol added (to remove boric acid as methyl borate). Crystalline IV was obtained in 80-percent yield from a solution in ethanol by the addition of pentane; mp 84.5–85.5°; $[\alpha]_D^{22}$ +10° (*c*, 2; water). A sirupy IV was reported by Ballou [11].

Anal. Calculated for $C_8H_{16}O_5$: C, 50.0; H, 8.4. Found: C, 50.2; H, 8.6.

3.6. 2,3-*O*-Isopropylidene-β-D-erythrofuranose (V)

A solution of 0.192 g of IV, treated with 0.225 g of sodium metaperiodate, showed within 5 min $[\alpha]_D^{22}$ −66° (calculated as V), and the rotation did not change in the next hour. For isolation of crystalline V, 0.95 g of I in 20 ml of water was reduced at room temperature with 0.1 g of sodium borohydride. After the solution had been kept overnight, carbon dioxide was bubbled through it for 1 hr, and then 1.18 g of sodium metaperiodate was added. One hour later, the mixture was repeatedly extracted with ether. The combined extracts were evaporated to dryness, to yield a crystalline residue. This was redissolved in ether, and the solution was filtered and re-evaporated. For purification, the product was sublimed at 0.03 mm at a bath temperature of 52°. An ether solution of the product gave, on drying, crystalline V; weight 0.7 g; mp 32.5—34.5°; $[\alpha]_D^{22}$ −68°→−66° in 2 min (*c*, 4.2; water); $[\alpha]_D^{22}$ −77.6°→−76.2° in 3 hr (*c*, 7; methanol). Sirupy V has been reported [11], and mp 29 to 31° and $[\alpha]_D^{20}$ +72° (in methanol) were reported [12] for the crystalline enantiomorph of V.

Anal. Calculated for $C_7H_{12}O_4$: C, 52.4; H, 7.5. Found: C, 52.6; H, 7.7.

A sample of V in water containing cation-exchange resin (see footnote 3) was heated at 80° for 1 hr. The hydrolyzate was chromatographed on paper. The compound migrated like an authentic specimen of D-erythrose that had been prepared from crystalline, "dimeric" 2,4-*O*-ethylidene-D-erythrose [9].

3.7. Calcium 2,3-*O*-Isopropylidene-D-erythronate Hemihydrate (VI)

The oxidation of 0.16 g of V with a mixture of 22 ml of 0.1 *N* iodine solution and 35 ml of 0.1 N sodium hydroxide was carried out as described in section 3.2. The crystalline product was obtained from 95-percent ethyl alcohol; weight, 0.17 g; $[\alpha]_D^{22}$ +65.6° (*c*, 1; water). It is hygroscopic; a sample was dried at 110° under vacuum before analysis.

Anal. Calculated for $C_{14}H_{22}CaO_{10} \cdot 0.5\ H_2O$: C, 42.1; H, 5.8; Ca, 10.0. Found: C, 42.3; H, 5.8; Ca, 10.2.

A solution (9 ml) of 0.0975 g of VI in water, on treatment with 1 ml of *N* hydrochloric acid, showed $[\alpha]_D^{22}$ +22.2° (l=2 dm) initially (calculated for 2,3-*O*-isopropylidene-D-erythronic acid). After 4 hr, the observed rotation (see footnote 5) was −1.7 °S, and, during the next 16 hr, the rotation at first continued to become more levorotatory and then less levorotatory; a final rotation of −1.25 °S was observed.

3.8. 2,3-*O*-Isopropylidene-D-erythrono-1,4-lactone (VII) From VI

A solution of 0.1 g of VI in ice-cold water was passed through a column of 5 ml of ice-cold, ion-exchange resin (see footnote 3), and was then concentrated under diminished pressure to a thin sirup and reconcentrated several times with absolute ethanol; VII crystallized from the sirup. The product was recrystallized from ice-cold ether; yield 0.06 g; mp 65 to 67.5°; initial $[\alpha]_D^{22}$ −116° (*c*, 1; water). The rotation (see footnote 5), observed in a 2-dm tube, changed to −1.2 °S in 6 days.

Anal. Calculated for $C_7H_{10}O_4$: C, 53.2; H, 6.4. Found: C, 53.0; H, 6.4.

A sample of VII in water was hydrolyzed by means of a cation-exchange resin (see footnote 3) at 80° for 2 hr, and paper chromatography of the hydrolyzate showed a product that migrated like D-erythrono-1,4-lactone [10].

3.9. Preparation of VII by Bromine Oxidation of V

A stirred solution of 0.164 g of V in 10 ml of ice-cold water was treated with 1.2 g of barium carbonate, and with 10 ml of a solution containing 1.2 g of barium bromide dihydrate, 0.4 ml of bromine, and 0.08 ml of concentrated hydrobromic acid. After 2 hr, the mixture was debrominated with ethylene, and filtered; the filtrate had $[\alpha]_D^{22}$ −103°, and this slowly changed to less levorotatory values. The solution was quickly extracted several times with chloroform, and evaporation of the combined extracts gave VII in about 90-percent yield.

3.10. 1,5-Di-*O*-acetyl-2,3-*O*-isopropylidene-α-D-lyxofuranose

A solution of 1 ml of acetic anhydride in 9 ml of pyridine rapidly dissolved 0.3 g of I. After 18 hr at room temperature, 50 g of ice (from distilled water) was added, and the mixture was stirred until the ice had melted; the solution was then freeze-dried. On dissolving the sirupy residue in 1.0 ml of absolute ethanol, cooling the solution to 0°, and adding water dropwise, the crystalline diacetate was obtained in 90-percent yield; mp 49.5–50.5°; $[\alpha]_D^{22}$ +62.8° (*c*, 1; chloroform).

Anal. Calculated for $C_{12}H_{18}O_7$: C, 52.5; H, 6.6. Found: C, 52.3; H, 6.5.

3.11. 1,5-Di-*O*-benzoyl-2,3-*O*-isopropylidene-α-D-lyxofuranose

A solution of 0.25 g of I in 8 ml of pyridine and 2 ml of benzoyl chloride was kept at 0° for several hours and then at room temperature for 3 days. The mixture was poured into 100 ml of ice and water, and, after being stirred for 2 hr, was extracted with chloroform. The combined extracts were successively washed with aqueous sulfuric acid, aqueous sodium bicarbonate solution, and water, and then dried. The product was crystallized from ethanol; yield 0.3 g; mp 93.5—94.5°; $[\alpha]_{25}^{D}$ +17.3° (*c*, 1; chloroform).

Anal. Calculated for $C_{22}H_{22}O_7$: C, 66.3; H, 5.6. Found: C, 66.1; H, 5.6.

The author expresses his appreciation to H. S. Isbell and R. S. Tipson for highly valued discussions and encouragement throughout this work; to E. R. Deardorff and R. J. Bowen for the microanalyses; and to S. C. Wait, Jr., J. J. Comeford, and F. P. Czech for recording the infrared absorption spectra of the compounds described.

4. References

[1] R. S. Tipson, H. S. Isbell, and J. E. Stewart, J. Research NBS **62,** 257 (1959) RP2960.
[2] P. A. Levene and R. S. Tipson, J. Biol. Chem. **115,** 731 (1936).
[3] S. A. Barker and R. Stephens, J. Chem. Soc. **1954,** 4550.
[4] K. Freudenberg and A. Wolf, Ber. **58,** 300 (1925); E. H. Goodyear and W. N. Haworth, J. Chem. Soc. **1927,** 3136.
[5] G. M. Kline and S. F. Acree, BS J. Research **5,** 1063 (1930) RP247.
[6] H. S. Isbell and C. S. Hudson, BS J. Research **8,** 327 (1932) RP418; H. S. Isbell, BS J. Research **8,** 615 (1932) RP441; H. S. Isbell, J. Am. Chem. Soc. **55,** 2166 (1933).
[7] M. Abdel-Akher, J. K. Hamilton, and F. Smith, J. Am. Chem. Soc. **73,** 4391 (1951).
[8] For a review of the periodate oxidation of carbohydrates, see J. M. Bobbitt, Advances in Carbohydrate Chem. **11;** 1 (1956).
[9] R. Schaffer, J. Am. Chem. Soc. **81,** 2838 (1959).
[10] O. Ruff, Ber. **32,** 3672 (1899).
[11] C. E. Ballou, J. Am. Chem. Soc. **79,** 165 (1957).
[12] J. N. Baxter and A. S. Perlin, Can. J. Chem. **38,** 2217 (1960).
[13] R. S. Rasmussen and R. R. Brittain, J. Am. Chem. Soc. **71,** 1073 (1949); S. A. Barker, E. J. Bourne, R. M. Pinkard, and D. H. Whiffen, Chem. & Ind. (London) **1958,** 658.
[14] C. S. Hudson, J. Am. Chem. Soc. **31,** 66 (1909).

(Paper 65A6–133)

JOURNAL OF RESEARCH of the National Bureau of Standards—A. Physics and Chemistry
Vol. 65A, No. 6, November-December 1961

Effect of Perchloryl Fluoride Additions on the Flame Speed of Methane

Carl Halpern

(June 7, 1961)

The effects of addition of small quantities of perchloryl fluoride and of oxygen on the flame speed of methane-air mixtures have been determined and are compared with each other and with the effect of moderately preheating the burning mixture. Only small additions of perchloryl fluoride, up to 3 percent by volume, could be used because of the corrosiveness of its combustion products. Perchloryl fluoride is more effective than oxygen in increasing the flame speed of methane but less effective, in the amounts added, than preheating the burning mixture to 330°F. Maximum flame speeds for given experimental conditions were found to vary linearly with increasing additions of either perchloryl fluoride or oxygen.

1. Introduction

The determination of the effect on flame speed of small additions of perchloryl fluoride was carried on concurrently with another task in which gross effects in the combustion of hydrocarbons with perchloryl fluoride addition in a large duct were measured. Results of experiments in the duct reflected the combined influences of high temperature, variation of pressures, turbulence, and fuel-oxidant mixture ratio. Since closer control of conditions is possible in a small burner, the effects of the parameters considered on the flame speed are more clearly identified, and thus the information obtained is more basic. Methane was chosen as the fuel because we had had much experience in the determination of flame speeds of methane-air mixtures. At the conclusion of the experiments with perchloryl fluoride, a series of experiments was run with similar quantities of oxygen added to methane-air mixtures to compare the effects of oxygen and perchloryl fluoride.

Perchloryl fluoride (ClO_3F) is a relatively new compound, discovered in 1952 [1].[1] It is stated [2] to be an inert gas at room temperature, stable and noncorrosive when dry; its freezing point is −146 °C and its boiling point is −46.8 °C. In the presence of water, it is very corrosive to most metals. Its heat of formation is −5.12 kcal/mole [3]; thus it can be expected, under the proper conditions, to be very active chemically, with high heats of reaction.

Lodwig and Margrave [4], in a study of perchloryl fluoride flames, have reported a few determinations of the flame speeds of mixtures of 65–75 percent methane and 35–25 percent perchloryl fluoride, by volume. Their values for flame speeds of these mixtures range from about 185 to 195 cm/sec (centimeters per second) and average about 190 cm/sec (6.2 fps) (feet per second). However, their method for determining flame speeds, which is based on the measurement of the area of the visible inner cone of a Bunsen flame, is not now considered to yield reliable values. The preferred method is considered to be that based on the measurement of the schlieren cone [5, 6].

2. Apparatus and Procedure

A description of the apparatus and the method used to measure flame speeds has been presented earlier [7]. Briefly, this apparatus comprises drying and metering systems for both air and fuel, a conditioning chamber for the mixture of fuel and oxidant, and a nozzle, the exit of which is the burner port. Means are provided to control the temperature of the combustible mixture issuing from the nozzle.

For the present experiments it was decided to prepare mixtures of air and the added oxidant (perchloryl fluoride or oxygen) of the desired strength and to meter this mixture, rather than to set up a third metering system. Some error in the measurement of the flow of these mixtures was inevitable, since the calibration of the sharp-edged orifice used to meter the gas depended on the density of the gas. However, in view of the small quantities of additive used (5 percent by volume maximum for perchloryl fluoride and 6 percent for oxygen), it was felt that the error so introduced would be tolerable. The mixtures of air and added oxidant were prepared in a 120 gal (16.05 cu ft) galvanized steel tank. The tank was evacuated to a pressure of several microns, and the oxidant was admitted from its container; pressure of the oxidant was measured by a mercury

[1] Figures in brackets indicate the literature references at the end of this paper.

manometer, read to 0.01 in. Air from a compressor was dried by passing first through a column of activated alumina and then through a cold trap immersed in a slush of dry ice in a mixture of equal parts by weight of carbon tetrachloride and chloroform. It was then slowly admitted to the tank. Water content was thus kept to 0.03 percent by volume. The final pressure in the mixing tank was generally about 150 psig and was read on a calibrated Bourdon gage to 0.1 lb.

Because the products of combustion of perchloryl fluoride include hydrogen chloride and hydrogen fluoride, the exhaust gas was drawn by a large capacity vacuum pump from the enclosure surrounding the burner nozzle, and then through a chamber packed with copper turnings before being exhausted into the air.

Mixtures of 0.5, 1, 2, 3, 4, and 5 percent by volume of perchloryl fluoride in air were prepared. For each mixture, attempts were made to determine the variation of flame speed with mixture ratio, by weight, of methane to air plus added perchloryl fluoride, with the velocity of the gas at the port of the nozzle held constant. The mixture ratio ranged from 0.054 to 0.072 and the velocity of the gas mixture at the port of the nozzle ranged from 4 to 7 fps.

Burning mixtures prepared with methane and air containing 1 and 2 percent, respectively, by volume of perchloryl fluoride yielded stable flames over the entire range of mixture ratios and gas velocities used.

Table 1 lists the conditions at which blowoff and flashback were encountered with the other mixtures. Blowoff represents the lean limit of operation of the burner, at which flames cannot be maintained; flashback represents the rich limit of operation.

TABLE 1. *Limits of operation of burner*

Percent ClO_3F by volume added to air	Percent O_2 by volume added to air	$\frac{\text{wt methane}}{\text{wt air+oxidant}}$	Gas velocity fps
		Blowoff	
0.5	0	0.054	6
.5	0	.056	6
.5	0	.054	7
.5	0	.056	7
0	.5	.054	6
0	.5	.054	7
0	.5	.056	7
0	1.0	.054	6
0	1.0	.054	7
0	2.0	.054	7
		Flashback	
3.0	0	.066	4
0	6.0	.066	4

Formation of a white deposit on the lip of the port of the nozzle during combustion of methane with air-perchloryl fluoride mixtures interfered with the gas flow and resulted in unstable, misshapen flames. Hydrogen fluoride and hydrogen chloride in the mantle of hot gas surrounding the inner cone of the flame undoubtedly had reacted with the metal of the nozzle to form a mixture of chlorides and fluorides. This deposit of salts was soft and easily removed. Rate of deposition was slow with weak mixtures of perchloryl fluoride and air; with proper care, stable conical flames were maintained. Rate of deposition with 4 and 5 percent mixtures, however, was so fast that undistorted flames could not be maintained. Hence, flame speeds could not be determined.

In a zone beginning about 0.03 in from the lip of the port of the nozzle and extending for about 0.2 in, the metal was eaten away to a depth of about 0.02 in, leaving a thin rim of untouched metal surrounding the port of the nozzle. During the first experiments with the 3 percent mixture of perchloryl fluoride, this rim burned through at one spot, thus creating permanently distorted flames. Experimentation with perchloryl fluoride was discontinued and the nozzle was removed from the burner system for repairs. Of the six bronze screens used to smooth the gas flow in the conditioning chamber of the burner assembly, the two top ones were heavily corroded and had to be replaced. Since flashback of perchloryl fluoride flames had taken place several times, it was felt that the corrosion of the screens was a result of these occurrences. The other four screens were in good condition. The reflecting surface of the spherical mirror used to focus light on the schlieren stop was eaten away in spots; this mirror was also replaced. The sharp-edged orifice used to meter the mixtures of air and perchloryl fluoride was in good condition.

Mixtures of air and 0.5, 1, 2, 3, 4, 5, and 6 percent, by volume, of added oxygen were prepared. Variation of flame speed with mixture ratio, by weight, of methane to air plus added oxygen was determined for each mixture. Velocity of the effluent gas at the nozzle port was held constant. As in the case of perchloryl fluoride, mixture ratio varied from 0.054 to 0.072, and gas velocity ranged from 4 to 7 fps.

Burning mixtures made from air containing 3, 4, and 5 percent by volume of added oxygen gave stable flames over the entire range of mixture ratios and gas velocities used. Table 1 lists the conditions at which blowoff and flashback occurred with mixtures of other strengths. As mentioned above, these represent the lean and rich limits of operation for the burner.

The temperature controlled nozzle was used throughout these experiments, but the control of temperature was not as good as had been in previous experiments. Because of the limited supply of oxidant mixture, the nozzle could not be brought to thermal equilibrium, so there was a change in temperature during an individual run. The largest temperature change during a run of about three hours' duration was a rise of nine degrees Fahrenheit; generally the temperature change did not exceed five degrees. Since the fluid circulating in the nozzle was cooled by tap water, temperature of the nozzle and hence of the incoming combustible mixture depended on the temperature of the tap water; as the experiments reported here lasted over a year, there was considerable seasonal variation

in the nozzle temperature. The winter temperature was about 80–85 °F, while the summer temperature was about 95–100 °F. The variation of flame speed with mixture temperature for methane-air flames had been found to be 0.0048 ft/°F [7]. The effect of temperature on methane-air-perchloryl fluoride and methane-air-oxygen flames, especially at low concentration of additives, should be of similar magnitude. Over a temperature range of 15 °F, this would amount to about 0.07 fps. For a flame speed of about 1.5 fps, poor temperature control could introduce a variation of about 7 percent between summer and winter, and about 2 percent in an individual determination when the change of the temperature of the nozzle and of the incoming combustible mixture is 5 °F.

3. Results

Results of the addition of perchloryl fluoride are shown in figures 1 and 2. Figure 1 shows the variation of flame speed with mixture ratio, by weight, of methane to air plus perchloryl fluoride at gas velocities, measured at the port of the nozzle, of 4, 5, 6, and 7 fps, when 0.5, 1, 2, and 3 percent by volume, respectively, of perchloryl fluoride was added to the combustion air. Results obtained with burning mixtures made from the 0.5 and 1 percent perchloryl fluoride-air mixtures show the flame speed increasing as the mixture becomes richer in fuel, rising to a maximum and then decreasing. With the 2 percent mixture, the flame speed increases as the burning mixture becomes richer in fuel, and a maximum value seems to occur at mixture ratio of 0.072. Only one set of observations could be made with the 3 percent mixture; at a gas velocity of 6 fps, flame speed increased as the burning mixture became richer in fuel until flashback occurred at a mixture ratio of 0.066. Maximum flame speeds and the experimental conditions at which they occurred are listed in table 2.

TABLE 2.—*Maximum flame speeds for perchloryl fluoride addition and the experimental conditions at which they were obtained*

Flame speed fps	wt methane / wt air + ClO_3F	Percent ClO_3F by volume added to air	Gas velocity fps	Gas temp. °F
1.449	0.068	0.5	4	87.8
1.475	.066	.5	5	88.0
1.480	.065	.5	6	88.1
1.455	.066	.5	7	88.4
1.652	.070	1.0	4	93.1
1.611	.066	1.0	5	90.6
1.705	.070	1.0	6	92.4
1.690	.072	1.0	7	94.4
1.970	.072	2.0	4	85.7
2.082	.072	2.0	5	90.3
1.770	.072	2.0	6	89.7
2.123	.072	2.0	7	88.4
2.386	.064*	3.0	6	82.0

* Flashback occurred at 0.066.

As may be noted from the data listed in table 2, the addition of perchloryl fluoride to the combustible mixture shifted the mixture ratio at which maximum flame speed occurs. It had been found previously [7] that maximum flame speed, 1.233 fps, for methane-air at a temperature of 84.4 °F occurred at mixture ratio of 0.062. The addition of 2 percent by volume of perchloryl fluoride moved the maximum flame speed to a mixture ratio for methane to air plus perchloryl fluoride of 0.072.

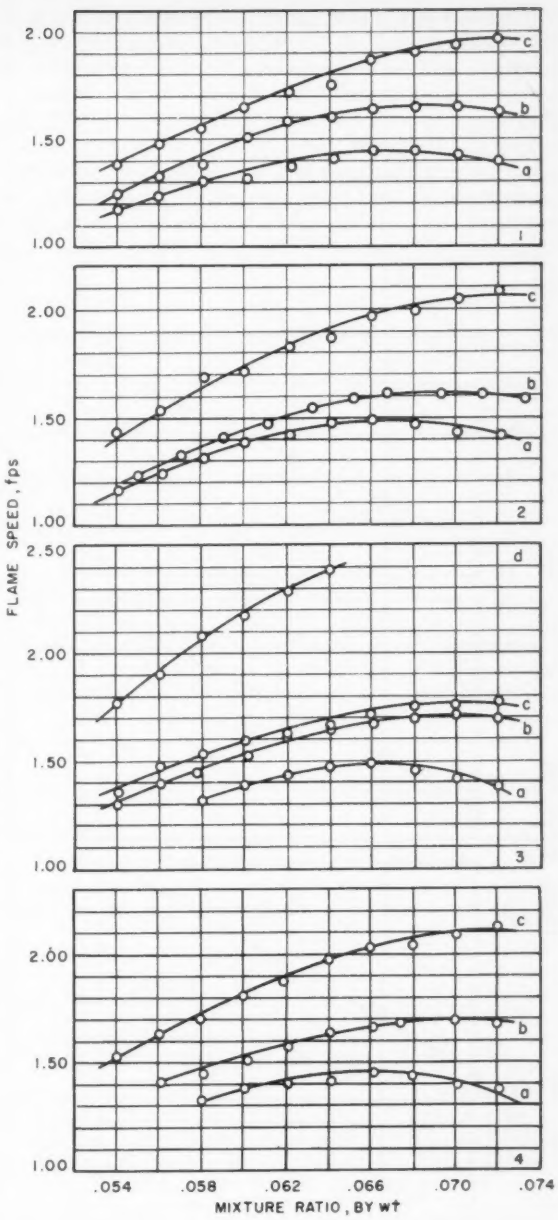

FIGURE 1. *Effect of mixture ratio, by weight, of methane to air plus perchloryl fluoride on flame speed.*

Percent, by volume, of added perchloryl fluoride=a, 0.5; b, 1.0; c, 2.0; and d, 3.0. Gas velocity=1, 4 fps; 2, 5 fps; 3, 6 fps; and 4, 7 fps.

Theoretically, flame speed is a property of the fuel and oxidant and of the physical condition of the mixture, and is independent of the apparatus in which it is measured. Hence, it was not expected that there be any variation of flame speed with gas velocity. However, there proved to be some variation. The 0.5 percent mixture of perchloryl fluoride in air showed practically no variation for lean burning mixtures. At richer mixtures, fuel-air plus perchloryl fluoride ratios of 0.068 and higher, there was a slight decrease of flame speed as gas velocity increases, which amounted to about 1.5 percent of the average value of the flame speed. The 1 percent mixture showed a small increase of flame speed as the gas velocity increases, also with a variation of about 1.5 percent. The 2 percent mixture showed a larger ncrease of flame speed with gas velocity, with a variation of 5 percent. (If the value of flame speed at 6 fps, which seems much too low, is ignored, then the variation becomes about 3 percent.) The flame speeds considered here have been corrected for temperature. The reasons for the variation of flame speed with gas velocity are obscure. Since these variations are small, they may be due to experimental difficulties, such as locating the flame front in the enlargements of the flame photographs, and thus they may fall within the experimental error. However, the trends seem to be consistent and, since a similar variation of flame speed with gas velocity had been found for methane-air flames previously [7], it is felt that the variation does exist. Conditions of the gas flow in the throat of the nozzle, e.g., the presence or absence, and the extent, of a boundary layer, are the most likely cause.

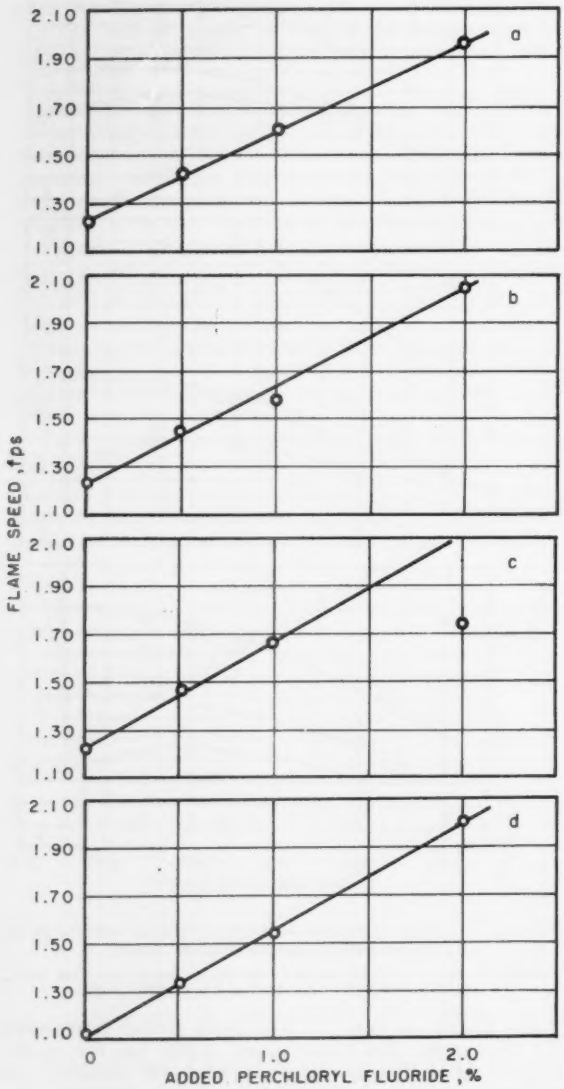

FIGURE 2. *Effect of added perchloryl fluoride on maximum flame speed.*

Gas velocity=a, 4 fps; b, 5 fps; c, 6 fps; and d, 7 fps.

From the data which are listed in table 5, it may be shown that flame speed increases linearly with increasing percentage of perchloryl fluoride, at least over the small range of perchloryl fluoride addition covered here, and as the burning mixture becomes richer in fuel, the rate of increase of flame speed becomes larger. The values of flame speed at 0 percent perchloryl fluoride, that is, for a methane-air flame, are taken from our previous work [7]. In figure 2 is shown the relation of maximum flame speed for each gas velocity to the percentage of perchloryl fluoride added. Maximum flame speed varies linearly with the percentage of added perchloryl fluoride, and the rate of increase at each gas velocity is about the same.

Figures 3 and 4 show the effect of addition of oxygen on the flame speed of methane-air mixtures. Figure 3 shows the variation of flame speed with mixture ratio, by weight, of methane to air plus oxygen at constant gas velocity and at various strengths of added oxygen. The maximum flame speeds observed for each set of experimental conditions are listed in table 3. It can be noted in figure 3 that, at low percentages of added oxygen, as the burning mixture becomes richer in fuel, the flame speed increases to a maximum and then decreases. As the burning mixture becomes richer in oxygen, the value of the mixture ratio at which the flame speed is a maximum gradually changes toward the fuel-rich side, and at 5 percent added oxygen, the maximum flame speed occurs about fuel to air plus oxygen ratio of 0.072. With 6 percent added oxygen, the maximum flame speed occurs beyond 0.072; i.e., an inflection point is not observed.

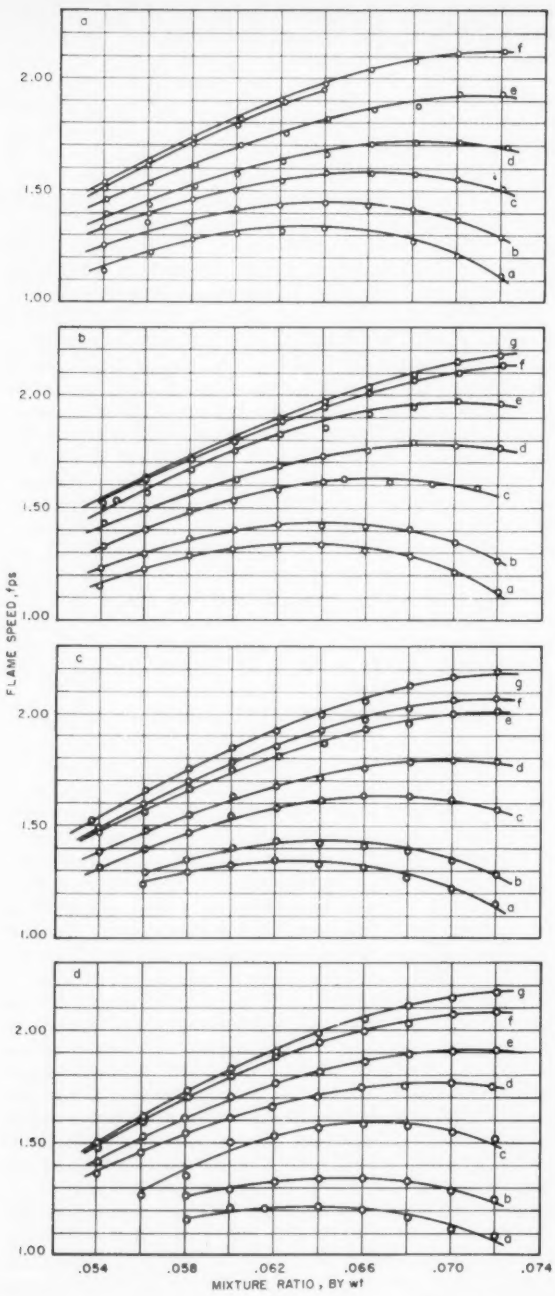

FIGURE 3(d). *Effect of mixture ratio, by weight, of methane to air plus added oxygen on flame speed.*
Percent added oxygen=a, 0.5; b, 1.0; c, 2.0; d, 3.0; e, 4.0; f, 5.0; and g, 6.0. Gas velocity=A, 4 fps; B, 5 fps· C, 6 fps; and D, 7 fps.

Flame speeds of methane-air mixtures to which oxygen had been added also proved to vary somewhat with gas velocity. In general, the flame speed decreased as the gas velocity increased. However,

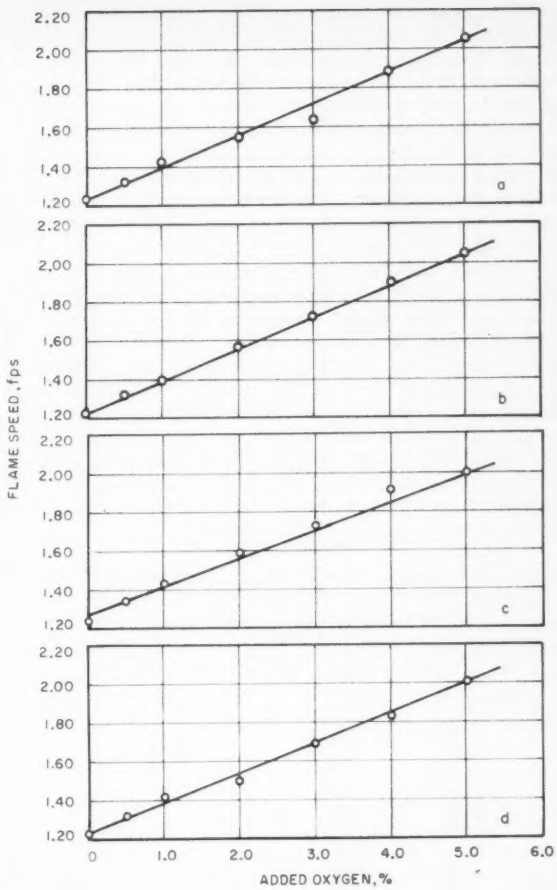

FIGURE 4. *Effect of added oxygen on maximum flame speed.*
Gas velocity=a, 4 fps; b, 5 fps; c, 6 fps; and d, 7 fps.

there were a few instances where an increase of flame speed with increasing gas velocity occurred: at 0.5 percent oxygen addition, at mixture ratio of 0.072; at 1 percent oxygen addition, at mixture ratio of 0.072; and at 6 percent oxygen addition, at mixture ratios of 0.056, 0.058, 0.060, 0.062, 0.064, 0.066, and 0.068. These variations of flame speeds, whether increase or decrease, are small and amount to about 1.2 percent of the average value of the flame speed. The flame speeds considered here have been corrected for temperature.

The data which are displayed in table 6 show the effect of increasing the amount of oxygen in the combustible mixture on the flame speed. It may be shown that flame speed increases linearly as the amount of oxygen is increased up to the addition of 4 or 5 percent; then the rate of increases changes abruptly and becomes less; the increase appears to be still linear. This effect is seen at all mixture ratios of fuel to air plus oxygen that were used and at all gas velocities. However, at gas velocities of 6 and 7 fps, the effect is less pronounced than at 4 and 5 fps. The rate of increase of flame speed (up

to 4 or 5 percent oxygen added) is greater with mixtures that are fuel-rich. If, as in figure 4, the maximum flame speed observed for each experimental condition is plotted against the percentage of oxygen added to the combustible mixture, then the result is a straight line and the slopes of the lines at each gas velocity are of similar magnitude. The values of flame speeds for 0 percent oxygen addition, that is, for methane-air, are taken from [7]. Since the maximum addition of oxygen was only 6 percent, one might question if there would not be a break in the curve at large oxygen addition. Lewis and von Elbe [8] reproduce a figure taken from the work of Jahn in which flame speed is plotted against the concentration of methane for "combustion airs" containing from 21 to 98.5 percent by volume of oxygen. A line drawn through the maximum flame speed found for each condition of "combustion air" is practically a straight line, showing a very slight degree of curvature, so that from 21 to 40 percent, by volume, of oxygen, the line is straight. In our experiments oxygen in the "combustion air" varied from 21 to 25.5 percent by volume.

TABLE 3. *Maximum flame speeds for oxygen addition and the experimental conditions at which they were obtained*

Flame speed fps	wt methane / wt air + oxygen	Percent O_2 by volume added to air	Gas velocity fps	Gas temp. °F
1 322	0.064	0.5	4	84 9
1.333	.064	.5	5	84.3
1.343	.062	.5	6	87.2
1.318	.064	.5	7	86.9
1.440	.064	1.0	4	88.2
1.422	.062	1.0	5	88.6
1.436	.062	1.0	6	88.0
1.443	.066	1.0	7	91.7
1.583	.064	2.0	4	92.4
1.634	.065	2.0	5	95.7
1.634	.068	2.0	6	97.4
1.581	.066	2.0	7	95.2
1.707	.070	3.0	4	100.0
1.788	.068	3.0	5	97.0
1.786	.070	3.0	6	98.4
1.765	.070	3.0	7	101.3
1.930	.070	4.0	4	95.3
1.970	.072	4.0	5	98.4
2.004	.072	4.0	6	102.4
1.915	.072	4.0	7	102.4
2.118	.072	5.0	4	98.3
2.139	.072	5.0	5	100.5
2.067	.072	5.0	6	101.2
2.080	.072	5.0	7	101.9
1.943	*.064	6.0	4	91.2
2.169	>.072	6.0	5	93.8
2.187	>.072	6.0	6	95.8
2.172	>.072	6.0	7	93.9

*Flash-back occurred at 0.066.

If it is assumed that the relation between maximum flame speed and oxygen content is, in fact, linear, then from the slope of the curves in figure 4 the maximum flame speed of methane in oxygen is estimated to be 16.5 fps (503 cm/sec). For comparison with experimental values, Jahn [9] gives 330 cm/sec, Fiock [10] lists 393 cm/sec, Singer and Heimel [11] give 445 cm/sec, and Singer, Grumer, and Cook [12] give 375 and 440 cm/sec for different types of burners. In a like manner from data given in figure 2, it is possible to estimate the maximum flame speed for methane and perchloryl fluoride to be about 42 fps (1,280 cm/sec). However, since the extrapolation involved is quite large, and the assumed linearity of the relation of maximum flame speed with added perchoryl fluoride over the entire range up to 100 percent perchlorly fluoride quite uncertain, this value of 42 fps should be regarded with caution.

The addition of perchloryl fluoride is more effective than the addition of oxygen in increasing the flame speeds of methane-air mixtures. The greatest flame speed observed in these experiments was 2.386 fps; this occurred with the addition of 3 percent perchloryl fluoride by volume to the combustion air at a mixture ratio, by weight, of methane to air plus perchloryl fluoride of 0.064. The gas velocity was 6 fps, the gas temperature, was 82.0 °F and the water content was 0.03 percent by volume. The greatest flame speed observed on addition of oxygen was 2.187 fps; this was found with the addition of 6 percent oxygen by volume to the combustion air. Mixture ratio, by weight, of methane to air plus oxygen was 0.072, gas velocity was 6 fps, gas temperature was 95.8 °F, and water content was 0.03 percent by volume. The above values for flame speeds should be compared with a maximum flame speed of 1.233 fps for a methane-air flame, mixture ratio, by weight, of methane to air of 0.062, gas velocity of 6 fps, gas temperature of 84.4 °F, and water content, 0.03 percent by volume.

The heat of combustion of methane burning in perchloryl fluoride is calculated to be −215.1 kcal/mole, while the heat of combustion of methane in oxygen is only −191.8 kcal/mole. Since there is more energy available in the perchloryl fluoride reaction, it is to be expected that flame speeds should be larger.

The flame speed of methane-air mixtures had been found previously [7] to depend strongly on the initial temperature of the combustible mixture. Increasing the temperature increased the flame speed. At 330 °F, the highest temperature used, maximum flame speed was 2.463 fps at a mixture ratio, by weight, of methane to air of 0.062. Gas velocity was 5 fps at the port of the nozzle and the water content was 0.03 percent by volume. This value of flame speed should be compared to 2.386 fps, the greatest found for perchloryl fluoride addition, and 2.187 fps for oxygen addition in the ranges covered in this report. From our previous work [7], it was found that to attain a flame speed of 2.386 fps in a methane-air flame, it was necessary to preheat the mixture to about 320 °F and to attain 2.187 fps, an initial gas temperature of about 295 °F is needed. Hence, it is apparent that a moderate increase in the initial temperature of the methane-air mixture is more effective in increasing flame speeds than is the addition of small quantities of other oxidants.

4. Experimental Observations

Tables 4, 5, and 6 present in detail some observations on the effect of some variables on the flame speed.

TABLE 4. *Effect of some variables on flame speed*

Wt methane / Wt air +ClO_3F	Flame speed fps	Gas temperature °F	Wt methane / Wt air +C_2	Flame speed fps	Gas temperature °F
A. 0.5 percent by volume ClO_3F added to air					
1. Gas velocity=4 fps			**2. Gas velocity=5 fps**		
0.05404	1.172	85.2	0.05407	1.159	88.5
.05597	1.233	85.7	.05661	1.241	85.2
.05805	1.303	86.1	.05809	1.315	86.1
.06017	1.320	86.4	.06003	1.385	86.7
.06217	1.376	86.8	.06212	1.418	87.2
.06414	1.418	87.2	.06406	1.470	87.8
.06603	1.445	87.4	.06606	1.475	88.0
.06802	1.449	87.8	.06806	1.462	88.4
.07006	1.421	88.0	.07014	1.429	88.9
.07191	1.400	87.4	.07212	1.412	88.9
3. Gas velocity=6 fps			**4. Gas velocity=7 fps**		
0.05802	1.315	88.6	0.05804	1.320	89.3
.06003	1.379	85.7	.06002	1.379	89.7
.06206	1.430	86.7	.06200	1.404	90.1
.06401	1.468	87.3	.06404	1.406	88.3
.06601	1.480	88.1	.06608	1.455	88.4
.06804	1.458	88.6	.06797	1.434	89.0
.07002	1.414	89.2	.07006	1.391	89.4
.07201	1.384	89.6	.07201	1.370	89.9
B. 1 percent volume ClO_3F added to air					
1. Gas velocity=4 fps			**2. Gas velocity=5 fps**		
0.05404	1.250	87.9	0.05496	1.234	91.0
.05603	1.328	88.6	.05701	1.321	91.0
.05802	1.380	89.2	.05903	1.406	90.6
.06012	1.504	89.8	.06108	1.473	91.8
.06201	1.578	90.3	.06312	1.546	89.9
.06410	1.600	90.7	.06513	1.580	90.6
.06603	1.641	91.2	.06669	1.611	91.1
.06807	1.646	92.8	.06926	1.608	89.6
.07007	1.652	93.0	.07128	1.600	89.6
.07208	1.637	93.1	.07332	1.587	91.6
3. Gas velocity=6 fps			**4. Gas velocity=7 fps**		
0.05404	1.306	91.1	0.05606	1.403	95.1
.05605	1.401	91.5	.05815	1.452	91.9
.05780	1.457	91.4	.06027	1.510	91.4
.06015	1.526	90.6	.06208	1.569	88.2
.06204	1.627	93.4	.06411	1.625	90.0
.06402	1.646	91.5	.06609	1.664	91.2
.06606	1.674	90.8	.06735	1.676	92.7
.06802	1.690	91.8	.07011	1.690	94.4
.07003	1.705	92.4	.07205	1.669	95.6
.07204	1.690	93.2			
C. 2 percent by volume ClO_3F added to air					
1. Gas velocity=4 fps			**2. Gas velocity=5 fps**		
0.05403	1.381	82.2	0.05402	1.435	84.9
.05596	1.482	82.5	.05601	1.534	86.0
.05798	1.544	83.1	.05807	1.681	86.5
.06003	1.649	83.6	.06004	1.712	86.6
.06197	1.719	83.6	.06207	1.828	87.7
.06404	1.754	85.0	.06407	1.869	88.4
.06597	1.871	85.0	.06604	1.969	88.9
.06801	1.903	85.6	.06809	1.987	89.0
.07000	1.945	85.9	.07009	2.043	89.7
.07200	1.970	85.7	.07201	2.082	90.3
3. Gas velocity=6 fps			**4. Gas velocity=7 fps**		
0.05409	1.357	87.9	0.05397	1.527	83.4
.05609	1.474	88.4	.05600	1.632	84.2
.05806	1.530	88.8	.05799	1.697	84.8
.06006	1.593	89.8	.06000	1.800	85.2
.06207	1.609	84.4	.06187	1.889	85.8
.06404	1.660	86.4	.06401	1.969	86.0
.06597	1.710	87.8	.06600	2.027	86.5
.06801	1.743	88.4	.06796	2.036	87.2
.07002	1.758	89.1	.06999	2.092	87.9
.07206	1.770	89.7	.07199	2.123	88.4

TABLE 4. *Effect of some variables on flame speed*—Continued

Wt methane / Wt air +ClO_3F	Flame speed fps	Gas temperature °F	Wt methane / Wt air +O_2	Flame speed fps	Gas temperature °F
D. 3 percent by volume ClO_3F added to air			**A. 0.5 percent by volume O_2 added to air**		
1. Gas velocity=6 fps			**1. Gas velocity=4 fps**		
0.05400	1.771	80.0	0.05411	1.140	80.4
.05601	1.904	79.8	.05612	1.223	81.4
.05802	2.079	80.4	.05807	1.279	82.4
.06003	2.168	80.3	.06031	1.305	83.4
.06205	2.276	80.6	.06210	1.318	84.3
.06400	2.386	82.0	.06399	1.322	84.9
			.06807	1.268	86.0
			.07001	1.209	86.4
			.07210	1.129	86.8

Wt methane / Wt air +O_2	Flame speed fps	Gas temperature °F	Wt methane / Wt air +O_2	Flame speed fps	Gas temperature °F
A. 0.5 percent by volume O_2 added to air					
2. Gas velocity=5 fps			**3. Gas velocity=6 fps**		
0.05398	1.147	81.3	0.05600	1.240	86.1
.05598	1.221	81.7	.05803	1.297	86.6
.05802	1.280	82.5	.06000	1.326	86.9
.05999	1.312	83.1	.06200	1.343	87.2
.06201	1.327	83.8	.06399	1.329	84.0
.06401	1.333	84.3	.06600	1.319	84.8
.06598	1.308	85.1	.06799	1.268	85.7
.06799	1.284	85.6	.07001	1.223	86.4
.07003	1.215	86.1	.07199	1.158	86.9
.07203	1.127	86.6			
A. 0.5 percent by volume O_2 added to air			**B. 1.0 percent by volume O_2 added to air**		
4. Gas velocity=7 fps			**1. Gas velocity=4 fps**		
0.05803	1.258	89.7	0.05404	1.255	84.3
.06005	1.305	90.5	.05599	1.358	85.3
.06172	1.305	86.3	.05796	1.359	86.1
.06400	1.318	86.9	.06004	1.418	86.7
.06601	1.301	87.6	.06202	1.432	87.4
.06804	1.271	88.5	.06406	1.440	88.2
.07001	1.219	89.4	.06596	1.433	88.0
.07201	1.187	90.4	.06801	1.416	89.2
			.07003	1.363	89.7
			.07206	1.298	90.1
B. 1.0 percent by volume O_2 added to air					
2. Gas velocity=5 fps			**3. Gas velocity=6 fps**		
0.05406	1.224	86.0	0.05604	1.293	90.6
.05598	1.284	86.8	.05799	1.352	90.8
.05801	1.359	87.4	.06003	1.404	91.3
.06003	1.400	88.0	.06203	1.436	88.0
.06201	1.422	88.6	.06400	1.426	88.8
.06402	1.418	89.4	.06600	1.411	89.4
.06607	1.417	89.9	.06802	1.384	90.1
.06803	1.402	90.3	.07003	1.347	90.7
.07006	1.342	90.6	.07202	1.260	91.1
.07204	1.267	91.0			
B. 1.0 percent by volume O_2 added to air			**C. 2.0 percent by volume O_2 added to air**		
4. Gas velocity=7 fps			**1. Gas velocity=4 fps**		
0.05802	1.365	93.6	0.05403	1.333	93.6
.05997	1.388	87.4	.05607	1.388	89.6
.06202	1.422	88.7	.05807	1.459	90.4
.06401	1.440	89.8	.05999	1.497	91.0
.06598	1.443	91.7	.06207	1.538	91.7
.06803	1.429	92.4	.06404	1.583	92.4
.07000	1.389	92.8	.06612	1.579	92.8
.07196	1.351	93.7	.06813	1.571	93.3
			.07008	1.543	93.7
			.07216	1.507	94.0

TABLE 4. *Effect of some variables on flame speed*—Continued

Wt methane / Wt air +O_2	Flame speed fps	Gas temperature °F	Wt methane / Wt air +O_2	Flame speed fps	Gas temperature °F
2. Gas velocity=5 fps			3. Gas velocity=6 fps		
0.05412	1.334	97.0	0.05405	1.319	97.3
.05604	1.400	92.4	.05609	1.397	93.2
.05804	1.480	93.4	.05808	1.467	94.1
.06008	1.531	94.0	.06004	1.540	94.7
.06206	1.579	94.5	.06206	1.574	95.4
.06308	1.611	95.1	.06407	1.614	96.3
.06502	1.634	95.7	.06602	1.622	96.7
.06704	1.617	96.1	.06804	1.634	97.4
.06898	1.607	96.7	.06999	1.613	97.8
.07104	1.583	97.1	.07205	1.576	98.4
C. 2.0 percent by volume O_2 added to air			D. 3.0 percent by volume of O_2 added to air		
4. Gas velocity=7 fps			1. Gas velocity=4 fps		
0.05602	1.371	96.6	0.05411	1.388	99.0
.05802	1.452	95.3	.05606	1.433	94.2
.06001	1.506	93.3	.05811	1.516	95.4
.06203	1.536	93.9	.06004	1.571	96.4
.06405	1.574	94.7	.06213	1.626	97.4
.06602	1.581	95.2	.06409	1.659	98.1
.06805	1.579	96.0	.06615	1.704	98.8
.07001	1.551	96.5	.06815	1.707	99.4
.07200	1.523	97.3	.07011	1.707	100.0
			.07226	1.696	100.5
D. 3.0 percent by volume of O_2 added to air			3. Gas velocity=6 fps		
2. Gas velocity=5 fps					
0.05413	1.429	97.7	0.05408	1.386	98.4
.05608	1.491	99.3	.05610	1.479	93.7
.05809	1.563	94.4	.05808	1.554	94.8
.06010	1.624	95.0	.06006	1.627	95.5
.06210	1.679	95.4	.06204	1.672	96.0
.06407	1.724	96.1	.06404	1.714	96.8
.06610	1.758	96.7	.06608	1.754	97.4
.06813	1.788	97.0	.06806	1.784	98.0
.07011	1.776	97.7	.07007	1.786	98.4
.07208	1.767	98.0	.07204	1.781	98.7
D. 3.0 percent by volume O_2 added to air			E. 4.0 percent by volume O_2 added to air		
4. Gas velocity=7 fps			1. Gas velocity=4 fps		
0.05396	1.359	100.4	0.05415	1.459	91.0
.05594	1.454	100.7	.05617	1.532	91.4
.05797	1.540	101.1	.05816	1.612	92.0
.05992	1.612	101.9	.06020	1.692	92.6
.06189	1.660	96.9	.06222	1.752	93.2
.06391	1.704	98.2	.06415	1.818	93.7
.06593	1.749	99.4	.06624	1.851	94.2
.06793	1.756	100.5	.06822	1.866	94.5
.06995	1.765	101.3	.07018	1.930	94.9
.07188	1.756	102.3	.07226	1.924	95.3
2. Gas velocity=5 fps			3. Gas velocity=6fps		
0.05467	1.522	93.1	0.05405	1.476	95.4
.05609	1.571	93.8	.05607	1.559	96.3
.05806	1.668	94.5	.05810	1.664	97.3
.06008	1.746	95.2	.06004	1.749	98.4
.06210	1.822	95.7	.06209	1.809	99.1
.06416	1.853	96.6	.06414	1.864	99.8
.06612	1.915	97.1	.06607	1.932	100.4
.06811	1.950	97.8	.06807	1.959	101.1
.07012	1.974	98.4	.07006	1.996	101.8
.07210	1.970	99.0	.07202	2.004	102.4

TABLE 4. *Effect of some variables on flame speed*—Continued

Wt methane / Wt air +O_2	Flame speed fps	Gas temperature °F	Wt methane / Wt air +O_2	Flame speed fps	Gas temperature °F
E. 4.0 percent by volume O_2 added to air			F. 5.0 percent by volume O_2 added to air		
4. Gas velocity=7 fps			1. Gas velocity=4 fps		
0.05403	1.418	102.2	0.05406	1.536	93.2
.05604	1.526	100.8	.05608	1.632	94.3
.05797	1.604	100.7	.05805	1.729	94.9
.06002	1.702	100.8	.06016	1.815	95.4
.06205	1.763	101.3	.06216	1.894	96.0
.06404	1.816	101.9	.06403	1.970	96.7
.06602	1.872	102.3	.06610	2.035	97.1
.06804	1.897	102.7	.06811	2.073	97.6
.07003	1.908	102.8	.07014	2.108	97.8
.07197	1.915	102.0	.07216	2.118	98.3
F. 5.0 percent by volume O_2 added to air					
2. Gas velocity=5 fps			3. Gas velocity=6 fps		
0.05405	1.516	94.3	0.05400	1.487	94.0
.05606	1.624	95.3	.05608	1.593	95.3
.05805	1.714	96.2	.05808	1.697	96.5
.06008	1.794	97.0	.06004	1.786	97.3
.06214	1.883	97.7	.06203	1.849	98.0
.06409	1.949	98.1	.06408	1.926	98.6
.06610	2.004	98.7	.06605	1.970	99.3
.06814	2.068	99.4	.06805	2.025	100.0
.07013	2.097	99.9	.07006	2.063	100.5
.07217	2.139	100.5	.07204	2.067	101.2
F. 5.0 percent by volume O_2 added to air			G. 6.0 percent by volume O_2 added to air		
4. Gas velocity=7 fps			1. Gas velocity=4 fps		
0.05400	1.478	92.8	0.05403	1.501	87.2
.05603	1.594	95.0	.05603	1.610	88.2
.05802	1.708	96.4	.05808	1.704	88.9
.06002	1.796	97.7	.06006	1.791	89.9
.06202	1.887	98.6	.06206	1.898	90.6
.06401	1.950	99.3	.06402	1.943	91.2
.06602	1.996	99.9			
.06802	2.036	100.6			
.07005	2.068	101.3			
.07202	2.080	101.9			
G. 6.0 percent by volume O_2 added to air					
2. Gas velocity=5 fps			3. Gas velocity=6 fps		
0.05404	1.514	88.1	0.05366	1.526	90.1
.05608	1.620	89.0	.05605	1.660	90.5
.05802	1.719	89.7	.05808	1.755	91.0
.06009	1.800	90.3	.06004	1.846	91.8
.06205	1.884	90.8	.06208	1.930	92.6
.06407	1.963	91.5	.06404	2.001	93.1
.06607	2.029	92.1	.06604	2.062	94.0
.06812	2.090	92.8	.06806	2.126	94.4
.07011	2.144	93.3	.07006	2.169	95.1
.07208	2.169	93.8	.07203	2.187	95.8
4. Gas velocity=7 fps					
0.05403	1.494	88.0	.06396	1.986	91.4
.05605	1.610	88.7	.06604	2.054	92.0
.05807	1.734	89.5	.06802	2.111	92.7
.06001	1.833	90.2	.07002	2.146	93.4
.06202	1.904	90.9	.07201	2.172	93.9

TABLE 5. *Effect of perchloryl fluoride addition on flame speed of methane*

Vol. percent ClO_3F added to air	Flame speed fps	Vol. percent ClO_3F added to air	Flame speed fps
A. Gas velocity=4 fps			
1. $\frac{\text{Wt methane}}{\text{Wt air}+ClO_3F}$=0.054		2. $\frac{\text{Wt methane}}{\text{Wt air}+ClO_3F}$=0.056	
0.0	1.094	0.0	1.156
0.5	1.168	0.5	1.226
1.0	1.232	1.0	1.304
2.0	1.392	2.0	1.492
3. $\frac{\text{Wt methane}}{\text{Wt air}+ClO_3F}$=0.058		4. $\frac{\text{Wt methane}}{\text{Wt air}+ClO_3F}$=0.060	
0.0	1.188	0.0	1.219
0.5	1.294	0.5	1.310
1.0	1.356	1.0	1.477
2.0	1.548	2.0	1.653
5. $\frac{\text{Wt methane}}{\text{Wt air}+ClO_3F}$=0.062		6. $\frac{\text{Wt methane}}{\text{Wt air}+ClO_3F}$=0.064	
0.0	1.233	0.0	1.223
0.5	1.364	0.5	1.404
1.0	1.548	1.0	1.568
2.0	1.723	2.0	1.751
7. $\frac{\text{Wt methane}}{\text{Wt air}+ClO_3F}$=0.066		8. $\frac{\text{Wt methane}}{\text{Wt air}+ClO_3F}$=0.068	
0.0	1.190	0.0	1.148
0.5	1.433	0.5	1.432
1.0	1.622	1.0	1.604
2.0	1.868	2.0	1.897
9. $\frac{\text{Wt methane}}{\text{Wt air}+ClO_3F}$=0.070		10. $\frac{\text{Wt methane}}{\text{Wt air}+ClO_3F}$=0.072	
0.0	1.094	0.0	1.017
0.5	1.403	0.5	1.385
1.0	1.609	1.0	1.593
2.0	1.937	2.0	1.963
B. Gas velocity=5 fps			
1. $\frac{\text{Wt methane}}{\text{Wt air}+ClO_3F}$=0.054		2. $\frac{\text{Wt methane}}{\text{Wt air}+ClO_3F}$=0.056	
0.0	1.094	0.0	1.156
0.5	1.138	0.5	1.237
1.0	1.201	1.0	1.288
2.0	1.432	2.0	1.526
3. $\frac{\text{Wt methane}}{\text{Wt air}+ClO_3F}$=0.058		4. $\frac{\text{Wt methane}}{\text{Wt air}+ClO_3F}$=0.060	
0.0	1.188	0.0	1.219
0.5	1.306	0.5	1.372
1.0	1.375	1.0	1.436
2.0	1.436	2.0	1.670
5. $\frac{\text{Wt methane}}{\text{Wt air}+ClO_3F}$=0.062		6. $\frac{\text{Wt methane}}{\text{Wt air}+ClO_3F}$=0.064	
0.0	1.233	0.0	1.223
0.5	1.404	0.5	1.453
1.0	1.518	1.0	1.549
2.0	1.701	2.0	1.849

TABLE 5. *Effect of perchloryl fluoride addition on flame speed of methane*—Continued

Vol. percent ClO_3F added to air	Flame speed fps	Vol. percent ClO_3F added to air	Flame speed fps
7. $\frac{\text{Wt methane}}{\text{Wt air}+ClO_3F}$=0.066		8. $\frac{\text{Wt methane}}{\text{Wt air}+ClO_3F}$=0.068	
0.0	1.190	0.0	1.148
0.5	1.457	0.5	1.442
1.0	1.577	1.0	1.582
2.0	1.946	2.0	1.964
9. $\frac{\text{Wt methane}}{\text{Wt air}+ClO_3F}$=0.070		10. $\frac{\text{Wt methane}}{\text{Wt air}+ClO_3F}$=0.072	
0.0	1.094	0.0	1.017
0.5	1.406	0.5	1.389
1.0	1.574	1.0	1.551
2.0	2.016	2.0	2.052
C. Gas velocity=6 fps			
1. $\frac{\text{Wt methane}}{\text{Wt air}+ClO_3F}$=0.054		2. $\frac{\text{Wt methane}}{\text{Wt air}+ClO_3F}$=0.056	
0.0	1.094	0.0	1.156
0.5	-----	0.5	-----
1.0	1.272	1.0	1.365
2.0	1.339	2.0	1.452
3.0	1.749	3.0	1.881
3. $\frac{\text{Wt methane}}{\text{Wt air}+ClO_3F}$=0.058		4. $\frac{\text{Wt methane}}{\text{Wt air}+ClO_3F}$=0.060	
0.0	1.188	0.0	1.219
0.5	1.304	0.5	1.372
1.0	1.422	1.0	1.495
2.0	1.508	2.0	1.566
3.0	2.059	3.0	2.147
5. $\frac{\text{Wt methane}}{\text{Wt air}+ClO_3F}$=0.062		6. $\frac{\text{Wt methane}}{\text{Wt air}+ClO_3F}$=0.064	
0.0	1.233	0.0	1.223
0.5	1.418	0.5	1.453
1.0	1.582	1.0	1.610
2.0	1.589	2.0	1.650
3.0	2.257	3.0	2.374
7. $\frac{\text{Wt methane}}{\text{Wt air}+ClO_3F}$=0.066		8. $\frac{\text{Wt methane}}{\text{Wt air}+ClO_3F}$=0.068	
0.0	1.190	0.0	1.148
0.5	1.461	0.5	1.437
1.0	1.632	1.0	1.653
2.0	1.693	2.0	1.723
9. $\frac{\text{Wt methane}}{\text{Wt air}+ClO_3F}$=0.070		10. $\frac{\text{Wt methane}}{\text{Wt air}+ClO_3F}$=0.072	
0.0	1.094	0.0	1.017
0.5	1.390	0.5	1.358
1.0	1.665	1.0	1.646
2.0	1.734	2.0	1.743
D. Gas velocity=7 fps			
1. $\frac{\text{Wt methane}}{\text{Wt air}+ClO_3F}$=0.054		2. $\frac{\text{Wt methane}}{\text{Wt air}+ClO_3F}$=0.056	
0.0	1.094	0.0	1.156
0.5	-----	0.5	-----
1.0	-----	1.0	1.349
2.0	1.532	2.0	1.633

TABLE 5. *Effect of perchloryl fluoride addition on flame speed of methane*—Continued

Vol. percent ClO_3F added to air	Flame speed fps	Vol. percent ClO_3F added to air	Flame speed fps
3. $\frac{\text{Wt methane}}{\text{Wt air} + ClO_3F} = 0.058$		4. $\frac{\text{Wt methane}}{\text{Wt air} + ClO_3F} = 0.060$	
0.0	1.188	0.0	1.219
0.5	1.295	0.5	1.352
1.0	1.414	1.0	1.475
2.0	1.695	2.0	1.760
5. $\frac{\text{Wt methane}}{\text{Wt air} + ClO_3F} = 0.062$		6. $\frac{\text{Wt methane}}{\text{Wt air} + ClO_3F} = 0.064$	
0.0	1.233	0.0	1.223
0.5	1.375	0.5	1.386
1.0	1.550	1.0	1.597
2.0	1.882	2.0	1.961
7. $\frac{\text{Wt methane}}{\text{Wt air} + ClO_3F} = 0.066$		8. $\frac{\text{Wt methane}}{\text{Wt air} + ClO_3F} = 0.068$	
0.0	1.190	0.0	1.148
0.5	1.435	0.5	1.411
1.0	1.630	1.0	1.634
2.0	2.016	2.0	2.022
9. $\frac{\text{Wt methane}}{\text{Wt air} + ClO_3F} = 0.070$		10. $\frac{\text{Wt methane}}{\text{Wt air} + ClO_3F} = 0.072$	
0.0	1.094	0.0	1.017
0.5	1.366	0.5	1.342
1.0	1.640	1.0	1.613
2.0	2.074	2.0	2.103

TABLE 6. *Effect of oxygen addition on flame speed of methane*

Vol percent O_2 added to air	Flame speed fps	Vol percent O_2 added to air	Flame speed fps
A. Gas velocity = 4 fps			
1. $\frac{\text{Wt methane}}{\text{Wt air} + O_2} = 0.054$		2. $\frac{\text{Wt methane}}{\text{Wt air} + O_2} = 0.056$	
0.0	1.074	0.0	1.079
0.5	1.140	0.5	1.223
1.0	1.233	1.0	1.338
2.0	1.267	2.0	1.347
3.0	1.295	3.0	1.369
4.0	1.406	4.0	1.482
5.0	1.472	5.0	1.567
6.0	1.467	6.0	1.576
3. $\frac{\text{Wt methane}}{\text{Wt air} + O_2} = 0.058$		4. $\frac{\text{Wt methane}}{\text{Wt air} + O_2} = 0.060$	
0.0	1.178	0.0	1.214
0.5	1.279	0.5	1.305
1.0	1.340	1.0	1.401
2.0	1.419	2.0	1.459
3.0	1.451	3.0	1.506
4.0	1.564	4.0	1.646
5.0	1.666	5.0	1.755
6.0	1.671	6.0	1.758
5. $\frac{\text{Wt methane}}{\text{Wt air} + O_2} = 0.062$		6. $\frac{\text{Wt methane}}{\text{Wt air} + O_2} = 0.064$	
0.0	1.232	0.0	1.223
0.5	1.318	0.5	1.322
1.0	1.416	1.0	1.421
2.0	1.501	2.0	1.543
3.0	1.560	3.0	1.590
4.0	1.707	4.0	1.771
5.0	1.825	5.0	1.908
6.0	1.866	6.0	1.909

TABLE 6. *Effect of oxygen addition on flame speed of methane*—Continued

Vol percent O_2 added to air	Flame speed fps	Vol percent O_2 added to air	Flame speed fps
7. $\frac{\text{Wt methane}}{\text{Wt air} + O_2} = 0.066$		8. $\frac{\text{Wt methane}}{\text{Wt air} + O_2} = 0.068$	
0.0	1.190	0.0	1.148
0.5		0.5	1.260
1.0	1.411	1.0	1.392
2.0	1.537	2.0	1.472
3.0	1.632	3.0	1.632
4.0	1.802	4.0	1.815
5.0	1.971	5.0	2.007
9. $\frac{\text{Wt methane}}{\text{Wt air} + O_2} = 0.070$		10. $\frac{\text{Wt methane}}{\text{Wt air} + O_2} = 0.072$	
0.0	1.094	0.0	1.017
0.5	1.200	0.5	1.117
1.0	1.336	1.0	1.269
2.0	1.496	2.0	1.459
3.0	1.629	3.0	1.615
4.0	1.877	4.0	1.871
5.0	2.041	5.0	2.048

B. Gas velocity = 5 fps

1. $\frac{\text{Wt methane}}{\text{Wt air} + O_2} = 0.054$		2. $\frac{\text{Wt methane}}{\text{Wt air} + O_2} = 0.056$	
0.0	1.078	0.0	1.142
0.5	1.147	0.5	1.221
1.0	1.200	1.0	1.258
2.0	1.255	2.0	1.348
3.0	1.347	3.0	1.409
4.0	1.463	4.0	1.510
5.0	1.451	5.0	1.556
6.0	1.480	6.0	1.583
3. $\frac{\text{Wt methane}}{\text{Wt air} + O_2} = 0.058$		4. $\frac{\text{Wt methane}}{\text{Wt air} + O_2} = 0.060$	
0.0	1.178	0.0	1.212
0.5	1.280	0.5	1.312
1.0	1.334	1.0	1.375
2.0	1.425	2.0	1.476
3.0	1.503	3.0	1.564
4.0	1.698	4.0	1.685
5.0	1.645	5.0	1.724
6.0	1.688	6.0	1.764
5. $\frac{\text{Wt methane}}{\text{Wt air} + O_2} = 0.062$		6. $\frac{\text{Wt methane}}{\text{Wt air} + O_2} = 0.064$	
0.0	1.230	0.0	1.222
0.5	1.327	0.5	1.333
1.0	1.398	1.0	1.392
2.0	1.525	2.0	1.557
3.0	1.621	3.0	1.665
4.0	1.762	4.0	1.771
5.0	1.813	5.0	1.908
6.0	1.849	6.0	1.927
7. $\frac{\text{Wt methane}}{\text{Wt air} + O_2} = 0.066$		8. $\frac{\text{Wt methane}}{\text{Wt air} + O_2} = 0.068$	
0.0	1.190	0.0	1.148
0.5	1.304	0.5	1.278
1.0	1.389	1.0	1.372
2.0	1.577	2.0	1.558
3.0	1.665	3.0	1.725
4.0	1.851	4.0	1.883
5.0	1.932	5.0	1.990
6.0	1.990	6.0	2.048

TABLE 6. *Effect of oxygen addition on flame speed of methane*—Continued

Vol percent O_2 added to air	Flame speed fps	Vol percent O_2 added to air	Flame speed fps
9. $\frac{\text{Wt methane}}{\text{Wt air} + O_2} = 0.070$		10. $\frac{\text{Wt methane}}{\text{Wt air} + O_2} = 0.072$	
0.0	1.094	0.0	1.017
0.5	1.206	0.5	1.116
1.0	1.311	1.0	1.234
2.0	1.545	2.0	1.519
3.0	1.710	3.0	1.699
4.0	1.904	4.0	1.897
5.0	2.019	5.0	2.058
6.0	2.099	6.0	2.122

C. Gas velocity = 6 fps

1. $\frac{\text{Wt methane}}{\text{Wt air} + O_2} = 0.054$		2. $\frac{\text{Wt methane}}{\text{Wt air} + O_2} = 0.056$	
0.0	1.094	0.0	1.156
0.5	-----	0.5	1.231
1.0	-----	1.0	1.262
2.0	1.254	2.0	1.353
3.0	1.316	3.0	1.432
4.0	1.421	4.0	1.499
5.0	1.439	5.0	1.538
6.0	1.497	6.0	1.629
3. $\frac{\text{Wt methane}}{\text{Wt air} + O_2} = 0.058$		4. $\frac{\text{Wt methane}}{\text{Wt air} + O_2} = 0.060$	
0.0	1.188	0.0	1.219
0.5	1.286	0.5	1.313
1.0	1.320	1.0	1.369
2.0	1.418	2.0	1.488
3.0	1.500	3.0	1.571
4.0	1.599	4.0	1.679
5.0	1.636	5.0	1.721
6.0	1.722	6.0	1.809
5. $\frac{\text{Wt methane}}{\text{Wt air} + O_2} = 0.062$		6. $\frac{\text{Wt methane}}{\text{Wt air} + O_2} = 0.064$	
0.0	1.233	0.0	1.221
0.5	1.329	0.5	1.329
1.0	1.418	1.0	1.402
2.0	1.519	2.0	1.552
3.0	1.614	3.0	1.650
4.0	1.735	4.0	1.785
5.0	1.781	5.0	1.853
6.0	1.889	6.0	1.955
7. $\frac{\text{Wt methane}}{\text{Wt air} + O_2} = 0.066$		8. $\frac{\text{Wt methane}}{\text{Wt air} + O_2} = 0.068$	
0.0	1.190	0.0	1.148
0.5	1.317	0.5	1.261
1.0	1.386	1.0	1.355
2.0	1.560	2.0	1.569
3.0	1.689	3.0	1.716
4.0	1.852	4.0	1.875
5.0	1.895	5.0	1.947
6.0	2.014	6.0	2.076
9. $\frac{\text{Wt methane}}{\text{Wt air} + O_2} = 0.070$		10. $\frac{\text{Wt methane}}{\text{Wt air} + O_2} = 0.072$	
0.0	1.094	0.0	1.017
0.5	1.213	0.5	1.146
1.0	1.315	1.0	1.256
2.0	1.546	2.0	1.506
3.0	1.716	3.0	1.709
4.0	1.909	4.0	1.914
5.0	1.982	5.0	1.983
6.0	2.115	6.0	2.130

TABLE 6. *Effect of oxygen addition on flame speed of methane*—Continued

Vol percent O_2 added to air	Flame speed fps	Vol percent O_2 added to air	Flame speed fps
D. Gas velocity = 7 fps			
1. $\frac{\text{Wt methane}}{\text{Wt air} + O_2} = 0.054$		2. $\frac{\text{Wt methane}}{\text{Wt air} + O_2} = 0.056$	
0.0	1.094	0.0	1.156
0.5	-----	0.5	-----
1.0	-----	1.0	-----
2.0	-----	2.0	1.310
3.0	1.279	3.0	1.372
4.0	1.329	4.0	1.444
5.0	1.436	5.0	1.541
6.0	1.476	6.0	1.588
3. $\frac{\text{Wt methane}}{\text{Wt air} + O_2} = 0.058$		4. $\frac{\text{Wt methane}}{\text{Wt air} + O_2} = 0.060$	
0.0	1.188	0.0	1.219
0.5	1.231	0.5	1.274
1.0	1.319	1.0	1.373
2.0	1.397	2.0	1.461
3.0	1.456	3.0	1.524
4.0	1.522	4.0	1.629
5.0	1.648	5.0	1.729
6.0	1.708	6.0	1.804
5. $\frac{\text{Wt methane}}{\text{Wt air} + O_2} = 0.062$		6. $\frac{\text{Wt methane}}{\text{Wt air} + O_2} = 0.064$	
0.0	1.233	0.0	1.223
0.5	1.295	0.5	1.306
1.0	1.400	1.0	1.413
2.0	1.488	2.0	1.522
3.0	1.561	3.0	1.590
4.0	1.678	4.0	1.728
5.0	1.816	5.0	1.825
6.0	1.871	6.0	1.951
7. $\frac{\text{Wt methane}}{\text{Wt air} + O_2} = 0.066$		8. $\frac{\text{Wt methane}}{\text{Wt air} + O_2} = 0.068$	
0.0	1.190	0.0	1.148
0.5	1.285	0.5	1.251
1.0	1.406	1.0	1.389
2.0	1.527	2.0	1.521
3.0	1.632	3.0	1.632
4.0	1.782	4.0	1.805
5.0	1.918	5.0	1.955
6.0	2.016	6.0	2.069
9. $\frac{\text{Wt methane}}{\text{Wt air} + O_2} = 0.070$		10. $\frac{\text{Wt methane}}{\text{Wt air} + O_2} = 0.072$	
0.0	1.094	0.0	1.017
0.5	1.194	0.5	1.157
1.0	1.347	1.0	1.304
2.0	1.490	2.0	1.458
3.0	1.680	3.0	1.666
4.0	1.816	4.0	1.827
5.0	1.983	5.0	1.992
6.0	2.099	6.0	2.124

5. Conclusions

Both perchloryl fluoride and oxygen increase the flame speed when added to burning mixtures of methane and air, and the effect of perchloryl fluoride, on a molar basis, is greater than that of oxygen. However, preheating the methane-air mixture moderately, up to temperatures of 330° F, is more effective in increasing flame speeds than the addition of small amounts of either oxidant. The mixture ratio at which maximum flame speed occurs is dis-

placed beyond 0.072 by only small additions of either perchloryl fluoride or oxygen. In the range of addition of oxidants covered in this report, the maximum flame speed increases linearly with the addition of either perchloryl fluoride or oxygen, although at different rates.

6. References

[1] A. Engelbrecht and H. Atzwanger, Monatsh. Chem. **83,** 1087 (1952).

[2] Private communication from the Pennsylvania Salt Manufacturing Co.

[3] C. Neugebauer and J. L. Margrave, J. Am. Chem. Soc. **79,** 1138 (1957).

[4] R. M. Lodwig and J. L. Margrave, Combustion and Flame **3,** 147 (1959).

[5] A. G. Gaydon and H. G. Wolfhard, Flames, their structure, radiation and temperature, Chapman and Hall, Ltd., London, p. 68–72 (1960).

[6] J. W. Linnett, Fourth Symposium (International) on Combustion, 1952. Williams and Wilkins, Baltimore, Md., p. 20 (1953).

[7] C. Halpern, J. Research NBS **60,** 535 (1958) RP2867.

[8] B. Lewis and G. von Elbe, Combustion, flames and explosions of gases. Academic Press, Inc., N.Y., p. 465 (1951).

[9] Reported in Lewis and von Elbe, op. cit., p. 466.

[10] E. F. Fiock, Physical measurements in gas dynamics and combustion, Princeton University Press, Princeton, N.J., p. 433 (1954).

[11] Reported in Lewis and von Elbe, op. cit., p. 467.

[12] J. M. Singer, J. Grumer, and E. B. Cook, Proc. gas dynamics symp. aerothermodynamics, 1955. Northwestern University, Evanston, Ill., p. 139 (1956).

(Paper 65A6–134)

JOURNAL OF RESEARCH of the National Bureau of Standards A. Physics and Chemistry
Vol. 65A, No. 6, November–December 1961

Publications of the National Bureau of Standards*

(Including papers in outside journals)

Selected Abstracts

Analysis of pyrolyzates of polystyrene and Poly(methyl methacrylate) by gas chromatography, *F. A. Lehmann and G. M. Brauer, Anal. Chem.* **33,** *No. 6, 673–676 (May 1961).*

Pyrolyzates of polystyrene and poly(methyl methacrylate) were studied at temperatures from 400 to 1100°C using gas chromatographic techniques. A small Vycor boat surrounded by a platinum heating coil was placed in the inlet system of the chromatograph. A 2 to 3 mg sample was degraded at a series of temperatures which were measured by means of a thermocouple placed in an indentation at the bottom of the boat. Helium carried the volatile products into the heated column of the chromatograph. Analyses of the products could usually be accomplished with a reproducibility of better than 1%. Polystyrene degraded mainly to monomer below 700°C and poly(methyl methacrylate) behaves similarly below 450°C. At higher temperatures some gaseous and liquid decomposition products are formed which were identified by their characteristic retention times. The technique uses inexpensive equipment and is generally applicable for the study of the thermal stability of polymers and their pyrolyzates. Results obtained are very helpful in identifying reaction products and in the elucidation of degradation mechanisms over wide temperature ranges. The procedure is also useful in the rapid characterization and quantitative estimation of the composition of complex copolymer systems.

Microwave spectrum of isobutylene. Dipole moment, internal barrier, equilibrium conformation, structure, *V. W. Laurie, J. Chem. Phys.* **34,** *No. 5, 1516–1519 (May 1961).*

The microwave spectra of isobutylene and isobutylene-*d*-3 have been studied in the region 17–36 kMc. Observed rotational constants (Mc) for isobutylene are $a_0=9133.32$, $b_0=8381.75$, $c_0=4615.99$; for *sym*-isobutylene-*d*-3, $a_0=9132.59$, $b_0=7788.98$, $c_0=4431.05$; for *asym*-isobutylene-*d*-3, $a_0=8819.46$, $b_0=7981.08$, $c_0=4469.59$. The most likely structure compatible with these data is $r_{c-c}=1.50_7$ A, $r_{c-c}=1.34$ A, $r_{CH}(\text{methyl})=1.08_5$ A, $r_{CH}(\text{ethylenic})=1.08_6$ A, $<\text{Me}-\text{C}-\text{Me}=115.9°$, $<\text{HCH}(\text{methyl})=108°$, $<\text{HCH}(\text{ethylenic})=117.5°$. Measurements of the Stark effect show that the dipole moment $\mu=0.503\pm0.009$ *D*. Fine structure leads to a barrier height hindering internal rotation of the methyl groups of 2.21 kcal/mole. The equilibrium conformation is C_{2v} with two methyl hydrogens in the plane of the carbon atoms and the CH bonds pointing away from the symmetry axis. It is concluded that although CC single bonds are shortened when adjacent to a double bond, the double bond length is probably not much affected by the presence of an adjacent CH_3 group.

Nonequilibrium processes in isotopically disordered crystals. Dependence on degree of order, *R. Zwanzig, J. Math. Phys.* **2,** *No. 3, 370–372 (May–June 1961).*

Maradudin, Weiss, and Jepsen have shown that approximate normal modes of isotopically disordered crystals decay irreversibly when the arrangement of isotopes is completely random. We generalize their results to crystals with an arbitrary degree of order. In particular, we show that irreversible behavior occurs whenever the spatial correlation between isotopic species extends over a fixed finite range, as the size of the crystal tends to infinity.

Intermolecular forces from optical spectra of impurities in molecular crystals, *R. W. Zwanzig, Molecular Phys.* **3,** *No. 4, 305–311 (July 1960).*

A procedure is outlined by which one can get information about the effects of electronic excitation on the interactions between molecules. The absorption and emission spectra of impurities in molecular crystals, and specifically the mean positions and widths of the lines are required as functions of temperature. A theory of M. Lax is used to relate mean position and width to intermolecular forces. The preliminary treatment of this problem by McCarty and Robinson is evaluated and extended: their procedure is expected to be valid for very narrow lines only.

Spin-lattice relaxation in cerous magnesium nitrate, *R. P. Hudson and R. S. Kaeser, Il Nuovo Cimento* **19,** *Serie X, 1275–1277 (Mar. 16, 1961).*

Measurements of the spin-lattice relaxation time, τ, at low audiofrequencies for cerous magnesium nitrate in the region of 2°K confirm the existence of an excited level at about 25 cm^{-1}. The consequent exponential dependence of τ on temperature, T, gives way below 2°K to a term varying as T^{-5}. It seems likely that the latter arises from the combined effect of a direct relaxation process (T^{-1}) and a "Raman-type" process (T^{-7}), here making comparable contributions to the relaxation at an unusually low temperature.

The photolysis of ethyl vinyl ether, *E. Murad, J. Am. Chem. Soc.* **83,** *1327–1330 (1961).*

This direct photolysis of ethyl vinyl ether has been studied and the primary photochemical processes determined. The same processes have been found to occur in the mercury-sensitized decomposition, viz,

$$\text{CH}_2=\text{CHOCH}_2\text{CH}_3+h\nu\rightarrow\text{C}_2\text{H}_5+\text{CH}_2=\text{CHO} \quad \text{I}$$
$$\rightarrow\text{C}_2\text{H}_4+\text{CH}_3\text{CHO} \quad \text{II}$$

An additional primary process was found to occur in the $Co^{60}\gamma$-radiolysis, viz,

$$\text{CH}_2=\text{CHOCH}_2\text{CH}_3+\gamma\rightarrow\text{C}_2\text{H}_5\text{O}+\text{CH}_2=\text{CH} \quad \text{IV}$$

The configuration of the excited state leading to process II is suggested to be a six-membered ring intermediate.

Vapor phase gamma-radiolysis of azomethane, *L. J. Stief and P. Ausloos, J. Phys. Chem.* **65,** *877–881 (1961).*

The effect of scavengers, pressure, temperature, and added zenon on the vapor phase γ-radiolysis of azomethane has been investigated. Most of the results can be explained on the basis of free radical reactions similar to those occurring in the photolysis of azomethane. Values for the ratio of rate constants $k^1/k_{2l}^{1/2}$ for the reactions

$$[\text{CH}_3+\text{CH}_3\text{N}_2\text{CH}_3\rightarrow\text{CH}_4+\text{CH}_2\text{N}_2\text{CH}_3 \quad (1)$$
$$\text{CH}_3+\text{CH}_3\rightarrow\text{C}_2\text{H}_3 \quad (2)$$

determined from the radiolysis data are in excellent agreement with values based on photolysis experiments, indicating that methane and ethane are formed by the reactions of thermalized methyl radicals. The results are best explained on the basis of the decomposition of an electronically excited molecule, formed either by direct excitation or by ionization followed by neutralization. Ion decomposition and ion-molecule reactions of the usual type are shown to be inconsistent with the results.

Electron interferometer studies of iron whiskers, *H. A. Fowler, L. Marton, J. A. Simpson, and J. A. Suddeth, J. Appl. Phys.* **32,** *No. 6, 1153 (June 1961).*

Electron interference patterns have been obtained by using an iron whisker as the electrostatic fiber of a Möllenstadt (1) interferometer. The tilted fringes in the shadow pattern resemble those observed by Chambers (2) and show the relationship between flux leakage and geometrical shape of the whisker. Chambers' general model of the flux configuration is confirmed.

(1) G. Möllenstadt and H. Düker, Z. Physik **145**, 377 (1956);
(2) R. G. Chambers, Phys. Rev. Letters **5**, 3 (July 1960).

Dissociation constant of the protonated acid form of 2-amino-2-(hydroxymethyl)-1, 3-propanediol [*tris* (hydroxymethyl)-aminomethane] and related thermodynamic quantities from 0 to 50°, *R. G. Bates and H. B. Hetzer, J. Phys. Chem.* **65,** *667–671 (1961).*
The thermodynamic dissociation constant (K_{bA}) of the protonated form (BH^+) of 2-amino-2-(hydroxymethyl)-1,3-propanediol [*tris* (hydroxymethyl)aminomethane] has been determined at 11 temperatures from 0 to 50° by measurement of the electromotive force of hydrogen-silver chloride cells without liquid junction. The results are given by the equation

$$-\log K_{bA}=\frac{2981.4}{T}-3.5888+0.005571\ T,$$

where T is in °K. The changes of free energy, enthalpy, entropy, and heat capacity were computed for the dissociation of the cation acid BH^+ in the standard state, as well as for the basic dissociation, $B+H_2O=BH^++OH^-$.
For the acidic dissociation at 25°, $\Delta G°$ is 46,075 j $mole^{-1}$, $\Delta H°$ is 47,600 j $mole^{-1}$, $\Delta S°=5.1$ j deg^{-1} $mole^{-1}$, and $\Delta C_p°$ is -64 j deg^{-1} $mole^{-1}$. The activity-coefficient term is consistent with an ion-size parameter of zero; hence, incomplete dissociation of the salt BHCl is suggested. The entropy changes for the isoelectric dissociation of cation acids (BH^+) appear to indicate restrictive orientation of solvent molecules about the ions and the attendant hindrance of free rotation about carbon-carbon bonds. This simple picture is, however, unable to account satisfactorily for the observed changes in heat capacity.

Hyperfine structure and isotope shifts in the 2537–A line of mercury, *W. G. Schweitzer, Jr., J. Opt. Soc. Am.* **51,** *No. 6, 692–693 (June 1961).*
The hyperfine structure and isotope shifts in the 2537 Å line of natural mercury have been measured with high precision using interferometric techniques on the absorption spectrum of an atomic beam.

Paramagnetic substances for nuclear orientation, *R. P. Hudson, Prog. in Cryogenics,* **3,** *99–127 (1961).*
An account is given of the magnetic and thermal properties of the substances which have proved most useful for producing nuclear orientation at very low temperatures. This is prefaced by a discussion of factors affecting the choice of substance.

Age to indium resonance for D-D neutrons in heavy water, *V. Spiegel, Jr., and A. C. B. Richardson, Nuclear Sci. and Eng.* **10,** *No. 1, 11–15 (1961).*
The neutron age to the 1.44 ev resonance in indium has been determined from activation measurements for a $D(d,n)He^3$ neutron source in heavy water. Appropriately averaged and corrected indium foil activities yield the value 115.5 ± 1.4 cm^2 for the age in an infinite medium. Independent theoretical calculations for exactly this experimental arrangement by Cooper and for a comparable case by Sullivan both yield values in agreement with this experimental result. It appears, therefore, that there is at present no discrepancy between theory and experiment for the age of 2–3 Mev neutrons in heavy water.

Magnetic properties and optical absorption spectrum of K_2ReCl_6, *J. C. Eisenstein, J. Chem. Phys.* **34,** *No. 5, 1628–1648 (May 1961).*
A phenomenological theory of certain physical properties of the $(ReCl_6)^{2-}$ complex ion is presented here. The ion can be described in terms of a set of parameters which includes the strength of the octahedral ligand field, the Coulomb integrals, the spin-orbit coupling constant and the orbital reduction factors. The interaction matrices for the three electron system are given in algebraic form. With an appropriate choice of the parameters the eigenvalues of these matrices are in fair agreement with the observed energy levels of the system. The effect of a departure from strict octahedral symmetry is discussed. The matrix elements of the magnetic moment operator are also given in algebraic form and then used in a calculation of the susceptibility. The discripancy between theory and experiment is attributed to a super-exchange interaction with leads, at sufficiently low temperatures, to antiferromagnetism of the compound. Finally, the results of paramagnetic resonance experiments on K_2ReCl_6 are considered.

Calculations of the neutron age in water and heavy water for D–D sources, *J. W. Cooper, Nuclear Sci. and Eng.* **10,** *No. 1, 1–10 (May 1961).*
Calculations of the age to indium resonance of neutrons from the reaction $D(d,n)He^3$ in water and heavy water have been performed by the Monte Carlo method. The calculations were designed to simulate the experiments of Spiegel et al. The effect of the duct used to lead the deuteron beam into the medium was investigated. The computations show agreement with the experimental results and with a similar calculation performed by C. R. Mullin.

Magnetic susceptibility of cerous magnesium nitrate, *R. P. Hudson and W. R. Hosler, Phys. Rev.* **122,** *No. 5, 1417–1420 (June 1961).*
The most striking features of the behavior of cerous magnesium nitrate at liquid helium temperatures—extremely anisotropic susceptibility with $g_\parallel\approx0$, a large temperature-independent term in $\chi_\perp$, the spin-lattice relaxation time varying as the twelfth or higher power of T in the region of 2°K—have until very recently received no detailed explanation. A measurement of $\chi_\perp$ between 4°K and 300°K was undertaken to elicit information on the energies of the excited doublets within the $J=5/2$ ground multiplet, and thus to provide a guide for the reassessment of the crystal field parameters. We find δ_1 and δ_2 to be 30 and (roughly) 200 cm^{-1} respectively, in contrast to the 113 and 150 cm^{-1} of of existing theory. The results are at variance with the published data for $\chi_\perp$ above 85°K, but are in fairly good agreement with the recent findings of Leask and Wolf at low temperatures.

Use of gaussian orbitals for atoms-in-molecule calculations, *M. Kraus, J. Chem. Phys.* **34,** *No. 2, 692–693 (February 1961).*
The use of Gaussian functions is proposed for "atoms-in-molecule" calculations and applied for the case of H_2. Reasonably accurate results are obtained for the equilibrium internuclear distance and the binding energy. The results justify further work with more complicated systems.

Measurement of minority carrier lifetime in SiC by a novel electroluminescent method, *G. G. Harman and R. L. Raybold, J. Appl. Phys.* **32,** *No. 6, 1168–1169 (June 1961).*
A new method of measuring the lifetime of minority carriers in large energy gap semiconductors is described. This consists of injecting and subsequently extracting carriers with a sine wave generator while monitoring the average carrier concentration by observing the emitted recombination radiation. When 1/f seconds is comparable to the lifetime this average emitted light falls off sharply. The method was applied to silicon carbide crystals and it was found that the majority had lifetimes$\sim10^{-5}$ sec but a few were as long as 10^{-6} sec.

Absolute measurement of W for Po^{210} alpha particles in air, nitrogen and carbon dioxide, *Z. Bay, P. A. Newman, and H. H. Seliger, Radiation Research* **14,** *No. 5, 551–565 (May 1961).*
The average energy (W) expended in producing an ion pair in air nitrogen, and carbon dioxide was measured for the alpha particles of Po^{210} while they are slowed down from their initial energy (5.305 Mev) to zero energy. The ionization chamber was used simultaneously in these measurements as an integrating current-measuring chamber and as a pulse ionization chamber. In this way, the ratio of the total charge measured to the total number of pulses counted is independent of the random statistical fluctuations in the emission rate of the low activity sources used. A small part of the chamber wall (which served as the high-voltage electrode) holding the alpha source and separated AC-wise from the rest of the chamber was used for pulse counting. A careful investigation of

the various factors involved helped to obtain a final accuracy of the measurements of about 0.1%. The results are $W_{air}=35.2\pm0.1$ ev/ion pair, $W_{N_2}=36.4\pm0.1$ ev/ion pair and $W_{CO_2}=34.3\pm0.2$ ev/ion pair. The indicated uncertainties include the standard errors of the respective means plus an allowance for other known sources of possible errors.

The structure of the monoclinic form of sodium tetrametaphosphate tetrahydrate, *H. M. Ondik, C. H. MacGillavry, and S. Block, Acta. Cryst.* **14,** *555 (1961).*

Crystals of monoclinic sodium tetrametaphosphate tetrahydrate, $Na_4P_4O_{12}\cdot4H_2O$, are needlelike in habit, elongated along c. The unit cell dimensions are $a=9.667\pm0.002$, $b=12.358\pm0.002$, $c=6.170\pm0.001$ Å, $\beta=92°16'\pm10'$; space group $P2_1/a$, $Z=2$. Two sets of three-dimensional X-ray diffraction data were collected with CuK_α radiation using Weissenberg multiple-film techniques and the intensities were measured photometrically. The structure was determined by a combination of three-dimensional Patterson and electron-density syntheses, and a complete-matrix least-squares reduction of data. The final R value for 831 nonzero reflections is 0.108. Individual isotropic temperature factors were used.

The tetrametaphosphate rings are on centers of symmetry The sodium ions are coordinated by six oxygen atoms in roughly octahedral configuration. One sodium ion links the rings in a network parallel to the *ab* plane. The other alternates with the rings linking them along *c*.

Mass spectrometric study of cyanogen and cyanoacetylenes, *V. H. Dibeler, R. M. Reese, and J. L. Franklin, J. Am. Chem. Soc.* **83,** *1813–1818 (1961).*

Relative abundances and appearance potentials are reported for the principal ions in the mass spectra of cyanogen, cyanoacetylene, dicyanoacetylene, and dicyanodiacetylene. Heats of formation of radicals and radical ions are calculated and the energetically probable ionization-dissociation processes are tabulated. Carbon-carbon and carbon-nitrogen bond dissociation energies are calculated for various ionized and neutral molecular species.

Energy levels and magnetic dipole transitions in the $4p^4$ ground configuration of singly ionized atomic bromine (Br II), *W. C. Martin and J. L. Tech, J. Opt. Soc. Am.* **51,** *No. 6, 591–594 (June 1961).*

Improved values of the previously known Br II energy levels relative to the $4p^4\ ^3p_2$ ground level at 0.0 cm^{-1}, have been obtained from preliminary observations in the vacuum ultraviolet region. The position of the $4p^4\ ^1S_0$ level was found from the "forbidden" transition, $4p^4\ ^3p_1-4p_4\ ^1S_0$ at 4042.42 A. An observation of the transverse Zeeman effect for this line yields a Lorentz triplet with the usual polarizations reversed and approximately the expected splitting. It is thus confirmed that the line arises from magnetic-dipole radiation. A similar line at 8269.65 A, due to the transition $4p^4\ ^3p_2-4p^4\ ^1D_2$, shows hyperfine-structure broadening consistent with the calculated structure. New values for the excited levels of $4p^4$ are: $^3p_1=3136.4$ cm^{-1}, $^3p_0=3837.5$ cm^{-1}, $^1D_2=12089.1$ cm^{-1}, and $^1S_0=27867.1$ cm^{-1}. The values for the levels of all configurations above $4p^4$, as given in *Atomic Energy Levels*, Vol. II, should be reduced by 5.9 ± 0.5 cm^{-1}. Previous values for the levels of $4p^4$ were also in error by several cm^{-1}, and earlier evidence for the position of $4p^4\ ^1S_0$ was inconclusive. Intermediate-coupling parameter values which yield a good fit for Br II $4p^4$ are $F_2(4p,4p)=1690$ cm^{-1} and $\zeta(4p)=2800$ cm^{-1}.

An improved structure determination for vinyl fluoride, *D. R. Lide, Jr., and D. Christensen, Spectrochim. Acta* **17,** *665–668 (1961).*

The previously published rotational constants of 8 isotopic species of vinyl fluoride have been used to calculate an r_s (substitution) structure for the molecule. The results are: r (CC) $=1.329\pm0.006$ A, r (CF) $=1.347\pm0.009$ A, $\measuredangle$FCC $=120.8°\pm0.3°$, $\measuredangle$FCH $=110°\pm1°$, r (CH) $=1.032\pm0.004$ A; in the $=CH_2$ group: r (CH) $=1.077\pm0.003$ A and $\measuredangle$ HCC $=119.0°\pm0.3°$ for the CH bond *trans* to *F*; r (CH) $=1.087\pm0.002$ A and $\measuredangle$ HCC $=120.9°\pm0.3°$ for the CH bond *cis* to *F*.

Other NBS Publications

Journal of Research 65C (Eng. and Instr.) No. 4, (Oct.-Dec. 1961) 75 cents.

A new airglow photometer. C. M. Purdy, L. R. Megill, and F. E. Roach.

A guide to the use of the modified reflectometer technique of VSWR measurement. W. J. Anson.

An X-ray diffractometer cryostat providing temperature control in the range 4 to 300 °K. F. A. Mauer and L. H. Bolz.

Apparatus for determination of pressure-density-temperature relations and specific heats of hydrogen to 350 atmospheres at temperatures above 14 °K. Robert D. Goodwin.

The use of a thermistor for detecting eluent fronts in liquid-solid chromatography. G. S. Ross.

Radiation field from a circular disk source. J. H. Hubbell, R. L. Bach, and R. J. Herbold.

The Bauschinger effect and residual microstresses in alpha brass. C. J. Newton.

A study by polarization techniques of the corrosion rates of aluminum and steel underground for sixteen months. W. J. Schwerdtfeger.

Journal of Research 65D, (Radio Prop.) No. 6, (Nov.–Dec. 1961) 70 cents.

The solar wind. E. N. Parker.

Attentuation coefficients for propagation at very low frequencies (VLF) during a sudden ionospheric disturbance (SID). E. T. Pierce.

Dipole radiation in a conducting half space. R. K. Moore and W. E. Blair.

Reliability of atmospheric radio noise predictions. J. R. Herman.

Effects of the ionosphere on VLF navigational aids. W. T. Blackband.

On the spectrum of terrestrial radio noise at extremely low frequencies. H. R. Raemer.

The nonsingular embedding of transition processes within a more general framework of coupled variables. J. Heading.

Worldwide VLF standard frequency and time signal broadcasting. A. D. Watt, R. W. Plush, W. W. Brown, and A. H. Morgan.

Design of panoramic ionospheric resources. L. H. Heisler and L. D. Wilson.

A quick method for estimating the stage of the sunspot cycle. W. B. Chadwick.

Measurements of low-angle radiation from a monopole. A. C. Wilson.

Capacities of stacks in sanitary drainage systems for buildings, R. S. Wyly and H. N. Eaton, NBS Mono. **31** (1961), 35 cents.

Mean electron density variations of the quiet ionosphere 4—June 1959, J. W. Wright, L. R. Wescott, and D. J. Brown, NBS TN40–4 (PB151399–4) (1961) $1.50.

Bibliography on ionospheric propagation of radio waves (1923–1960), W. Nupen, NBS TN84 (PB161585) (1961) $7.00.

Collisions of liquid drops with liquids, O. G. Engel, NBS TN89 (PB161590) (1961) $1.00.

Determination of the K fluorescence yield of argon by proportional-counter spectrometry, C. Godeau, NBS TN91 (PB161592) (1961) 50 cents.

On the climatology of ground-based radio ducts and associated fading regions, E. J. Dutton, NBS TN96 (PB161597) (1961) $1.75.

A fixed frequency, 9.1 Gc, field intensity recording receiver with extremely narrow bandwidth, R. W. Hubbard and J. V. Cateora, NBS TN107 (PB161608) (1961) 75 cents.

Data reduction instrumentation for radio propagation research, W. E. Johnson, NBS TN111 (PB161612) (1961) $1.00.

The glass electrode, R. G. Bates, Book, Reference Electrodes, edited by D. J. G. Ives and G. J. Janz (Academic Press Inc., New York, N.Y.), ch. **5,** 231–269 (1961).

A recalibration of the NBS standard thermal neutron flux, E. R. Mosburg, Jr., and W. M. Murphey, J. Nuclear Eng. (Reactor Science and Technology Pt.) **14,** 25–30 (1961).

The relationship of low-height ionosonde echoes to auroral-zone absorption and VHF *D* scatter, J. K. Olesen and J. W. Wright, J. Geophys. Research **66,** No. 4, 1127–1134 (Apr. 1961).

Trends in the technology of automatic data processing, S. N. Alexander, AMA Report **43,** 38–42 (1960).

Use of the bulge test for determining mechanical properties of stainless steel foil, D. B. Ballard, Materials Research and Standards **1,** No. 6, 471–473 (June 1961).

Some comments on the use and preparation of hard gallium alloys, G. G. Harman, Rev. Sci. Instr. **32,** No. 4, 465–466 (Apr. 1961).

On the nature of equatorial spread *F*, R. Cohen and K. L. Bowles, J. Geophys. Research **66,** No. 4, 1081–1106 (Apr. 1961).

A study of the chemical reactions in kilning bone char, F. G. Carpenter, and V. R. Deitz, Proc. 6th Tech. Session on Bone Char 1959, p. 321 (Bone Char Research Project Inc., Charlestown, Massachusetts, 1961).

Rate of vaporization of refractory substances, R. F. Walker, J. Efimnokof, and N. L. Lofgren, Book, Physical Chemistry in Aerodynamics and Space Flight (Pergamon Press, Inc., London, England), p. 24–30 (1961).

A note on phase velocity of VLF radio waves, J. R. Wait and K. P. Spies, J. Geophys. Research **66,** No. 3, 992–993 (Mar. 1961).

On the excitation of electromagnetic surface waves on a curved surface, J. R. Wait, IRE Trans. Ant. Prop. **AP–8,** No. 4, 445–448 (July 1960).

Solubility product phenomena in hydroxyapatite—water systems, R. M. Rootare, V. R. Deitz, and F. G. Carpenter, Proc. 6th Tech. Session on Bone Char 1959, p. 287 (Bone Char Research Project Inc., Charlestown, Massachusetts 1961).

Reproducibilities of carbon and germanium thermometers at 4.2° K, M. H. Edlow and H. H. Plumb, Proc, Cryogenic Eng. Conf., Boulder, Colo., Aug. 1960, 6, 542–547 (1961).

The automatic chloride titrator in the analysis of some ionic constituents, M. D. Peiperl, F. G. Carpenter, and V. R. Deitz, Proc. 6th Tech. Session on Bone Char 1959, p. 53 (Bone Char Research Project Inc., Charlestown Massachusetts 1961).

Changes in dentures during storage in water and in service, J. B. Woefel, G. C. Paffenbarger, and W. T. Sweeney, J. Am. Dental Assoc, **62,** No. 6, 643–657 (June 1961).

Solar disturbances and radio communication forecasts, J. F. Brockman, Sky and Telescope **XXI,** No. 6. 322–326 (June 1961).

Long-distance one-hop F_1 propagation through the auroral zone, L. H. Tveten, J. Geophys. Research **66,** No. 6, 1683–1684 (June 1961).

Resonators for millimeter and submillimeter wavelengths, W. Culshaw, IRE Trans. Microwave Theory and Tech. **MTT–9,** No. 2, 135–144 (March 1961).

A five-attribute system of describing visual appearance, D. B. Judd, Am. Soc. Testing Materials Spec. Tech. Pub. No. 297 (1961).

Circumferentially uniform electroplating of tube bores, J P. Young and H. I. Salmon, Plating **48,** No. 7, 763; 787–8 (July 1961).

Solar flare effects in the *F* region of the ionosphere, R. W. Knacht and K. Davies, Nature **190,** No. 4778, 797–798 (May 1961).

Convective circulation in water induced by evaporation cooling, W. G. Spangenberg and W. R. Rowland, Phys. of Fluids **4,** No. 6, 743–750 (June 1961).

Photoionization heating in the *F* region of the atmosphere, D. C. Hunt and T. E. Van Zandt, J. Geophys. Research **66,** No. 6, 1673–1682 (June 1961).

Identification of fiber blends by infrared spectroscopy' M. K. Wharton and F. H. Forziati, Am. Dyestuff Rep. **50,** No. 14, 33–36 (July 1961).

Residual losses in a guard-ring micrometer-electrode holder for solid-disk dialectric specimens, A. H. Scott and W. P. Harris, 1960 Annual Report, Conference on Electrical Insulation, Natl. Acad. Sci.-Natl. Research Council, 11–17 (1961).

Comparative *p*H measurements on papers by water extraction and glass electrode spot tests, J. H. Flynn and L. E. Smith, Tappi **44,** No. 3, 223–228 (March 1961).

A comparison between theoretical and experimental data on phase velocity of VLF radio waves, J. R. Wait, Proc. IRE **49,** No. 6, 1089–1090 (June 1951).

A diffraction theory for LF sky-wave propagation, J. R. Wait, J. Geophys. Research **66,** No. 6, 1713–1724 (June 1961); An additional note, J. R. Wait and A. M. Conda, J. Geophys. Research **66,** No. 6, 1725–1729 (June 1961).

An analysis of errors in the calibration of electric instruments, F. L. Hermach, Communication and Electronics, 1–6 (May 1961).

Incoherent scattering by free electrons as a technique for studying the ionosphere and exosphere; Some observations and theoretical considerations, K. L. Bowles, pp. 223–243 of AGARDograph **42,** The upper atmosphere above *F*2-maximum. North Atlantic Treaty Organization, Advisory Group for Aeronautical Research and Development, Avionics Panel. Papers presented at the Symposium of the Ionospheric Research Committee, Paris, France, May 1959.

A *p*H standard for blood and other physiologic media, V. E. Bower, M. Paabo, and R. G. Bates, Clin. Chem. **7,** No. 3, 292 (June 1961).

Evidence on the laminar nature of the exosphere obtained by means of guided high-frequency wave propagation, R. M. Galley and W. F. Utlaut, Phys. Rev. Letters **6,** No. 11, 591–594 (June 1, 1961).

Comparison of the ionization produced in air by alpha particles near 5 Mev and by beta particles, Z. Bay and P. A. Newman, Radiation Research **14,** No. 5, 566–572 (May 1961).

A century-old razor, S. J. Rosenberg, Metal Progress, 94–96 (1961).

Some applications of Hardy's formula in Brownian motion (Abstract), A. Chaffari, Am. Math. Soc. Notices **8,** No. 54, 238 (June 1961).

On the classical approximation in the statistical theory of mass spectra, H. M. Rosenstock, J. Chem. Phys. **34,** 2182 (1961).

Optical calibration of vibration pickups at small amplitudes, V. A. Schmidt, S. Edelman, E. R. Smith, and E. Jones, J. Acoust. Soc. Am. **33,** Mo. 6, 748–751 (June 1961).

Superconductivity of Nb_3Sn in pulsed fields of 185 kilogauss, V. D. Arp, R. H. Kropschot, and J. H. Wilson, Phys. Rev. Letters **6,** No. 9, 542–453 (May 1961).

Proposed nomenclature for linear viscoslastic behavior, H. Leaderman and F. Schwarzl, Rheologica Acta **1,** No. 4/6, 674–676 (1961).

FM and SSB radiotelephone tests on a VHF ionospheric scatter link during multipath conditions, IRE Trans. Commun. Systems **CS–8,** No. 3, 183–186 (Sept. 1960).

**Publications for which a price is indicated (except for Technical Notes) are available only from the Superintendent of Documents, U.S. Government Printing Office, Washington 25, D.C. (foreign postage, one-fourth additional). Technical Notes are available only from the Office of Technical Services, U.S. Department of Commerce, Washington 25, D.C. (Order by PB number.) Reprints from outside journals and the NBS Journal of Research may often be obtained directly from the authors.*

UNIVERSITY MICROFILMS INC
EDITORIAL DEPARTMENT
313 NORTH FIRST ST
ANN ARBOR MICH
SJR-A OCT

UNITED STATES
GOVERNMENT PRINTING OFFICE
DIVISION OF PUBLIC DOCUMENTS
WASHINGTON 25, D.C.

OFFICIAL BUSINESS

PENALTY FOR PRIVATE USE TO AVOID PAYMENT OF POSTAGE, $300 (GPO)

JOURNAL OF RESEARCH of the National Bureau of Standards Vol. 65A, No. 6 November–December 1961
A. Physics and Chemistry

Contents

Page

Comparison of lens response for sinusoidal and square-wave targets at several focal positions. Sayeda H. Emara. 465

Wavelength shifts in Hg^{198} as a function of temperature. Sayeda H. Emara. 473

Variability of spectral tristimulus values. Isadore Nimeroff, Joan R. Rosenblatt, and Mary C. Dannemiller. 475

Extension of the Flory-Rehner theory of swelling to an anisotropic polymer system. Stephen D. Bruck. 485

Fiber structure-property relationships: a disulfide-crosslinked self-crimping polyamide. Stephen D. Bruck. 489

Acidity functions. Values of the quantity $p(a_H\gamma_{Cl})$ for buffer solutions from 0 to 95 °C. Roger G. Bates and R. Gary. 495

2,3-O-Isopropylidene-α-D-lyxofuranose, the monoacetone-D-lyxose of Levene and Tipson. Robert Schaffer. 507

Effect of perchloryl fluoride additions on the flame speed of methane. Carl Halpern. 513

Publications of the National Bureau of Standards. 525

Index to volume 65A, January to December 1961. 529

For sale by the Superintendent of Documents, U.S. Government Printing Office, Washington 25, D.C. Price 70 cents (single copy)
Subscription price: $4.00 a year; 75 cents additional for foreign mailing.

UNITED STATES GOVERNMENT PRINTING OFFICE, WASHINGTON : 1961